Highlights

- A numerical procedure for the three-dimensional frictional contact modelling of anisotropic coupled magneto-electro-elastic materials in presence of both electric and magnetic fields is presented.

- An orthotropic frictional law is considered, so anisotropy is present both in the bulk and in the surface.

- The methodology uses the boundary element method with explicit evaluation of the fundamental solutions in order to compute the magneto-electro-elastic influence coefficients.

- The contact model is based on an augmented Lagrangian formulation and it uses an iterative Uzawa scheme of resolution.

- Conducting, semi-conducting and insulated electric and/or magnetic indentation conditions, as well as orthotropic frictional contact conditions are considered.

- The methodology is validated by comparison with benchmark analytical solutions. Then, additional exploration examples are presented and discussed in detail, revealing that magneto-electric material coupling, conductivity contact conditions lead to a significant effect on the indentation force and contact pressure distributions.

- The influence of friction in electric and magnetic potential responses has been also proved to be very significant. Moreover, tangential loads exhibit an important influence both on the maximum values of the electric and magnetic potentials as well as on their distributions.

3D coupled multifield magneto-electro-elastic contact modelling

L. Rodríguez-Tembleque*[1], F. C. Buroni[1], A. Sáez[1], M. H. Aliabadi[2]

[1] *Escuela Técnica Superior de Ingeniería, Universidad de Sevilla, Camino de los Descubrimientos s/n , Sevilla E-41092, Spain.*

[2] *Department of Aeronautics, Faculty of Engineering, Imperial College of London, South Kensington Campus, London SW7 2AZ, UK.*

Abstract

The present work deals with the general contact problem for coupled magneto-electro-elastic materials. Despite of the relevant technological applications, this topic of research has been treated only in some analytical works. But analytical solutions lack the generality of numerical methodologies, being restricted typically to simple geometries, loading conditions, idealized contact conditions and mostly taking into account transversely isotropic material symmetry with the symmetry axis normal to the contact surface. In this work, a numerical procedure for the three-dimensional frictional contact modelling of anisotropic coupled magneto-electro-elastic materials in presence of both electric and magnetic fields is presented for the first time. An orthotropic frictional law is considered, so anisotropy is present both in the bulk and in the surface. The methodology uses the boundary element method with explicit evaluation of the fundamental solutions in order to compute the magneto-electro-elastic influence coefficients. The contact model is based on an augmented Lagrangian formulation and it uses an iterative Uzawa scheme of resolution. Conducting, semi-conducting and insulated electric and/or magnetic indentation conditions, as well as orthotropic frictional contact conditions are considered. The methodology is validated by comparison with benchmark analytical solutions. Then, additional exploration examples are presented and discussed in detail, revealing that magneto-electric material

*corresponding author
Email address: luisroteso@us.es (L. Rodríguez-Tembleque[1])

coupling, conductivity contact conditions lead to a significant effect on the indentation force and contact pressure distributions. The influence of friction in electric and magnetic potential responses has been also proved to be very significant. Moreover, tangential loads exhibit an important influence both on the maximum values of the electric and magnetic potentials as well as on their distributions.

Key words: Multifield contact, Contact mechanics, Magneto-electro-elastic materials, Friction, Indentation, Boundary Element Method

---

1. Introduction

The Magneto-Electro-Elastic (MEE) coupling present in multiferroic composites consisting of Piezoelectric (PE) and Piezomagnetic (PM) phases has been focus of intensive research in last years, due to its wide and important technological applications at multiple scales, such as sensors, actuators, filters, oscillators, phase shifters, memory devices, and general smart structures [1]. On the other hand, the study of the contact problem is necessary in order to address problems like positioning of micro- and nano-mechanisms and various functional devices, as well as in experimental testing and characterization of this kind of materials. Therefore, in this emerging topic of research, the pursuit of powerful and efficient capabilities for modelling this coupled multifield contact problem become crucial in order to predict and understand the underlying physics in the interaction of electro-magnetic and mechanical processes.

Because of the mentioned interest, several analytical works devoted to model the contact problem in coupled MEE materials have recently appeared. One of the first works which study this problem was due to Hou et al. [2], who obtain the Boussinesq and Cerruti solutions and apply them to the frictional Hertz problem in transversely isotropic materials. Analytical solutions for the half-space indentation by rigid flat-ended, conical, and spherical punches in transversely isotropic MEE materials have been presented and discussed in detail by Chen et al. [3]. Indenters may be in any combination of conducting and insulating for both electric and magnetic fields. Both works are based on Fabrikant's method of potential theory for elastic materials [4]. Moving rigid punch solutions in two-dimensions (2D) have been considered by Zhou et al., both for frictionless [5, 6] and frictional contact [7, 8, 9, 10, 11]. 2D graded materials are further considered in [12].

Most of the analytical works modelling the MEE problem are extensions of previous efforts related to the modelling of the contact problem for materials with electro-mechanical coupling. For instance some of those mentioned above are based on the works by Ding et al. [13, 14, 15]. It should be mentioned also the work by Giannakopoulos and Suresh [16] who presented a theory of indentation of piezoelectric materials by using the Hankel transform for the three typical indenters (i.e. flat, conical, and spherical). See also further references in Rodríguez-Tembleque et al. [17]. For transversely isotropic PM materials, the frictionless axisymmetric indentation by flat rigid punch has been studied by Giannakopoulos and Parmaklis [18]; and the 2D exact solution of the singular integral equation corresponding to the indentation by a sliding rigid punch with flat or cylindrical profile has been presented by Zhou and Lee [19].

But all these works lack the generality of numerical methodologies, being restricted to simple geometries (a few axisymmetric indenters on a half-space), loading conditions, idealized contact conditions and taking into account almost uniquely transversely isotropic material symmetry with the material symmetry axis being normal to the contact surface. These limitations can be overtaken with advanced numerical formulations. Mathematical models in variational form for coupled electro-elastic frictional contact problems have been proposed (e.g. [20, 21]); and some numerical schemes based in the Finite Element Method (FEM) have been implemented. Quasistatic 2D contact problems between solid-foundation and a PE material and an electro-visco-elastic material have been studied, for instance, by Sofonea et al. [22, 23, 24, 25] under frictionless conditions; and by Sofonea et al. [26] incorporating isotropic frictional contact conditions. Recently, Rodríguez-Tembleque et al. [17] presented a Boundary Element Method (BEM) formulation to study 3D frictional contact of piezoelectric bodies in the presence of electric fields. However, to the best of the authors' knowledge, no numerical formulation for solving the coupled MEE contact problem is available in the literature.

BEM is an alternative particularly advantageous over other numerical techniques when it is used for solving the contact problem in finite, semi-finite or infinite domains. The ability of the BEM to accurately represent steep solution gradients is well-known and the reduction in the degrees of freedom becomes particularly attractive to handle the concerning problem, since for multifield materials the number of degrees of freedom per node notably increases.

The aim of this work is to present and to implement a BEM formulation for the 3D coupled modelling of the sliding contact interaction between anisotropic magneto-electro-elastic materials in presence of both electric and magnetic fields. An orthotropic frictional law is considered, so anisotropy is present both in the bulk and in the surface. The paper is organized as follows: In Section 2, the basic governing equations are presented. Non-linear mechanical and magneto-electrical contact conditions are presented in Sections 3 and 4. The literature on BEM formulations is quite extensive, so in Section 5.1 we briefly present the basic ideas of the BEM with emphasis in the explicit evaluation procedure for the fundamental solutions. MEE contact discrete equations are presented as an algebraic equation system in Section 5.2. Then, the solution method is presented in Section 6. The methodology is validated by comparison with benchmark analytical solutions in Section 7, where additional exploration examples are presented and discussed in detail. We close the paper with some concluding remarks.

2. Coupled magneto-electro-elastic equations

Let consider a 3D region $\Omega \subset \mathbb{R}^3$ with a piecewise smooth boundary $\partial\Omega$ occupied by a homogeneous MEE anisotropic material, in reference at a Cartesian coordinate system (x_i) $(i = 1, 2, 3)$. Small deformations are considered, so the infinitesimal strain tensor $\boldsymbol{\gamma}$, the electric field $\boldsymbol{E}$ and the magnetic field $\boldsymbol{H}$ are obtained, respectively, from derivatives of the displacements $\boldsymbol{u}$, the electric potential $\boldsymbol{\varphi}$ and the magnetic potential $\boldsymbol{\psi}$ as

$$\begin{array}{lll} \gamma_{ij} = (u_{i,j} + u_{j,i})/2 & \text{in} & \Omega, \\ E_i = -\varphi_{,i} & \text{in} & \Omega, \\ H_i = -\psi_{,i} & \text{in} & \Omega. \end{array} \tag{1}$$

In the absence of any body sources, the mechanical stress $\boldsymbol{\sigma}$, the electric displacement $\boldsymbol{D}$ and the magnetic induction $\boldsymbol{B}$ are divergence-free fields, that is,

$$\sigma_{ij,j} = 0 \quad \text{in} \quad \Omega, \tag{2}$$

$$D_{i,i} = 0 \quad \text{in} \quad \Omega, \tag{3}$$

$$B_{i,i} = 0 \quad \text{in} \quad \Omega, \tag{4}$$

where repeated dummy indices indicate summation. In linear MEE materials, the elastic, electric and magnetic fields are coupled through the constitutive law

$$\sigma_{ij} = c_{ijkl}\gamma_{kl} - e_{lij}E_l - q_{lij}H_l \quad \text{in} \quad \Omega, \tag{5}$$

$$D_i = e_{ikl}\gamma_{kl} + \epsilon_{il}E_l + \lambda_{il}H_l \quad \text{in} \quad \Omega, \tag{6}$$

$$B_i = q_{ikl}\gamma_{kl} + \lambda_{il}E_l + \mu_{il}H_l \quad \text{in} \quad \Omega, \tag{7}$$

where $\boldsymbol{c}$, $\boldsymbol{\epsilon}$ and $\boldsymbol{\mu}$ denote the components of the elastic stiffness tensor, the dielectric permittivity tensor and the magnetic permeabilities tensor, respectively; $\boldsymbol{e}$, $\boldsymbol{q}$ and $\boldsymbol{\lambda}$ are the PE, PM and ME coupling coefficients, respectively. These tensors satisfy the following symmetries

$$c_{ijkl} = c_{jikl} = c_{ijlk} = c_{klij}, \quad e_{kij} = e_{kji}, \quad q_{kij} = q_{kji}, \tag{8}$$

$$\epsilon_{kl} = \epsilon_{lk}, \quad \lambda_{kl} = \lambda_{lk}, \quad \mu_{kl} = \mu_{lk}.$$

Moreover, the elastic constant, dielectric permittivity, magnetic permeability tensors are positive definite; and the PE, PM and ME coupling tensor are positive semi-definite.

Given a MEE region Ω, three partitions of the boundary $\partial\Omega$ are considered to define the mechanical, the electrical and the magnetic boundary conditions (see Fig. 1). The first one divides $\partial\Omega$ into three disjoint parts such that $\partial\Omega = \partial\Omega^u \cup \partial\Omega^t \cup \partial\Omega^c$. Here, $\partial\Omega^u$ denotes the boundary on which displacements $\tilde{u}_i$ are prescribed; $\partial\Omega^t$ denotes the boundary on which the tractions $\tilde{t}_i = \sigma_{ij}\nu_j$ are imposed, being ν_j the components of the outward unit normal vector to the boundary $\partial\Omega^t$; and $\partial\Omega^c$ represents the potential contact surface, which have outward unit normal vector with components ν_i^c. The second partition of $\partial\Omega$ is such that $\partial\Omega = \partial\Omega^\varphi \cup \partial\Omega^q \cup \partial\Omega^c$, being the electrical potential $\tilde{\varphi}$ prescribed on $\partial\Omega_\varphi$, and the electrical charge flux $\tilde{q} = D_i\nu_i$ known on $\partial\Omega_q$, where ν_i is the outward unit normal vector on this part of the boundary. Last partition of $\partial\Omega$ regards to the magnetic boundary conditions, so $\partial\Omega = \partial\Omega^\psi \cup \partial\Omega^s \cup \partial\Omega^c$ is satisfied. In this case, magnetic potential $\tilde{\psi}$ is prescribed on $\partial\Omega^\psi$ and the normal magnetic flux $\tilde{s} = B_i\nu_i$ on the boundary $\partial\Omega^s$, with outward unit normal components ν_i.

For a well-posed problem either Dirichlet or Neumann boundary conditions must be prescribed at each boundary point outside the contact zone $\partial\Omega^c$.

Under small displacement assumption, a common unit normal vector ν_i^c can be considered in $\partial\Omega^c$. So the nonlinear boundary contact conditions are:

$$\begin{array}{lll} \sigma_{ij}\nu_j^c = p_i & \text{on} & \partial\Omega^c, \\ D_i\nu_i^c = -\kappa_e(\varphi - \varphi_o) & \text{on} & \partial\Omega^c, \\ B_i\nu_i^c = -\kappa_m(\psi - \psi_o) & \text{on} & \partial\Omega^c, \end{array} \tag{9}$$

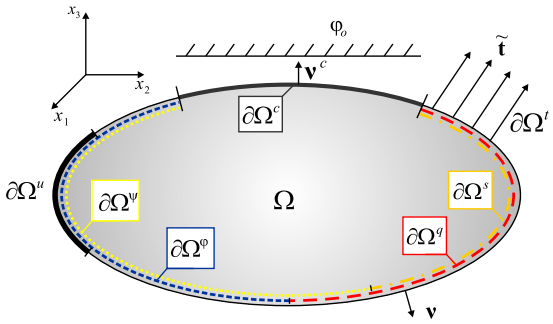

Figure 1: The physical setting.

where p_i is the contact traction: $p_\nu = \mathbf{p} \cdot \boldsymbol{\nu}^c$ is the normal contact pressure and $\mathbf{p}_\tau = \mathbf{p} - p_\nu \boldsymbol{\nu}^c$ is the tangential contact traction; κ_e and κ_m are the electrical and magnetic conductivity coefficients, respectively; and φ_o and ψ_o denote, respectively, the electric and magnetic potentials of the foundation or the indenter.

3. Mechanical contact conditions

The unilateral contact law involves Signorini's contact conditions in $\partial\Omega^c$:

$$g_\nu \geq 0, \quad p_\nu \leq 0, \quad g_\nu \, p_\nu = 0, \tag{10}$$

where $g_\nu = (g_o - u_\nu)$, being g_o the initial gap between the bodies and $u_\nu = \mathbf{u} \cdot \boldsymbol{\nu}^c$.

The normal contact constraints presented in (10) can be formulated as:

$$p_\nu - \mathbb{P}_{\mathbb{R}_-}(p_\nu^*) = 0, \tag{11}$$

where $\mathbb{P}_{\mathbb{R}_-}(\bullet)$ is the normal projection function ($\mathbb{P}_{\mathbb{R}_-}(\bullet) = min(0, \bullet)$) and $p_\nu^* = p_\nu + r_\nu g_\nu$ is the augmented normal traction. The parameters r_ν is the normal dimensional penalization parameter ($r_\nu \in \mathbb{R}^+$).

In general, an orthotropic frictional constitutive law is considered for anisotropic MEE materials: $||\mathbf{p}_\tau||_\mu \leq |p_\nu|$. According to [29, 30], this Coulomb friction restriction can be summarized as:

$$\begin{array}{lll} ||\mathbf{p}_\tau||_\mu < |p_\nu| \Rightarrow & \dot{\mathbf{g}}_\tau = \mathbf{0} & \text{on} \quad \partial\Omega_c, \\ ||\mathbf{p}_\tau||_\mu = |p_\nu| \Rightarrow & \mathbf{p}_\tau = -|p_\nu| \mathbb{M}^2 \dot{\mathbf{g}}_\tau / ||\dot{\mathbf{g}}_\tau||_\mu^* & \text{on} \quad \partial\Omega_c. \end{array} \tag{12}$$

In the expressions above, the tangential slip can be assumed for quasistatic contact problems as $\dot{\mathbf{g}}_\tau \approx \Delta \mathbf{g}_\tau = \mathbf{g}_{o,\tau} - \mathbf{u}_\tau$ (i.e. $\mathbf{g}_{o,\tau}$ is the tangential translation and $\mathbf{u}_\tau = \mathbf{u} - u_\nu \boldsymbol{\nu}_c$), $\mathbb{M}$ is a diagonal matrix (i.e. $\mathbb{M} = diag(\mu_1, \mu_2)$), $||\bullet||_\mu$ denotes the elliptic norm

$$||\mathbf{p}_\tau||_\mu = \sqrt{(p_{e_1}/\mu_1)^2 + (p_{e_2}/\mu_2)^2} \tag{13}$$

and the norm $||\bullet||_\mu^*$ is dual of $||\bullet||_\mu$

$$||\dot{\mathbf{g}}_\tau||_\mu^* = \sqrt{(\mu_1 \dot{g}_{e_1})^2 + (\mu_2 \dot{g}_{e_2})^2}, \tag{14}$$

being μ_1 and μ_2 the principal friction coefficients in the tangential directions $\{e_1, e_2\}$. In this work $\{e_1, e_2\}$ are coincident with the x_1 and x_2 axis, respectively.

The frictional contact constraints (12) can be also formulated using contact operators as:

$$\mathbf{p}_\tau - \mathbb{P}_{\mathbb{E}_\rho}(\mathbf{p}_\tau^*) = 0, \tag{15}$$

where $\mathbf{p}_\tau^* = \mathbf{p}_\tau - r_\tau \mathbb{M}^2 \dot{\mathbf{g}}_\tau$ ($r_\tau \in \mathbb{R}^+$) is the augmented tangential traction and $\mathbb{P}_{\mathbb{E}_\rho}(\bullet) : \mathbb{R}^2 \longrightarrow \mathbb{R}^2$ is the tangential projection function defined in [30] as

$$\mathbb{P}_{\mathbb{E}_\rho}(\mathbf{p}_\tau^*) = \begin{cases} \mathbf{p}_\tau^* & \text{if} \quad ||\mathbf{p}_\tau^*||_\mu < \rho, \\ \rho \ \mathbf{p}_\tau^* / ||\mathbf{p}_\tau^*||_\mu & \text{if} \quad ||\mathbf{p}_\tau^*||_\mu \geq \rho, \end{cases} \tag{16}$$

with $\rho = |\mathbb{P}_{\mathbb{R}_-}(p_\nu^*)|$.

4. Magneto-electrical contact conditions

The electrical and magnetic conductivity coefficients in (9) can be defined as: $\kappa_e = \kappa_e(p_\nu)$ and $\kappa_m = \kappa_m(p_\nu)$, being

$$\kappa_e(p_\nu) = \begin{cases} 0 & \text{if} \quad p_\nu = 0, \\ \kappa_e^* & \text{if} \quad p_\nu < 0, \end{cases} \tag{17}$$

and

$$\kappa_m(p_\nu) = \begin{cases} 0 & \text{if} \quad p_\nu = 0, \\ \kappa_m^* & \text{if} \quad p_\nu < 0, \end{cases} \tag{18}$$

what allows to describe perfect electrical and magnetic contact conditions similarly to the Signorini's contact conditions. In the expressions (17) and

(18), κ_e^* and κ_m^* are the conductivity parameter similar to [17]. So, according to (17) and (18), the electric and magnetic contact conditions (9) show that when there is no contact (i.e. $p_\nu = 0$) on $\partial\Omega_c$ the normal electric and magnetic fluxes vanish, and when there is contact, electric and magnetic charges appear.

5. Boundary element formuation

5.1. Discretized MEE boundary integral equations

In this section, the matricial Barnett-Lothe representation for MEE materials, summarized in Appendix A, is used, so upper-case sub-indices range from 1 to 5. This representation allow us to write the discretized boundary integral equation for extended displacements at the source point $\mathbf{x}' \in \partial\Omega$ in a compact form, and similar to its well-known purely mechanical counterpart as

$$\begin{aligned} c_{JK}(\mathbf{x}')u_J(\mathbf{x}') + \sum_{e=1}^{N_e} \left\{ \fint_{\partial\Omega_e} \check{T}_{JK}(\mathbf{x}' \mid \mathbf{x}) u_J(\mathbf{x}) dS(\mathbf{x}) \right\} \\ = \sum_{e=1}^{N_e} \left\{ \int_{\partial\Omega_e} \check{U}_{JK}(\mathbf{x}' \mid \mathbf{x}) t_J(\mathbf{x}) dS(\mathbf{x}) \right\}. \end{aligned} \tag{19}$$

In equation (19), u_J is the extended displacement vector containing the displacements and the electric and magnetic potentials (see Appendix A for its definition); t_J is the extended tractions vector containing the tractions, the normal electric charge flux and the normal magnetic flux (see also Appendix A). The matrix c_{JK} depends on the local geometry of the boundary $\partial\Omega$ at the point $\mathbf{x}'$. Particularly, for a smooth boundary at $\mathbf{x}'$ is equal to $\frac{1}{2}\delta_{JK}$ (being δ_{JK} the extended Kronecker delta). Tensors $\check{U}_{JK}$ and $\check{T}_{JK}$ are the extended displacement fundamental solution and the extended traction fundamental solution at a boundary point $\mathbf{x}$ due to a unit extended source applied at point $\mathbf{x}'$, respectively. A key point in boundary integral formulations is the availability and subsequent implementation of these fundamental solutions. In this work, the scheme for the evaluation of the extended fundamental solution proposed by Buroni and Sáez [32] has been implemented, which posses the remarkable characteristics that it is exact, explicit and valid for mathematical degenerate and non-degenerate materials in the Stroh formalism context. Appendix B presents a summary of these fundamental solutions for

completeness. The strongly singular integral on the left-hand side in (19) is evaluated in the Cauchy principal value sense, whereas the weakly singular integral on the right-hand side is evaluated as an improper integral. As usual in this methodology, the boundary $\partial\Omega$ has been discretized into N_e quadrilateral elements of surface $\partial\Omega_e$. The physical variables u_J and t_J are approximated over each element $\partial\Omega^e$ using linear shape functions in terms of the nodal values. Applying a collocation procedure at each one of the boundary nodes located at $\mathbf{x}'$, equation (19) leads to a system of equations, that, adding the boundary conditions, can be arranged such that the resulting system of algebraic equations is

$$\left[\begin{array}{ccccccc} \mathbf{A}_{\mathrm{x}_e} & \mathbf{A}_{u_c} & \mathbf{A}_{\varphi_c} & \mathbf{A}_{\psi_c} & \mathbf{A}_{p_c} & \mathbf{A}_{q_c} & \mathbf{A}_{s_c} \end{array} \right] \left\{ \begin{array}{c} \mathbf{x}_e \\ \mathbf{u}_c \\ \boldsymbol{\varphi}_c \\ \boldsymbol{\psi}_c \\ \mathbf{p}_c \\ \mathbf{q}_c \\ \mathbf{s}_c \end{array} \right\} = \mathbf{F}. \tag{20}$$

In expression (20), $\mathbf{x}_e$ collects the nodal external unknowns (i.e. the nodal unknowns which are outside the contact zone); $\mathbf{u}_c$, $\boldsymbol{\varphi}_c$ and $\boldsymbol{\psi}_c$ collect the nodal contact displacements, and electric and magnetic potentials, respectively; $\mathbf{p}_c$ contains the normal and tangential nodal contact tractions (i.e. $\mathbf{p}_\nu$ and $\mathbf{p}_\tau$); and, $\mathbf{q}_c$ and $\mathbf{s}_c$ contains the nodal electric charges and magnetic fluxes, respectively. Matrices $\mathbf{A}_{\mathrm{x}_e}$, $\mathbf{A}_{u_c}$, $\mathbf{A}_{\varphi_c}$, $\mathbf{A}_{\psi_c}$, $\mathbf{A}_{p_c}$, $\mathbf{A}_{q_c}$ and $\mathbf{A}_{s_c}$ contain the free-terms and corresponding integrals in equation (19) and vector $\mathbf{F}$ contains the terms corresponding to the prescribed boundary conditions.

5.2. MEE contact discrete equations

The electric charge and the magnetic flux on every contact node i can be expressed in terms of the electric and magnetic potential according to the magneto-electric contact condition (9), (17) and (18), as:

$$(\mathbf{q}_c)_i = -\kappa_e((\mathbf{p}_\nu)_i)((\boldsymbol{\varphi}_c)_i - (\boldsymbol{\varphi}_o)_i), \tag{21}$$

$$(\mathbf{s}_c)_i = -\kappa_m((\mathbf{p}_\nu)_i)((\boldsymbol{\psi}_c)_i - (\boldsymbol{\psi}_o)_i). \tag{22}$$

So equation (20) can be written as

$$\left[\begin{array}{ccccc} \mathbf{A}_{\mathrm{x}_e} & \mathbf{A}_{u_c} & \tilde{\mathbf{A}}_{\varphi_c} & \tilde{\mathbf{A}}_{\psi_c} & \mathbf{A}_{p_c} \end{array} \right] \left\{ \begin{array}{c} \mathbf{x}_e \\ \mathbf{u}_c \\ \boldsymbol{\varphi}_c \\ \boldsymbol{\psi}_c \\ \mathbf{p}_c \end{array} \right\} = \tilde{\mathbf{F}}, \tag{23}$$

being $\tilde{\mathbf{A}}_{\varphi_c} = \mathbf{A}_{\varphi_c} - \boldsymbol{\kappa}_e(\mathbf{p}_\nu)\mathbf{A}_{q_c}$, $\tilde{\mathbf{A}}_{\psi_c} = \mathbf{A}_{\psi_c} - \boldsymbol{\kappa}_m(\mathbf{p}_\nu)\mathbf{A}_{s_c}$,

$$\tilde{\mathbf{F}} = \mathbf{F} - \boldsymbol{\kappa}_e(\mathbf{p}_\nu)\mathbf{A}_{q_c}\boldsymbol{\varphi}_o - \boldsymbol{\kappa}_m(\mathbf{p}_\nu)\mathbf{A}_{s_c}\boldsymbol{\psi}_o \tag{24}$$

and $\boldsymbol{\kappa}_e(\mathbf{p}_\nu)$ and $\boldsymbol{\kappa}_e(\mathbf{p}_\nu)$ diagonal matrices, i.e.:

$$\boldsymbol{\kappa}_e(\mathbf{p}_\nu) = \mathbf{diag}\left[\, \kappa_e((\mathbf{p}_\nu)_1), \cdots, \kappa_e((\mathbf{p}_\nu)_i), \cdots, \kappa_e((\mathbf{p}_\nu)_{N_c}) \,\right], \tag{25}$$

$$\boldsymbol{\kappa}_m(\mathbf{p}_\nu) = \mathbf{diag}\left[\, \kappa_m((\mathbf{p}_\nu)_1), \cdots, \kappa_m((\mathbf{p}_\nu)_i), \cdots, \kappa_m((\mathbf{p}_\nu)_{N_c}) \,\right]. \tag{26}$$

Finally, the mechanical contact restrictions (11) and (15) are defined on every contact node i as:

$$(\mathbf{p}_\nu)_i - \mathbb{P}_{\mathbb{R}_-}(\ (\mathbf{p}_\nu)_i + r_\nu(\mathbf{g}_\nu)_i\ ) = 0, \tag{27}$$

$$(\mathbf{p}_\tau)_i - \mathbb{P}_{\mathbb{E}_\rho}(\ (\mathbf{p}_\tau)_i - r_\tau\mathbb{M}^2(\mathbf{g}_\tau)_i\ ) = \mathbf{0}, \tag{28}$$

where $\mathbf{p}_\nu$ and $\mathbf{p}_\tau$ contain the normal and tangential contact tractions of every contact node i and $\mathbf{g}_\nu$ and $\mathbf{g}_\tau$ contain the normal and tangential mechanical gap vectors, respectively.

Equations (23), (27) and (28) define the quasi-static MEE contact problem which can now be written in the following form

$$\boldsymbol{\Theta}(\mathbf{z}) = \left\{ \begin{array}{c} \mathbf{A}_{\mathrm{x}_e}\mathbf{x}_e + \mathbf{A}_{u_c}\mathbf{u}_c + \tilde{\mathbf{A}}_{\varphi_c}\boldsymbol{\varphi}_c + \tilde{\mathbf{A}}_{\psi_c}\boldsymbol{\psi}_c + \mathbf{A}_{p_c}\mathbf{p}_c - \widetilde{\mathbf{F}} \\ \mathbf{p}_c - \mathbb{P}_{\mathbb{C}_f}(\mathbf{p}_c^*) \end{array} \right\} = \mathbf{0}, \tag{29}$$

being $\mathbf{z} = (\mathbf{x}_e, \mathbf{u}_c, \boldsymbol{\varphi}_c, \boldsymbol{\psi}_c, \mathbf{p}_c)$ a vector which collects the unknowns variables and $\mathbb{P}_{\mathbb{C}_f}$ the contact operator: $\mathbb{P}_{\mathbb{C}_f}(\ (\mathbf{p}_c^*)_i\ ) = \left\{\mathbb{P}_{\mathbb{R}_-}(\ (\mathbf{p}_\nu^*)_i\ ), \mathbb{P}_{\mathbb{E}_\rho}(\ (\mathbf{p}_\tau^*)_i\ )\right\}$.

6. Solution method

The quasi-static MEE contact system (29) is solved using the Uzawa's method [27, 28, 29, 30]. To compute the variables at the load step (k), $\mathbf{z}^{(k)} = (\mathbf{x}_e^{(k)}, \mathbf{u}_c^{(k)}, \boldsymbol{\varphi}_c^{(k)}, \boldsymbol{\psi}_c^{(k)}, \mathbf{p}_c^{(k)})$, we iterate using $(n = 0, 1, 2, ...)$ index, initializing $\mathbf{z}^{(0)} = \mathbf{z}^{(k-1)}$ (i.e. $\mathbf{p}_c^{(0)} = \mathbf{p}_c^{(k-1)}$).

First, we solve the following system:

$$\left[\begin{array}{cccc} \mathbf{A}_{\mathrm{x}_e} & \mathbf{A}_{u_c} & \tilde{\mathbf{A}}_{\varphi_c} & \tilde{\mathbf{A}}_{\psi_c} \end{array} \right] \left\{ \begin{array}{c} \mathbf{x}_e \\ \mathbf{u}_c \\ \boldsymbol{\varphi}_c \\ \boldsymbol{\psi}_c \end{array} \right\}^{(n+1)} = -\mathbf{A}_{p_c}\, \mathbf{p}_c^{(n)} + \tilde{\mathbf{F}}, \tag{30}$$

being $\tilde{\mathbf{A}}_{\varphi_c} = \mathbf{A}_{\varphi_c} - \boldsymbol{\kappa}_e(\mathbf{p}_\nu^{(n)})\mathbf{A}_{q_c}$, $\tilde{\mathbf{A}}_{\psi_c} = \mathbf{A}_{\psi_c} - \boldsymbol{\kappa}_m(\mathbf{p}_\nu^{(n)})\mathbf{A}_{s_c}$ and $\tilde{\mathbf{F}} = \mathbf{F} - \boldsymbol{\kappa}_e(\mathbf{p}_\nu^{(n)})\mathbf{A}_{q_c}\boldsymbol{\varphi}_o - \boldsymbol{\kappa}_m(\mathbf{p}_\nu^{(n)})\mathbf{A}_{s_c}\boldsymbol{\psi}_o$.

After solving the system of equations (30), contact tractions for every contact node i are updated:

$$(\mathbf{p}_\nu^{(n+1)})_i = \mathbb{P}_{\mathbb{R}_-}(\ (\mathbf{p}_\nu^{(n)})_i + r_\nu(\mathbf{g}_\nu^{(n+1)})_i\ ), \tag{31}$$

$$(\mathbf{p}_\tau^{(n+1)})_i = \mathbb{P}_{\mathbb{E}_\rho}(\ (\mathbf{p}_\tau^{(n)})_i - r_\tau\ \mathbb{M}^2(\Delta\mathbf{g}_\tau^{(n+1)})_i\ ), \tag{32}$$

where $(\mathbf{g}_\nu^{(n+1)})_i = (\mathbf{g}_{o,\nu}^{(k)})_i - (\mathbf{u}_\nu^{(n)})_i$, $(\Delta\mathbf{g}_\tau^{(n+1)})_i = (\mathbf{g}_{o,\tau}^{(k)})_i - (\mathbf{u}_\tau^{(n)})_i$ and $\rho = |(\mathbf{p}_\nu^{(n+1)})_i|$.

Finally, if $\Psi(\mathbf{z}^{(n+1)}) \leq \varepsilon$ (being $\Psi(\mathbf{z}^{(n+1)}) = max\{\|\mathbf{u}_c^{(n+1)} - \mathbf{u}_c^{(n)}\|, \|\boldsymbol{\varphi}_c^{(n+1)} - \boldsymbol{\varphi}_c^{(n)}\|, \|\boldsymbol{\psi}_c^{(n+1)} - \boldsymbol{\psi}_c^{(n)}\|, \|\mathbf{p}_c^{(n+1)} - \mathbf{p}_c^{(n)}\|\}$), the solution for the instant (k) is reached, i.e. $\mathbf{z}^{(k)} = \mathbf{z}^{(n+1)}$. Otherwise, return to (30) evaluating $\mathbf{p}_c^{(n)} = \mathbf{p}_c^{(n+1)}$.

7. Numerical results

The capabilities of the proposed multifield contact formulation and some numerical results are shown in this section. First, the methodology is validated by comparison with the analytical results presented in [3], where the indentation response of a transversely isotropic MEE solid is considered. Then a fully orthotropic MEE solid indentation is solved under frictional and non-isolated MEE indentation conditions. Finally, the tangential load response of an orthotropic MEE solid is studied.

Table 1: Transversely isotropic MEE properties for ($BaTiO_3$-$CoFe_2O_4$).

Elastic coefficients (GPa)	
c_{1111}	226.00
c_{1122}	125.00
c_{1133}	124.25
c_{3333}	216.00
c_{2323}	44.15
Piezoelectric coefficients (C/m^2)	
e_{113}	5.80
e_{333}	9.30
e_{311}	-2.20
Piezomagnetic coefficients (N/Am)	
q_{113}	275.00
q_{333}	350.00
q_{311}	290.15
Dielectric constants (10^{-9} F/m)	
ϵ_{11}	5.64
ϵ_{33}	6.35
Magnetic constants (10^{-6} Ns^2/C^2)	
μ_{11}	297.50
μ_{33}	83.50

7.1. Indentation response of a transversely isotropic MEE solid

The problem illustrated in Fig. 2(a) presents a spherical indentation of a transversely isotropic MEE block, whose dimensions are $2L_1 \times 2L_1 \times L_2$, being $L_1 = 50 \times 10^{-3}$ m and $L_2 = 120 \times 10^{-3}$ m. The block is discretized by 1088 linear quadrilateral boundary elements, using 16×16 elements on the $L_o \times L_o$ potential contact zone ($L_o = 5 \times 10^{-3}$ m), as Fig. 2(b) shows. The material considered in this example was presented in [3] and it presents no coupling between the electric and magnetic field. It is a MEE composite material made of piezoelectric ($BaTiO_3$) and magnetostrictive ($CoFe_2O_4$) phases, whose material properties were estimated using the rule of mixture according to the volume fraction: $\chi = 0.5$. The resulting MEE composite material has a symmetry axis coinciding with x_3-direction, being its properties presented in Table 1.

The rigid sphere of radius $R = 100 \times 10^{-3}$ m is subjected to a normal

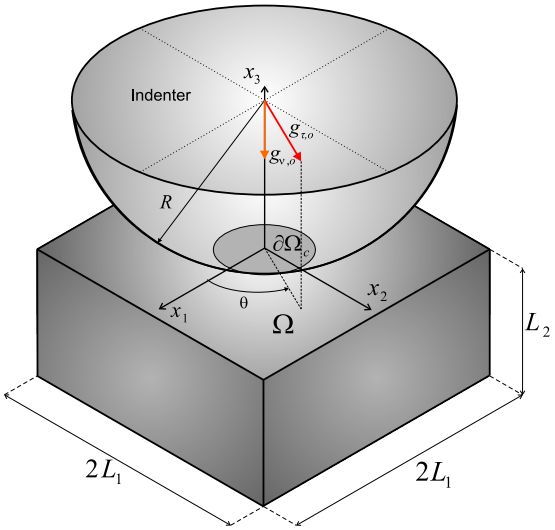

(a)

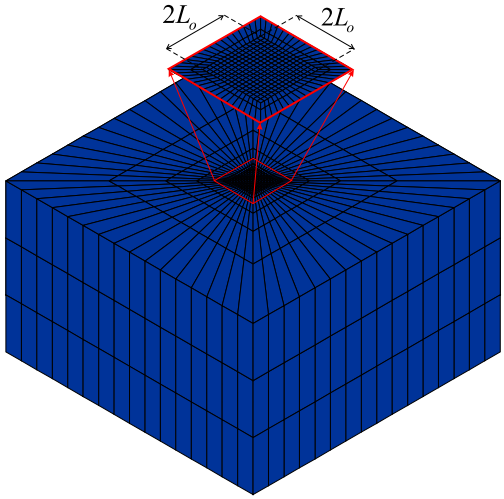

(b)

Figure 2: (a) The physical setting: rigid indenter over a magneto-electro-elastic domain. (b) Boundary element mesh details.

indentation of $g_{\nu,o} = 5 \times 10^{-5}$ m ($g_{\tau,o} = 0$) and the MEE block is assumed to be ideally bonded at the base ($x_3 = -L_2$). Different frictionless indentation conditions are considered, e.g.: electrically and magnetically insulating

Table 2: Basic indentation parameters presented in [3] for the MEE composite material.

$[\xi_{ij}]$	2.08613	1.77480	1.93900
		−2.35928	2.85507
	sym.		−1.00418
$\eta = \lvert\xi_{ij}\rvert$		5.14794	
$[\eta_{ij}]$	2.08613	1.77480	1.93900
		−2.35928	2.85507
	sym.		−1.00418

indentation (EMII), electrically conducting and magnetically insulating indentation (ECMII), electrically insulating and magnetically conducting indentation (EIMCI) or electrically and magnetically conducting indentation (EMCI). Chen et al. [3] present the analytical solutions for a transversely isotropic MEE under all these spherical indentation conditions. For example, the resultant indentation force are expressed as:

$$P_{EMII} = \frac{4a^3}{3\pi\xi_{11}R} \qquad \left(a = \sqrt{g_{\nu,o}R}\right), \tag{33}$$

$$P_{ECMII} = \frac{4\xi_{22}a^3}{3\pi\eta_{33}R} \qquad \left(a = \sqrt{g_{\nu,o}R - \xi_{12}\varphi_o/\xi_{22}}\right), \tag{34}$$

$$P_{EIMCI} = \frac{4\xi_{33}a^3}{3\pi\eta_{22}R} \qquad \left(a = \sqrt{g_{\nu,o}R - \xi_{13}\psi_o/\xi_{33}}\right), \tag{35}$$

and

$$P_{EMCI} = \frac{4a}{3\pi\eta}(\eta_{11}g_{\nu,o} + \eta_{21}\varphi_o + \eta_{31}\psi_o), \tag{36}$$

being $a = \sqrt{g_{\nu,o}R + (\eta_{21}\varphi_o + \eta_{31}\psi_o)/\eta_{11}}$. In the expressions (33-36), a is the contact radius, ξ_{ij} and η_{ij} are the MEE composite material parameters listed in Table 2 and ϕ_o and ψ_o are the indenter prescribed electric and magnetic potential, respectively. Similar expressions can be found in [3] for the total electric charge (Q), the total magnetic charge (M), the electric potential distribution or the magnetic potential distribution.

Boundary element results (namely the resultant indentation force and the total electric charge) for a electrically conducting and magnetically insulating

indentation (i.e. $\kappa_e^* \neq 0$ and $\kappa_m^* = 0$) are shown in Fig. 3 (a). We can appreciate how, when the conductivity parameter κ_e^* increases ($\kappa_e^* \to \infty$), the computed resultant indentation force and the total electric charge values converge to the analytic values $P_{_{ECMII}}$ and $Q_{_{ECMII}}$, presented in [3]. In those cases, the prescribed electric potential was $\varphi_o = 0$. Same behavior can be observed in Fig. 3 (b) for the total magnetic charge, in an electrically insulating and magnetically conducting indentation (i.e. $\kappa_e^* = 0$ and $\kappa_m^* \neq 0$): when the conductivity parameter κ_m^* increases ($\kappa_m^* \to \infty$), the computed resultant indentation force and the total magnetic charge values converge to the analytic values $P_{_{EIMCI}}$ and $M_{_{EIMCI}}$. In those cases, the prescribed magnetic potential was $\psi_o = 0$. The examples have been solved using the proposed algorithm, considering $r_\nu = 5 \cdot 10^3$ for the augmented Lagrangian, and $\varepsilon = 10^{-6}$ as a termination limit.

Normalized indentation response distributions as function of conductivity parameters for ECMII and EIMCI are presented in Fig. 4. Contact pressure distributions are presented in Fig. 4 (a) and electric and magnetic potential distributions are shown in Fig. 4 (b) and Fig. 4 (c), respectively. An excellent agreement between analytic and numerical solutions can be observed. For $\kappa_e^* = 0$ and $\kappa_m^* = 0$, perfectly insulating indentation responses (i.e., $p_{o,_{EMII}}$, $\varphi_{o,_{EMII}}$ and $\psi_{o,_{EMII}}$) are obtained by the boundary elements formulation. We observe in Fig. 4 (b) (left) that, for higher values of κ_e^* ($\kappa_e^* \to \infty$, $\kappa_m^* = 0$), the value of the electric potential at the contact region tends to the prescribed electric potential $\varphi_o = 0$. However, the magnetic potential remains unaltered (see Fig. 4 (c) (left)). This is due to fact that the MEE composite material (Table 1) considered for validation in [3] presents no coupling between the electric and magnetic fields. As expected, the opposite behavior is observed when $\kappa_m^* \to \infty$ and $\kappa_e^* = 0$: the value of the magnetic potential at the contact region tends to the prescribed potential $\psi_o = 0$ (see Fig. 4 (c) (right)) and the electric potential remains unaltered (see Fig. 4 (b) (right)).

7.2. Indentation response of an orthotropic MEE solid

In order to illustrate the capabilities of the proposed boundary element formulation, we next study the indentation response of an orthotropic MEE material whose MEE properties are presented in Table 3. We can appreciate a fully coupling between the magnetic, electric and elastic fields.

The influence of the conductivity boundary conditions on the MEE variables are studied in figure 5 and 6. The indentation response for resultant indentation force and total electric and magnetic charges under ECMII and

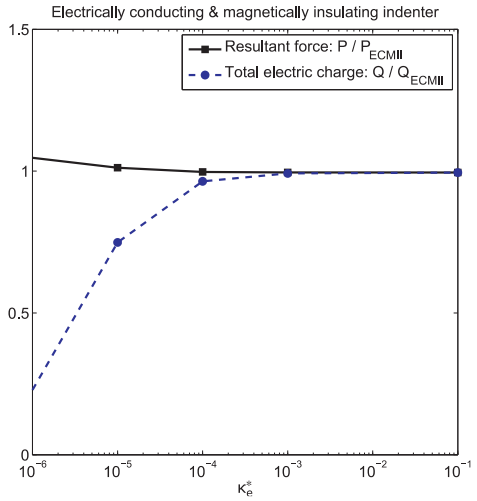

(a)

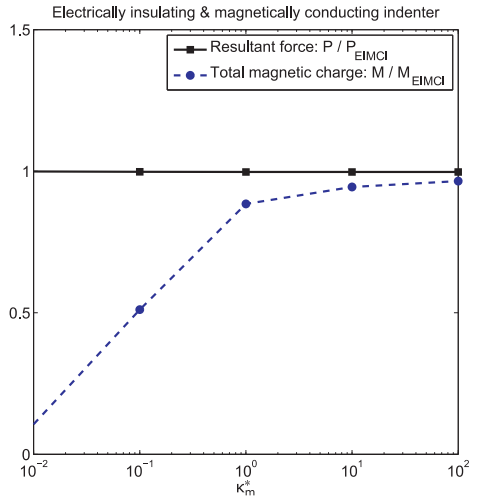

(b)

Figure 3: (a) Influence of the electrical conductivity parameter in electrically conducting and magnetically insulating indentation (ECMII) (i.e. $\kappa_e^* \neq 0$ and $\kappa_m^* = 0$). (b) Influence of the magnetic conductivity parameter in electrically insulating and magnetically conducting indentation (EIMCI) (i.e. $\kappa_e^* = 0$ and $\kappa_m^* \neq 0$).

EIMCI are presented in Fig. 5 and normalized indentation response distributions for normal contact pressure and electric and magnetic potentials are presented in Fig. 6. Numerical examples have been solved for $r_\nu = 5 \cdot 10^2$

Table 3: Orthotropic MEE properties for orthotropic MEE material.

Elastic coefficients (GPa)	
c_{1111}	3.61
c_{1122}	1.61
c_{1133}	1.42
c_{2222}	3.13
c_{2233}	1.31
c_{3333}	1.63
c_{2323}	0.55
c_{1313}	0.59
c_{1212}	0.69
Piezoelectric coefficients (C/m^2)	
e_{113}	-0.016
e_{223}	-0.013
e_{333}	-0.021
e_{311}	0.032
e_{322}	-0.004
Piezomagnetic coefficients (N/Am)	
q_{113}	550.00
q_{223}	570.00
q_{333}	699.70
q_{311}	580.30
q_{322}	590.00
Magneto-electric coefficients (Ns/Am)	
λ_{11}	0.60
λ_{22}	0.80
λ_{33}	0.10
Dielectric constants (10^{-9} C/Vm)	
ϵ_{11}	0.054
ϵ_{22}	0.066
ϵ_{33}	0.059
Magnetic constants (10^{-9} Ns^2/C^2)	
μ_{11}	5000
μ_{22}	7000
μ_{33}	10000

and $\varepsilon = 10^{-6}$. For a ECMII (see Fig. 5 (a) and Fig. 6 (left)), the conductivity parameter increments ($\kappa_e^* \to \infty$) only affect the electric variables (i.e. Q and φ), due to the low value of magneto-electric coefficient λ_{33}. However, for a EIMCI (see Fig. 5 (b) and Fig. 6 (right)), the conductivity increments ($\kappa_m^* \to \infty$) clearly modify all the MEE variables. Fig. 5 (b) shows that normal resultant indentation force for insulated indentation conditions (i.e. $\kappa_m^* \simeq 0$) is reduced by half when conducting indentation conditions (i.e $\kappa_m^* \to \infty$) are considered.

So normal contact compliance can be modified by the conductivity boundary conditions. This can be a key aspect when addressing technological applications in smart structures and systems.

7.3. Frictional indentation response of an orthotropic MEE solid

Now, the problem presented in Section 7.2 is studied under frictional contact conditions, considering both isotropic and orthotropic friction laws. Assuming an isotropic friction law ($\mu_1 = \mu_2 = \mu$), Fig. 7 (a) and Fig. 7 (b) present the influence of friction under EMII and EMCI, respectively, for different values of $\mu = \{0, 0.1, 0.3, 0.6, 0.9\}$. Fig. 7 (a) shows the influence of friction on the normalized resultant force, the maximum electric potential and the maximum magnetic potential. Their values increase with the value of μ, exhibiting an increment of 65% in the maximum electric potential or 30% in the maximum magnetic potential for $\mu = 0.9$. These increments are consequence of the stress state increment inside the bulk due to the frictional tangential contact tractions presence. Fig. 8(a) shows the normal and tangential contact tractions distribution for different values of μ and relative to maximum frictionless contact pressure p_o and 8(b) and 8(c) show the relative electric potential and the magnetic potential distributions, respectively. Fig. 7 (b) shows the influence of friction on the normalized resultant force, the total electric charge and the total magnetic charge. In the EMCI, their values are not significantly affected by the increment of μ values. These numerical results have been solved considering $r_\nu = 5 \cdot 10^3$, $r_\tau = 3 \cdot 10^3$ and $\varepsilon = 10^{-6}$.

Finally, in this section, orthotropic frictional EMII conditions influence is considered. Fig. 9 (a) shows the normalized electric potential distribution and Fig. 9 (b) presents the normalized magnetic potential relative to the frictionless EMII. Both results reveal that not only their values are affected by the orthotropic friction law, but also the electric and magnetic potential distribution shape.

7.4. Tangential load response of an orthotropic MEE solid

The influence of tangential load in the indentation response is studied in this section. In this case, the EMII presented in Section 7.3 is also subjected to a tangential displacement $g_{o,\tau}$ that generates a tangential load. The indentation response is studied under different values of tangential load (in particular, from tangential loading applying the full stick contact condition to tangential loading applying the full slip contact on $\partial\Omega_c$).

Fig. 10 shows the normalized indentation and tangential load response distributions as function of the friction coefficient for EMII. In this results, tangential load direction is $\theta = 0^o$ (see Fig. 2). Fig. 10 (a), Fig. 10 (b) and Fig. 10 (c) present the influence of tangential load in the contact tractions, in the magnetic potential distribution and in the electric potential distribution, respectively, for low friction $\mu = 0.1$ (left) and high friction $\mu = 0.6$ (right) conditions. Fig. 10(a) shows normal and tangential contact tractions distributions for different values of the normalized tangential load $F_{x_1}/\mu P$. We can see in Fig. 10 (a) that the stick zone decreases and it is moved to the left side of the contact zone (opposite to the tangential load direction) when the normalized tangential load increases, as it is expected [33]. Meanwhile, Fig. 10 (b) and Fig. 10 (c) show that the maximum of the electric and magnetic potential distribution is also moved in the same direction as the tangential load is applied, but its value exhibits a decrement when the normalized tangential load increases until full slip contact distribution is developed. This behavior is more pronounced when tangential loads occur under high friction conditions. Same results can be observed in Fig. 11 and Fig. 12 for the electric and magnetic potential distribution on the contact zone.

Finally, the influence of tangential load direction (θ) under orthotropic frictional contact conditions is considered in this example. Assuming $\mu_1 = 0.1$ and $\mu_2 = 0.6$, Fig. 13 shows the normalized electric potential distribution (top), normalized magnetic potential distribution (mid) and normalized contact traction distribution (bottom) for: (a) $\theta = 0^o$, (b) $\theta = 45^o$ and (c) $\theta = 90^o$. In the same way, Fig. 14 presents same results for $\mu_1 = 0.6$ and $\mu_2 = 0.1$. It is clear how the orthotropic frictional conditions and tangential load direction affect the MEE contact variables, not only in the intensity, but also in the distribution shape.

8. Conclusions

A boundary element formulation has been presented and applied to study 3D coupled multifield MEE contact under orthotropic frictional conditions. The proposed formulation has been applied for the analysis of a MEE half space configuration under different frictional indentation conditions. The main conclusions and findings of this work are the following:

- The boundary element formulation proves to be a very interesting numerical methodology to analyze these multifield systems with a high accuracy: the indentation results of a transversely isotropic MEE solid (Section 7.1) show an excellent agreement with the analytical solution presented in [3].

- The formulation is versatile, being able to consider conducting, semiconducting and insulated electric and magnetic indentation conditions, as well as orthotropic frictional indentation conditions.

- Numerical results reveal that the conductivity parameters (i.e. κ_e^* and κ_m^*) and the coupling between the elastic, electric and magnetic fields have a significant effect on the indentation force and the contact pressure. So normal contact compliance can be modified by the conductivity boundary conditions.

- The influence of friction in electric and magnetic potential response has been proved to be also very significant (i.e. an increment of 65% in the maximum electric potential can be observed for a half space indentation under high value of friction coefficient). This increment is a consequence of the stress state increment inside the bulk due to the frictional tangential contact tractions presence.

- Tangential loads have also an important influence not only in the values of the electric and magnetic potential but also on their distributions and the maximum of electric and magnetic potential values.

So all these aspect should be considered in coupled multifield contact modelling. In other case, we could over- or underestimate MEE contact magnitudes and its distribution over the contact zone, as it was shown in the numerical examples.

Finally, it is important to mention that the proposed BEM formulation can be extended to consider thermal field coupling in this multifield coupling and contact problems. Work in this direction is under way.

9. Acknowledgments

This work is supported by the *Ministerio de Ciencia e Innovación* (Spain) through the research project DPI2013-43267-P.

A. Barnett-Lothe representation

As proposed by Barnett & Lothe [31] for PE materials, the linear MEE problem may be formulated in an elastic-like fashion by considering a generalized displacement vector extended with the electric potential and the magnetic potential as

$$u_J = \begin{cases} u_j & J \leqslant 3 \\ \varphi & J = 4 \\ \psi & J = 5, \end{cases} \tag{37}$$

a traction vector extended with normal electric charge flux and normal magnetic flux

$$t_J = \begin{cases} t_j & J \leqslant 3 \\ q & J = 4 \\ s & J = 5, \end{cases} \tag{38}$$

a stress tensor extended with the electric displacements and the magnetic inductions as

$$\sigma_{iJ} = \begin{cases} \sigma_{ij} & J \leqslant 3 \\ D_i & J = 4 \\ B_i & J = 5, \end{cases} \tag{39}$$

and an extended elasticity tensor with the following components

$$C_{iJKm} = \begin{cases} c_{ijkm} & J, K \leqslant 3 \\ e_{mij} & J \leqslant 3;\ K = 4 \\ e_{ikm} & J = 4;\ K \leqslant 3 \\ q_{mij} & J \leqslant 3;\ K = 5 \\ q_{ikm} & J = 5;\ K \leqslant 3 \\ -\lambda_{im} & J = 4;\ K = 5 \text{ or } J = 5;\ K = 4 \\ -\epsilon_{im} & J, K = 4 \\ -\mu_{im} & J, K = 5. \end{cases} \tag{40}$$

By virtue of symmetries (8), $C_{iJKm} = C_{mKJi}$ is satisfied. In the above definitions the lower-case (elastic) and upper-case (extended) sub-indices take values 1, 2, 3 and 1, 2, 3 (elastic), 4 (electric), 5 (magnetic), respectively. Then, with the introduced representation the constitutive equations (5), (6) and (7) can be rewritten together as

$$\sigma_{iJ} = C_{iJKm} u_{K,m}. \tag{41}$$

B. Fundamental solutions

The explicit fundamental solutions proposed by Buroni & Sáez [32] are briefly described in this appendix. In homogeneous media they depend on the relative vector $\mathbf{x} - \mathbf{x}'$, henceforth, for simplicity, it is considered that the Cartesian coordinate system (x_i) $(i = 1, 2, 3)$ has the origin at the collocation point $\mathbf{x}'$.

Extended displacement fundamental solution can be expressed as a singular term by a modulation function $\mathbf{H}$ as

$$\check{U}_{JK}(\mathbf{x}) = \frac{1}{4\pi r} H_{JK}(\mathbf{x}) \tag{42}$$

where $\mathbf{x} = r\hat{\mathbf{e}}$ with $r = |\mathbf{x}| \neq 0$. The symmetric modulation function $H_{JK}(\mathbf{x})$ depends on the direction of $\mathbf{x}$ but not on its modulus, so $H_{JK}(\mathbf{x}) = H_{JK}(\hat{\mathbf{e}})$ and is known as one of the three extended Barnett-Lothe tensors. A general expression of the extended Barnett-Lothe tensor H_{JK} is obtained as [32]

$$H_{JK}(\hat{\mathbf{e}}) = \frac{2\mathrm{i}}{|\mathbf{T}|} \sum_{\alpha=1}^{N} \frac{1}{(m_\alpha - 1)!} \times \left[\frac{d^{m_\alpha - 1}}{dp^{m_\alpha - 1}} \left\{ \frac{\hat{\Gamma}_{JK}(p)}{(p - \bar{p}_\alpha)^{m_\alpha} \prod_{\substack{\xi=1 \\ \xi \neq \alpha}}^{N} [(p - p_\xi)(p - \bar{p}_\xi)]^{m_\xi}} \right\} \right]_{at\ p = p_\alpha} . \tag{43}$$

In equation (43), $\mathrm{i} = \sqrt{-1}$. $\hat{\Gamma}_{JK}$ is the adjoint of Γ_{JK} defined as $\Gamma_{PJ}(p)\hat{\Gamma}_{JK}(p) = |\mathbf{\Gamma}(p)|\delta_{PK}$ where δ_{PK} is the extended Kronecker delta and

$$\Gamma_{JK}(p) = Q_{JK} + (R_{JK} + R_{KJ})p + T_{JK}p^2, \tag{44}$$

being

$$Q_{JK} = C_{iJKm} n_i n_m, \quad R_{JK} = C_{iJKm} n_i m_m, \quad T_{JK} = C_{iJKm} m_i m_m, \tag{45}$$

where n_i and m_i are the components of any two mutually orthogonal unit vectors such that $(\mathbf{n}, \mathbf{m}, \hat{\mathbf{e}})$ is a right-handed triad. The determinant of $\mathbf{T}$ can be computed from equation (45). In the Stroh formalism context, p_ξ are known as the Stroh's eigenvalues and corresponds to the five roots of the tenth-order polynomial characteristic equation

$$|\mathbf{\Gamma}(p)| = 0 \tag{46}$$

with positive imaginary part. The bar over p_ξ denotes its complex conjugate. At most, there are N $(1 \leqq N \leqq 5)$ distinct Stroh's eigenvalues p_α of m_α-multiplicity.

The extended traction fundamental solution follows from the derivative of the extended displacement fundamental solution as

$$\check{T}_{JK} = C_{iJMl} \check{U}_{MK,l} \nu_i \tag{47}$$

where ν_i are the components of the external unit normal vector to the boundary $\partial\Omega$ at point $\mathbf{x}$. In similar way to equation (42), the derivative of the displacement fundamental solution may be expressed as

$$\check{U}_{PJ,q}(\mathbf{x}) = \frac{1}{4\pi r^2} \tilde{U}_{PJq}(\hat{\mathbf{e}}) \tag{48}$$

where the modulation function is

$$\tilde{U}_{PJq}(\hat{\mathbf{e}}) = -\hat{e}_q H_{PJ} + \frac{C_{rKMs}}{\pi} \left(M_{qsPKMJ} \hat{e}_r + M_{qrPKMJ} \hat{e}_s \right), \tag{49}$$

that only depends on the orientation of $\mathbf{x}$ $(\hat{\mathbf{e}})$ but not on its modulus r. The M_{ijPKMN} components have the following general expression [32]

$$M_{ijPKMN}(\hat{\mathbf{e}}) = \frac{2\pi \mathrm{i}}{|\mathbf{T}|^2} \sum_{\alpha=1}^{N} \frac{1}{(2m_\alpha - 1)!} \left[\frac{d^{2m_\alpha - 1}}{dp^{2m_\alpha - 1}} \{ \frac{\Phi_{ijPKMN}(p)}{\prod_{\substack{\xi=1 \\ \xi \neq \alpha}}^{N} [(p - p_\xi)]^{2m_\xi}} \} \right]_{at\ p = p_\alpha} \tag{50}$$

where the function

$$\Phi_{ijPKMN}(p) := \frac{\tilde{B}_{ij}(p)\hat{\Gamma}_{PK}(p)\hat{\Gamma}_{MN}(p)}{(p-\bar{p}_1)^2(p-\bar{p}_2)^2(p-\bar{p}_3)^2(p-\bar{p}_4)^2(p-\bar{p}_5)^2} \tag{51}$$

has been introduced together with definition

$$\tilde{B}_{ij} := n_i n_j + (n_i m_j + m_i n_j)p + m_i m_j p^2. \tag{52}$$

It can be shown that the components M_{qsPKMJ} satisfy the following symmetry conditions [32]

$$M_{qsPKMJ} = M_{qsMJPK} = M_{qsKPMJ} = M_{qsPKJM}, \tag{53}$$

$$M_{qsPKMJ} = M_{sqPKMJ}. \tag{54}$$

These symmetries allow considerable reduction in the number of components M_{qsPKMJ} to be calculated, and must be considered in the numerical implementation.

It is important to note that this scheme for the evaluation of fundamental solutions is general and valid for any kind of mathematical degeneracy, that is, when there exist repeated Stroh's eigenvalues of any multiplicity.

References

[1] Ce-Wen Nan, M. I. Bichurin, Shuxiang Dong, D. Viehland, and G. Srinivasan, Multiferroic magnetoelectric composites: Historical perspective, status, and future directions, J. Appl. Phys., 103 (2008) 031101

[2] P.F. Hou, A.Y.T. Leung and H. Ding, The elliptical Hertzian contact of transversely isotropic magnetoelectroelastic bodies, Int. J. Solids Struct., 40 (11) (2003) 2833–2850

[3] W. Chen, E. Pan, H. Wang and Ch. Zhang, Theory of indentation on multiferroic composite materials, J. Mech. Phys. Solids, 58 (2010) 1524–1551

[4] V.I. Fabrikant, Applications of Potential Theory in Mechanics: a Selection of New Results, Kluwer Academic Publishers, The Netherlands (1989)

[5] Zhou, Y.T. and Lee, K.Y, Contact problem for magneto-electro-elastic half-plane materials indented by a moving punch. Part I: Closed-form solutions, Int. J. Solids Struct., 49 (2012) 3853–3865

[6] Y.T. Zhou and T.W. Kim, Multi-field Response of Anisotropic Magneto-Electro-Elastic Materials at a Rigid Conducting Cylinder, J. Elast., 117 (2014) 63–94

[7] R. Elloumi, M.A. Guler, I. Kallel-Kamoun and S. El-Borgi, Closed-form solutions of the frictional sliding contact problem for a magneto-electro-elastic half-plane indented by a rigid conducting punch, Int. J. Solids Struct., 50 (2013) 3778–3792

[8] Y.T. Zhou and K.Y Lee, Theory of sliding contact for multiferroic materials indented by a rigid punch, Int. J. Mech. Sci., 66 (2013) 156–167

[9] R. Elloumi, I. Kallel-Kamoun, S. El-Borgi and M.A. Guler, On the frictional sliding contact problem between a rigid circular conducting punch and a magneto-electro-elastic half-plane, Int. J. Mech. Sci., 87 (2014) 1–17

[10] Y.T. Zhou and T.W. Kim, An exact analysis of sliding frictional contact of a rigid punch over the surface of magneto-electro-elastic materials, Acta Mech., 225 (2014) 625–645

[11] Y.T. Zhou and Z. Zhong, Frictional Indentation of Anisotropic Magneto-Electro-Elastic Materials by a Rigid Indenter, J. Appl. Mechanics, 81 (2014) 071001–1

[12] J. Ma, L.L. Ke and Y. S. Wang, Sliding Frictional Contact of Functionally Graded Magneto-Electro-Elastic Materials Under a Conducting Flat Punch, J. Appl. Mechanics, 82 (2015) 011009–1

[13] H.J. Ding, B. Chen and J. Liang, General solutions for coupled equations for piezoelectric media, Int. J. Solids Struct., 33 (1996) 2283–2298

[14] H.J. Ding, P.F. Hou and F.L. Guo, Elastic and electric fields for elliptical contact for transversely isotropic piezoelectric bodies, J. Appl. Mech., 66 (1999) 560–562

[15] H.J. Ding, P.F. Hou and F.L. Guo, The elastic and electric fields for three-dimensional contact for transversely isotropic piezoelectric materials, Int. J. Solids Struct., 37 (2000) 3201–3229.

[16] A.E. Giannakopoulos and S. Suresh, Theory of indentation of piezoelectric materials, Acta Mater., 47 (1999) 2153–2164.

[17] L. Rodríguez-Tembleque, F.C. Buroni and A. Sáez, 3D BEM for orthotropic frictional contact of piezoelectric bodies, Comput. Mech., 56 (2015) 491–502.

[18] A.E. Giannakopoulos and A.Z. Parmaklis, The contact problem of a circular rigid punch on piezomagnetic materials, Internat. J. Solids Struct., 44 (2007) 4593–4612

[19] Y.T. Zhou and K.Y. Lee, Exact Two-Dimensional Contact Analysis of Piezomagnetic Materials Indented by a Rigid Sliding Punch, ASME. J. Appl. Mech., 79 (2012) 041011–041011–12

[20] S. Migorski, A. Ochall and M. Sofonea, Variational analysis of fully coupled electro-elastic frictional contact problems, Math. Nachr., 283 (9) (2010) 1314 -1335

[21] S. Hüeber A. Matei and B. Wohlmuth, A contact problem for electro-elastic materials, ZAMM Z. Angew. Math. Mech., 93 (2013) 789–800

[22] Han, W., Sofonea, M., Kazmi, K., Analysis and numerical solution of a frictionless contact problem for electro-elastic-visco-plastic materials, Comput. Meth. Appl. Mech. Eng., 196 (2007) 3915–3926

[23] Barboteu, M., Fernández, J.R., Ouafik, Y., Numerical analysis of two frictionless elastic-piezoelectric contact problems, J. Math. Anal. Appl., 339 (2008) 905–917

[24] M. Barboteu and M. Sofonea, Solvability of a dynamic contact problem between a piezoelectric body and a conductive foundation, Appl. Math. Comput., 215 (2009) 2978–2991

[25] M. Barboteu and M. Sofonea, Modeling and analysis of the unilateral contact of a piezoelectric body with a conductive support, J. Math. Anal. Appl., 358 (2009) 110–124

[26] M. Sofonea, K. Kazmi, M. Barboteu and W.M. Han, Analysis and numerical solution of a piezoelectric frictional contact problem. Appl. Math. Model., 36 (2012) 4483–4501

[27] N. Kikuchi and J.T. Oden, Contact Problems in Elasticity: A Study of Variational Inequalities and Finite Element Methods, SIAM, Philadelphia, (1988)

[28] P. Alart and A. Curnier, A mixed formulation for frictional contact problems prone to Newton like solution methods, Comput. Meth. Appl. Mech. Eng. 92 (1991) 353–375

[29] L. Rodríguez-Tembleque, R. Abascal and M.H. Aliabadi, Anisotropic wear framework for 3D contact and rolling problems, Comput. Meth. Appl. Mech. Eng., 241 (2012) 1–19.

[30] L. Rodríguez-Tembleque and R. Abascal, Fast FE-BEM algorithms for orthotropic frictional contact, Int. J. Numer. Methods Eng. 94 (2013) 687–707.

[31] D.M. Barnett and J. Lothe, Dislocations and Line Charges in Anisotropic Piezoelectric Insulators, Phys. Stat. Sol., 67 (1975) 105–111.

[32] F.C. Buroni and A. Sáez, Three-dimensional Green's function and its derivative for materials with general anisotropic magneto-electro-elastic coupling, Proc. R. Soc. A 466 (2010) 515–537.

[33] W.W. Chen and Q.J. Wang, A numerical model for the point contact of dissimilar materials considering tangential tractions, Mech. of Mater., 40 (2008) 936–948.

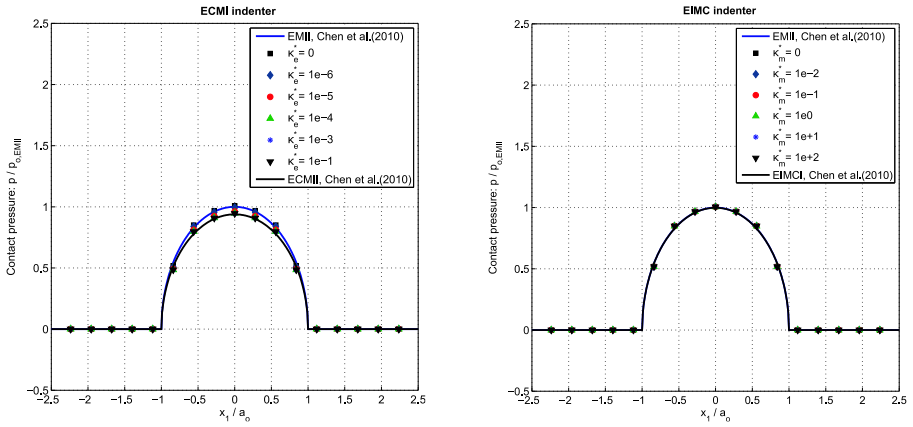

(a)

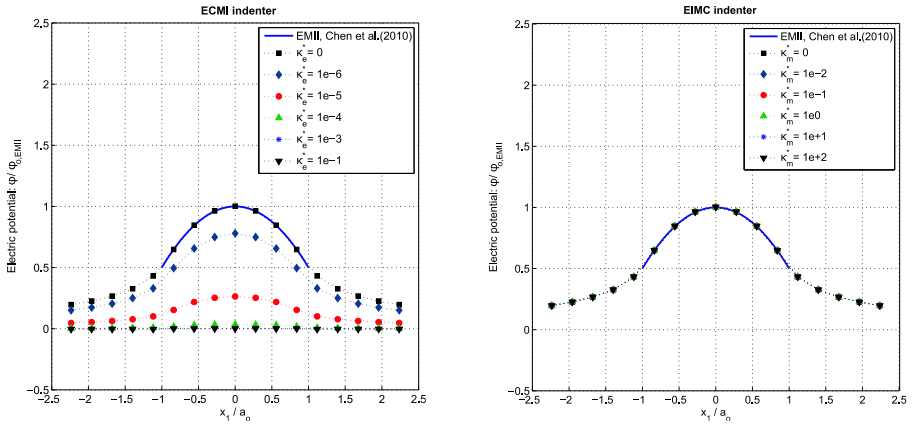

(b)

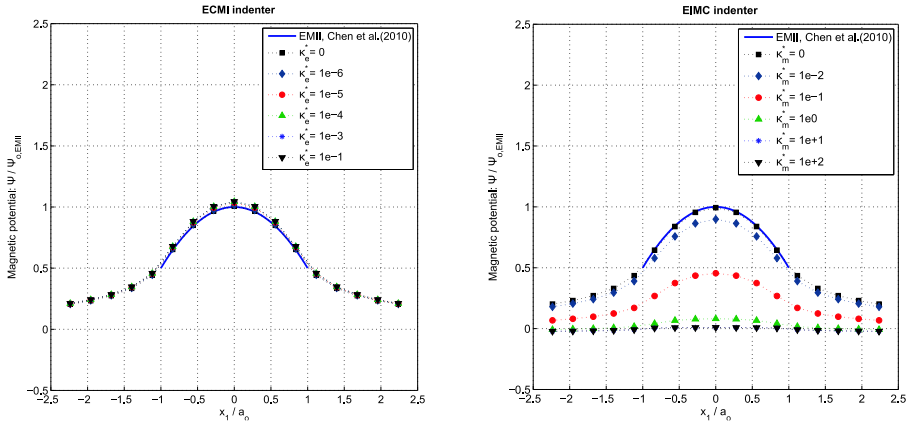

(c)

Figure 4: Normalized indentation response distributions as function of conductivity parameters for ECMII and EIMCI: (a) contact pressure, (b) electric potential and (c) magnetic potential.

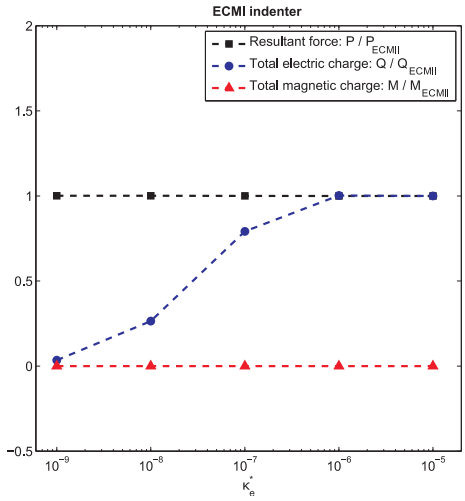

(a)

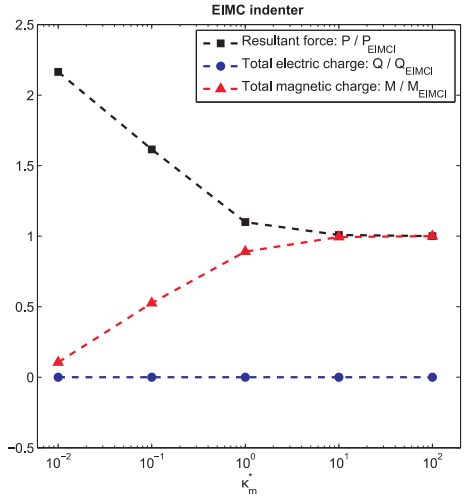

(b)

Figure 5: Influence of conductivity parameters in normalized resultant force, total electric charge and total magnetic charge for: (a) ECMII and (b) EIMCI.

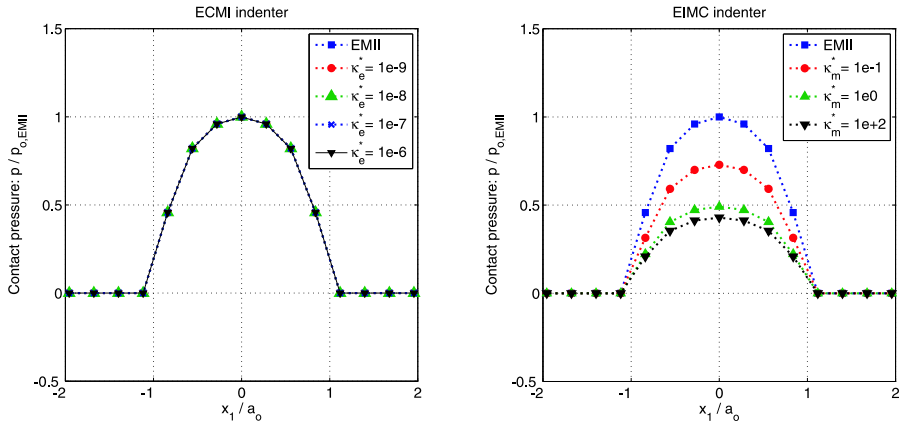

(a)

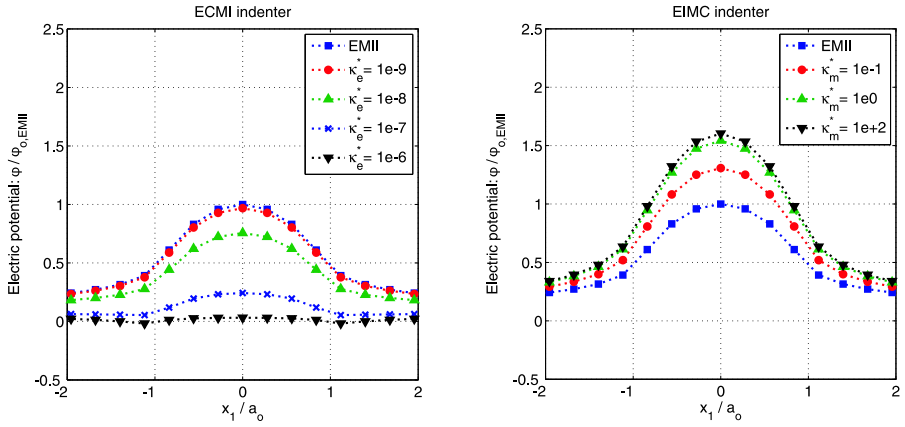

(b)

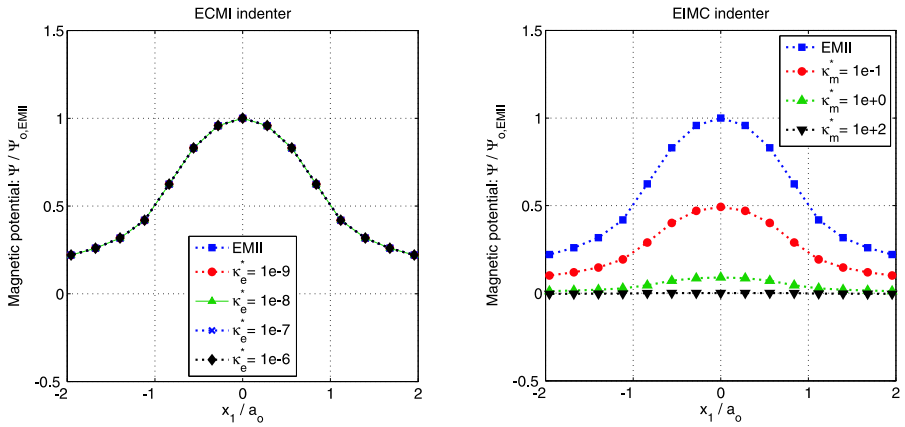

(c)

Figure 6: Normalized indentation response of a fully coupled MEE material as function of conductivity parameters for ECMII and EIMCI: (a) contact pressure, (b) electric potential and (c) magnetic potential.

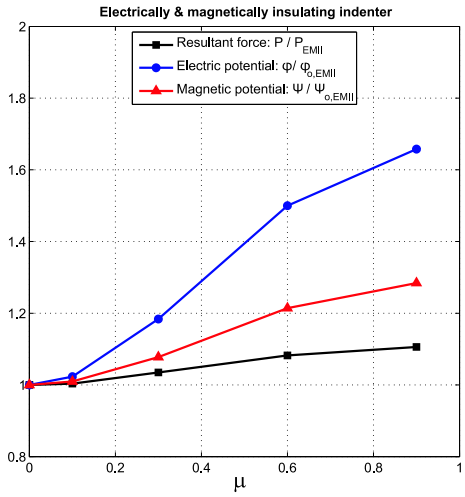

(a)

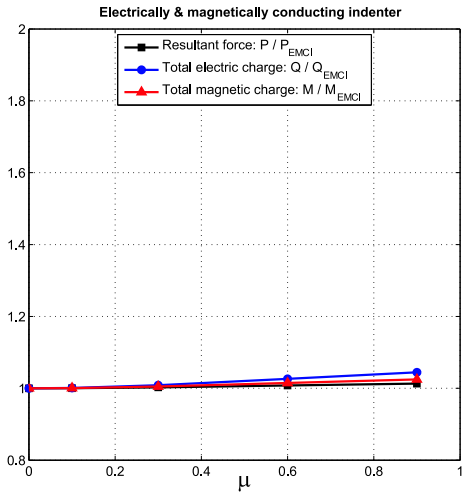

(b)

Figure 7: (a) Influence of friction on the normalized resultant force, maximum electric potential and maximum magnetic potential for a EMII. (b) Influence of friction on the normalized resultant force, total electric charge and total magnetic charge for a EMCI.

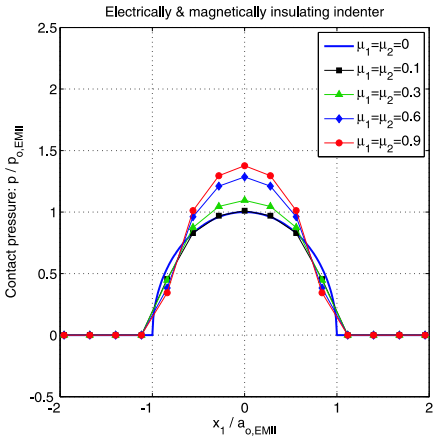

(a)

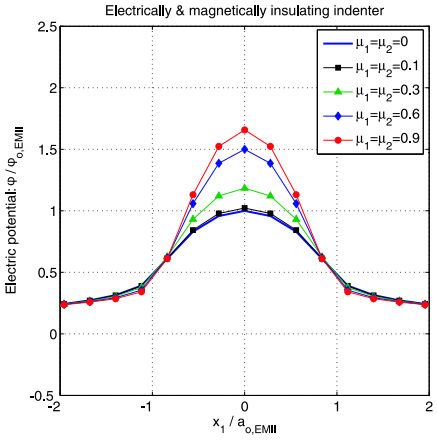

(b)

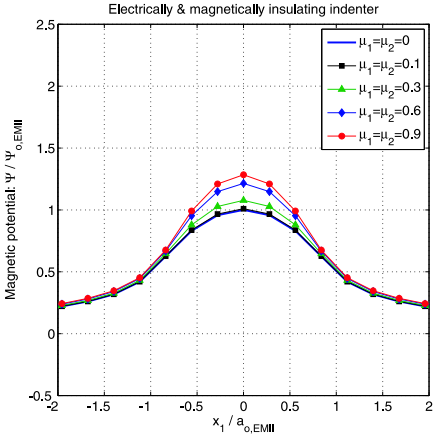

(c)

Figure 8: Influence of friction on the normalized resultant force (a), maximum electric potential (b) and maximum magnetic potential (c) for a EMII.

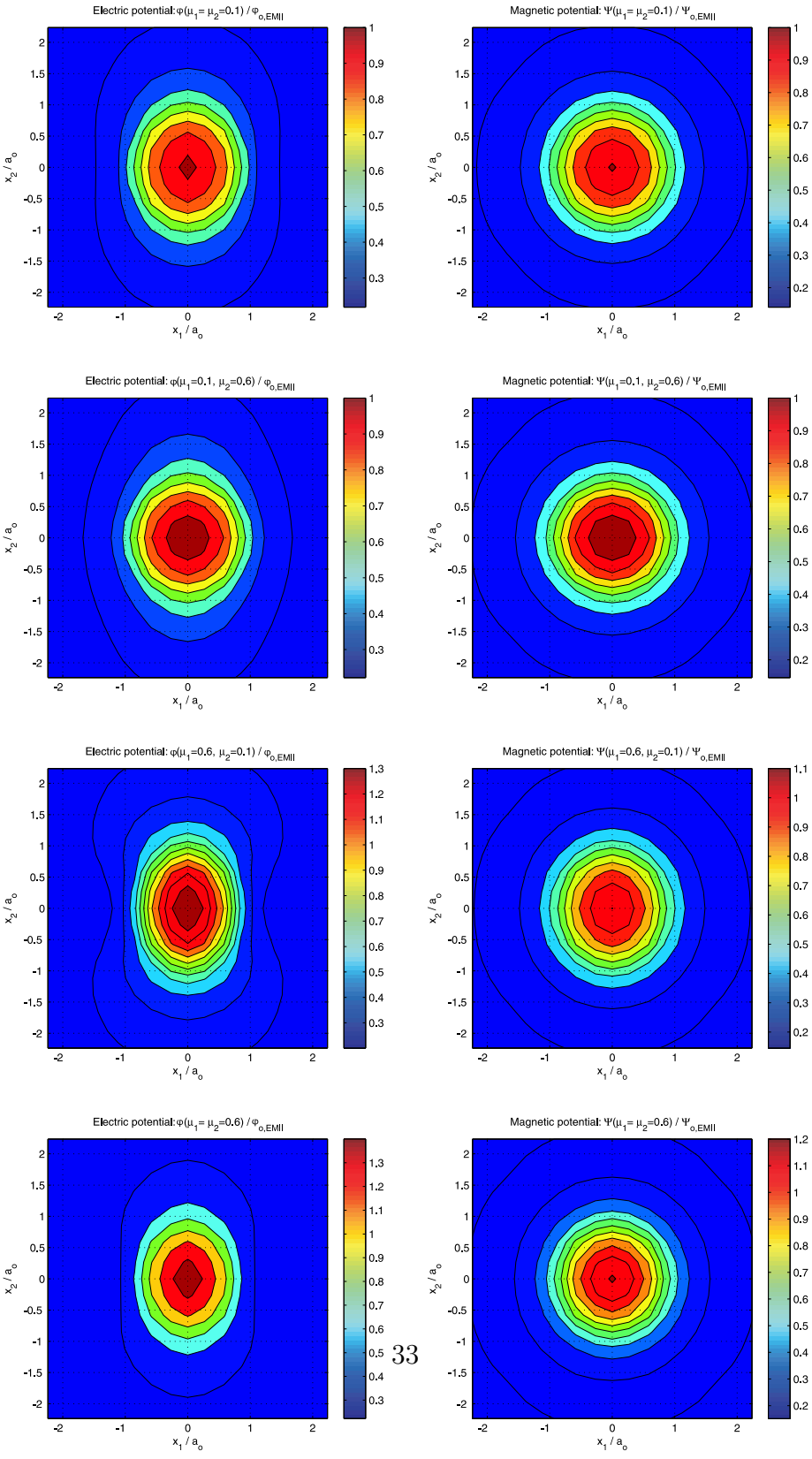

Figure 9: (a) Normalized electric potential distribution. (b) Normalized magnetic potential distribution.

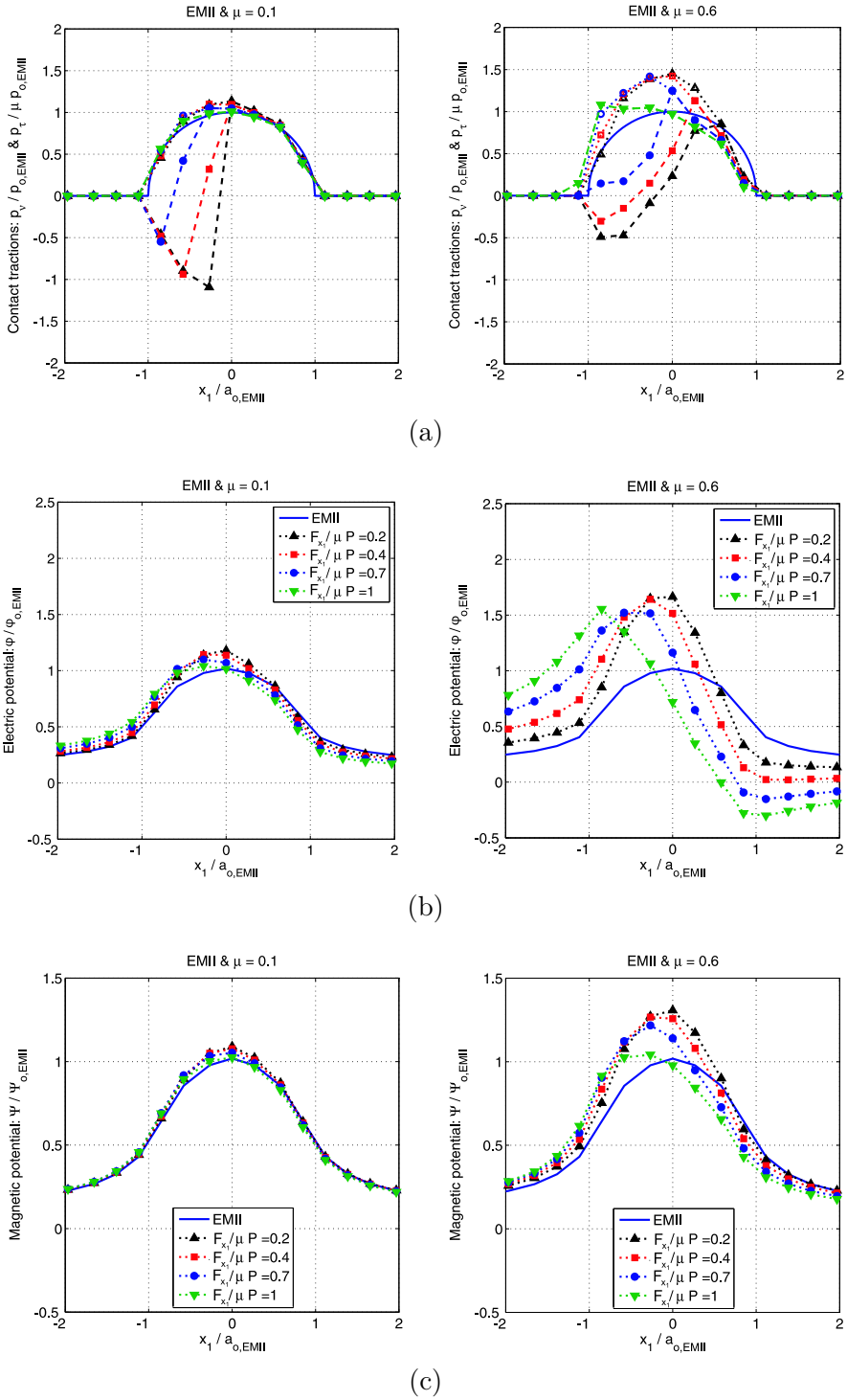

Figure 10: Normalized indentation and tangential load response distributions as function of the friction coefficient for EMII: (a) contact tractions, (b) electric potential and (c) magnetic potential.

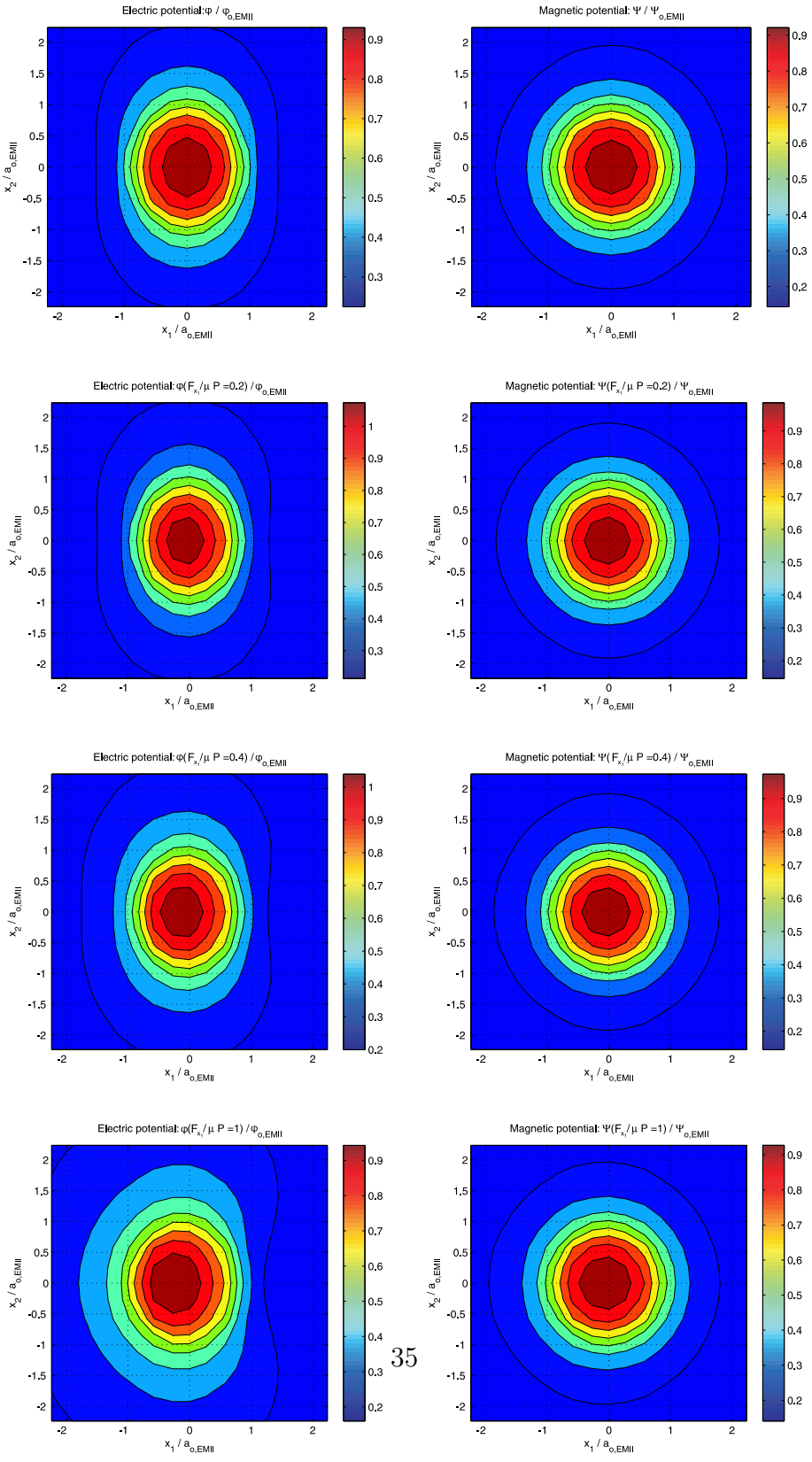

(a) (b)

Figure 11: Normalized electric potential (a) and normalized magnetic potential (b) for EMII under low friction conditions ($\mu = 0.1$).

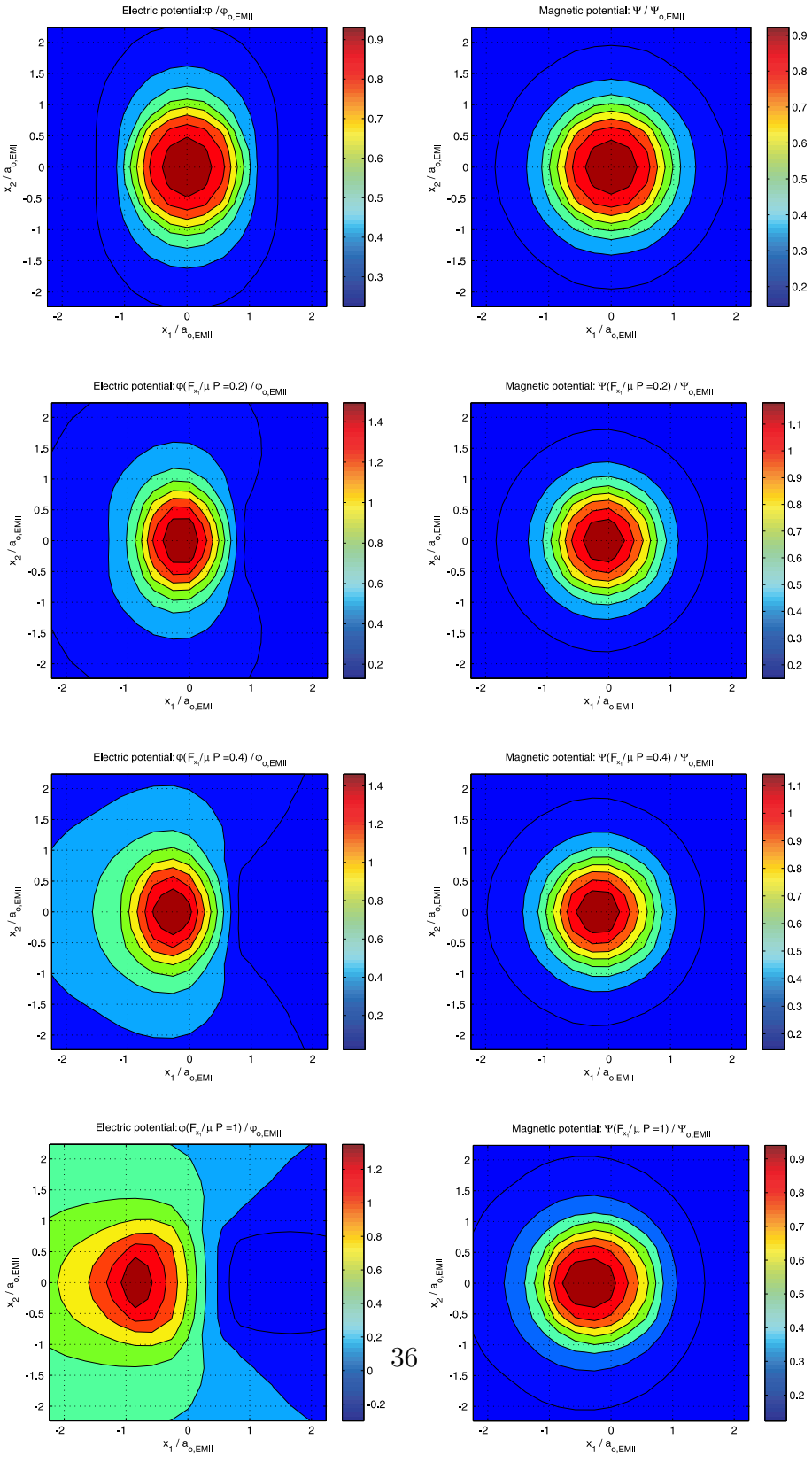

(a) (b)

Figure 12: Normalized electric potential (a) and normalized magnetic potential (b) for EMII under high friction conditions ($\mu = 0.6$).

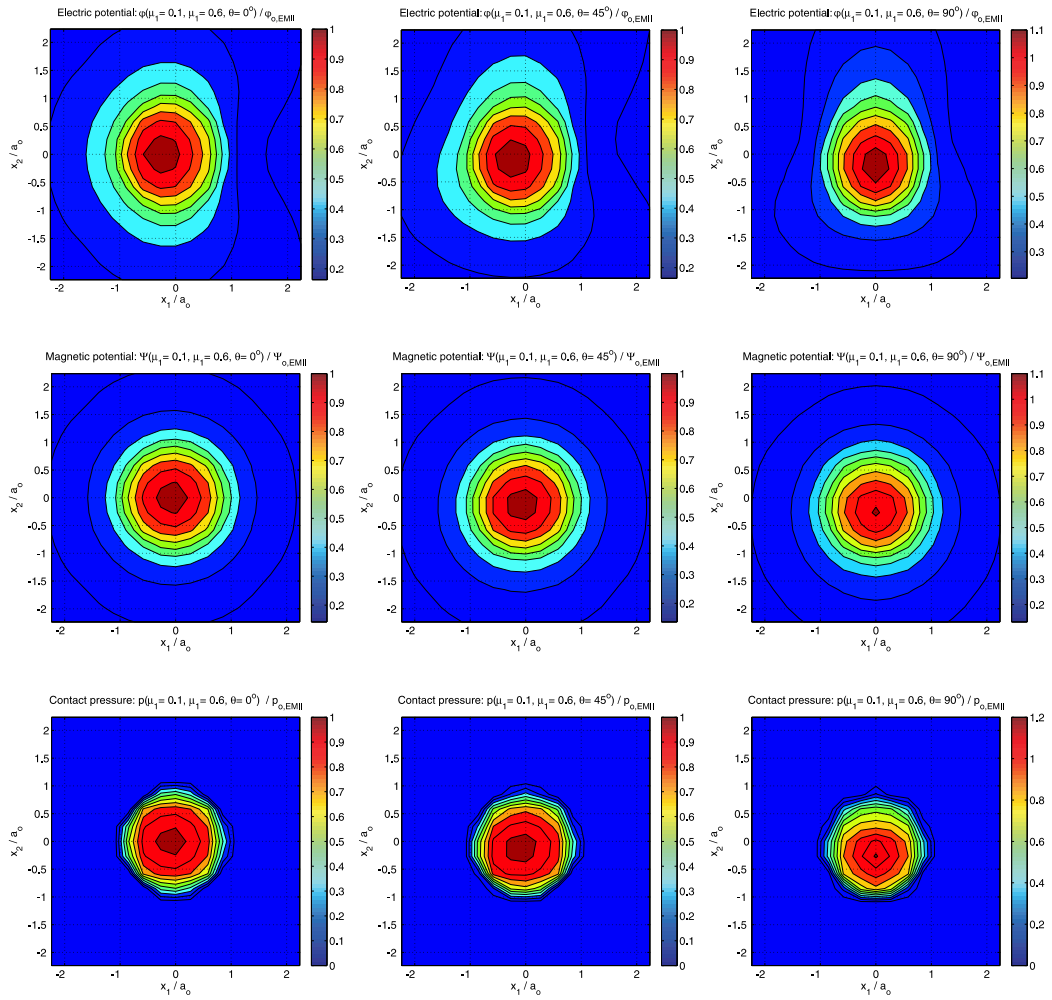

Figure 13: Normalized electric potential distribution (top), normalized magnetic potential distribution (mid) and normalized contact traction distribution (bottom) for: (a) $\theta = 0^o$, (b) $\theta = 45^o$ and (c) $\theta = 90^o$, under orthotropic friction conditions ($\mu_1 = 0.1$ and $\mu_2 = 0.6$).

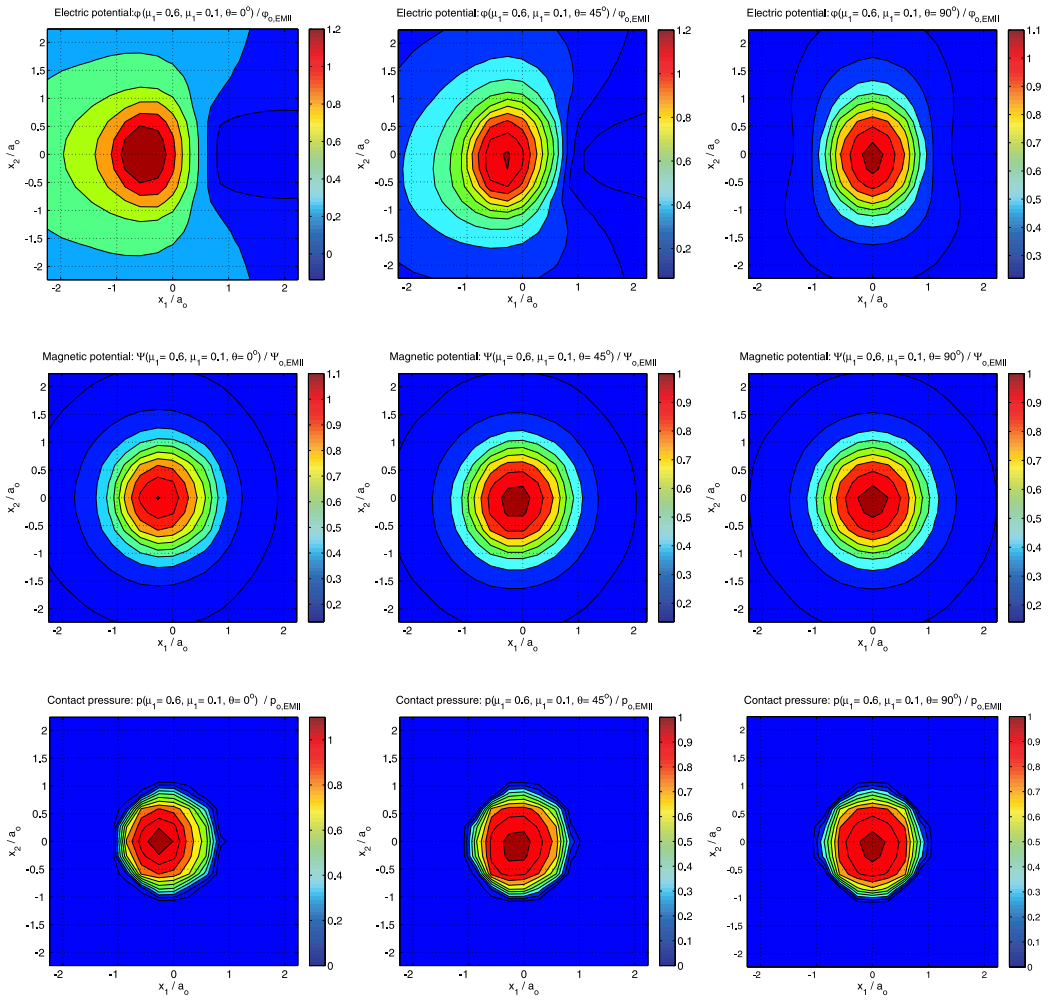

Figure 14: Normalized electric potential distribution (top), normalized magnetic potential distribution (mid) and normalized contact traction distribution (bottom) for: (a) $\theta = 0^o$, (b) $\theta = 45^o$ and (c) $\theta = 90^o$, under orthotropic friction conditions ($\mu_1 = 0.6$ and $\mu_2 = 0.1$).

Figure(s)

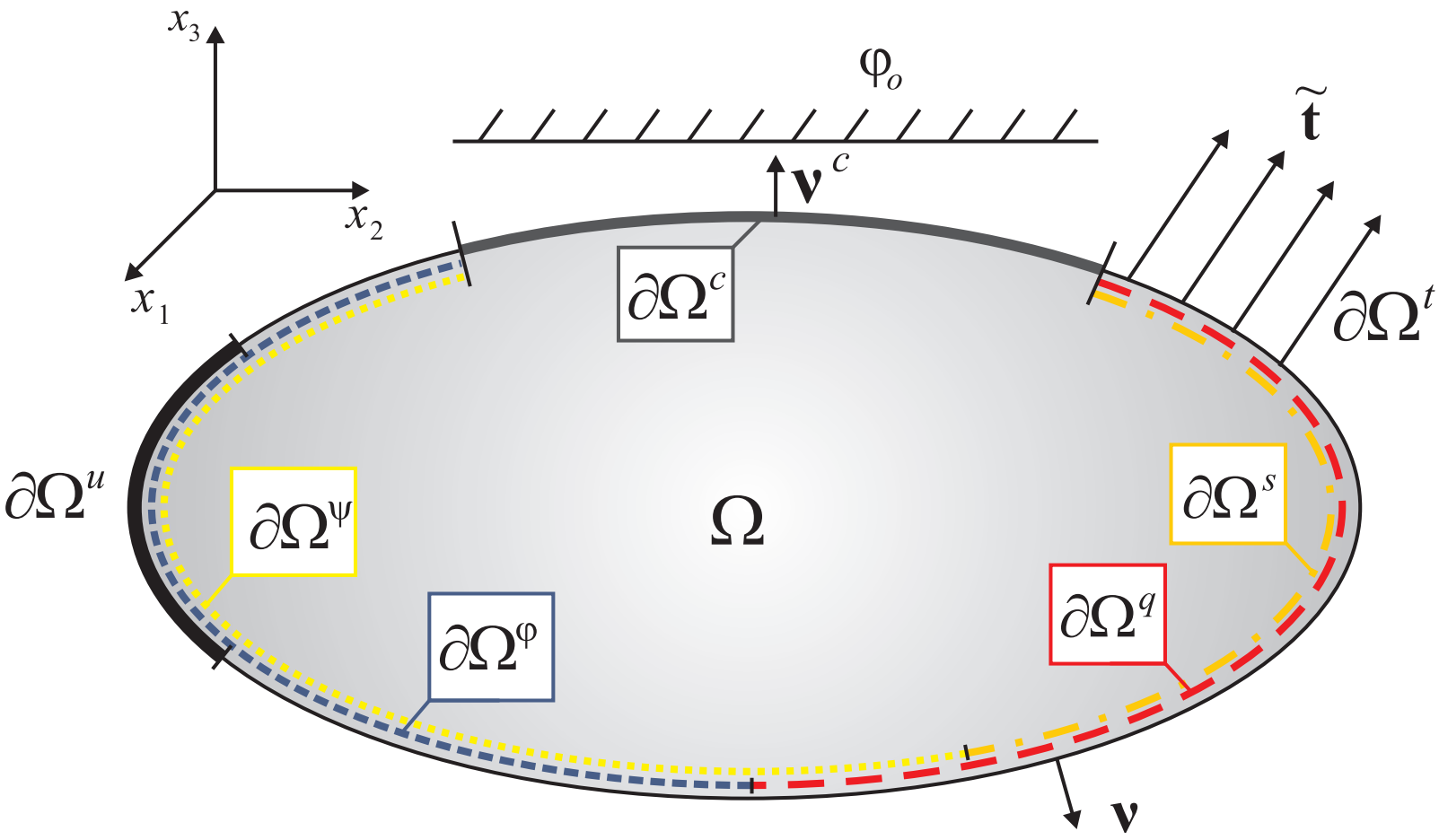
x_3
x_2
x_1
φ_o
$\mathbf{v}^c$
$\tilde{\mathbf{t}}$
$\partial\Omega^c$
$\partial\Omega^t$
$\partial\Omega^u$
$\partial\Omega^\psi$
Ω
$\partial\Omega^s$
$\partial\Omega^q$
$\partial\Omega^\varphi$
$\mathbf{v}$

Figure(s)

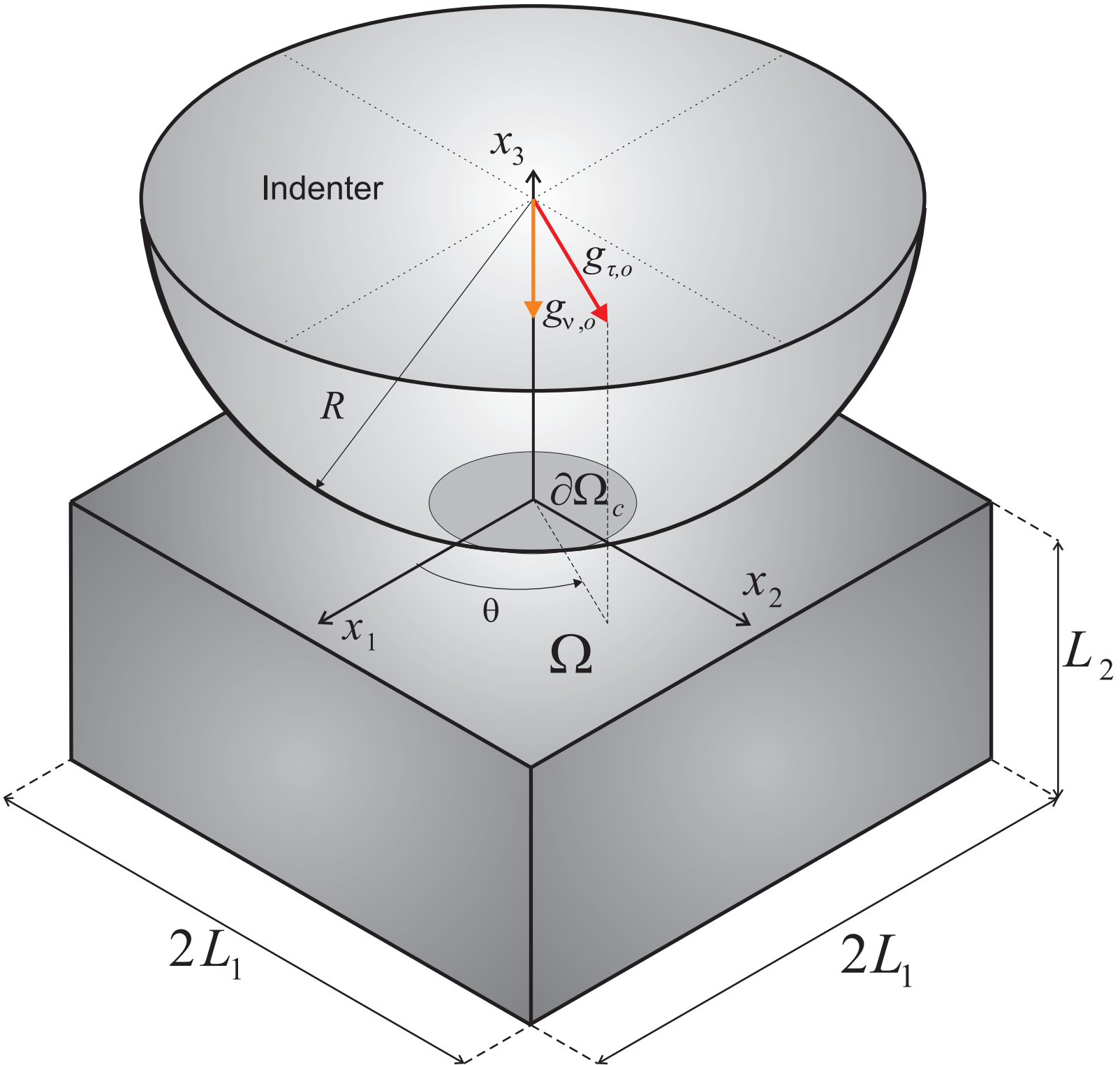
Indenter
x_3
$g_{\tau,o}$
$g_{\nu,o}$
R
$\partial\Omega_c$
x_1
x_2
θ
Ω
L_2
$2L_1$
$2L_1$

Figure(s)

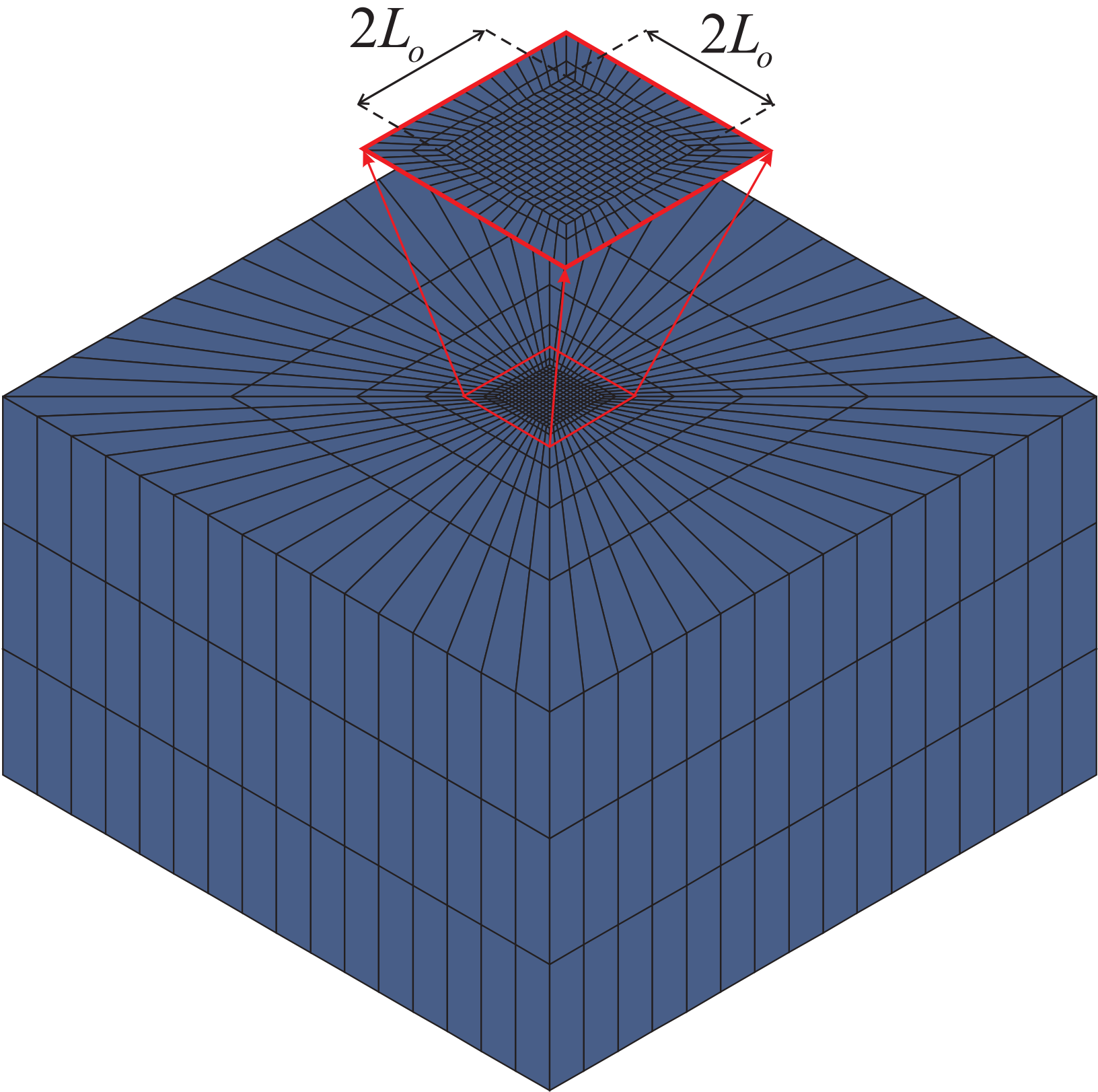

Figure(s)

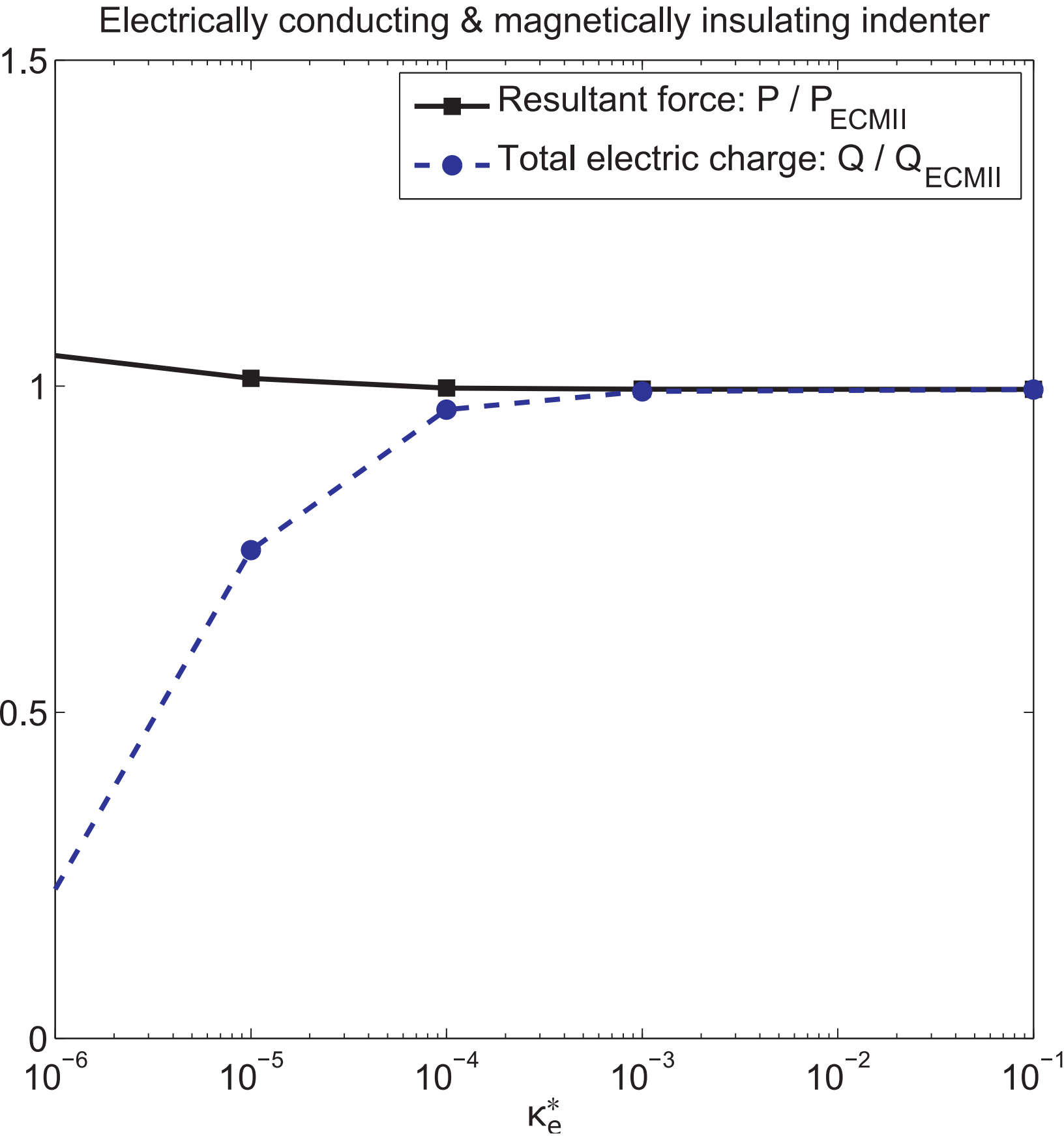
Electrically conducting & magnetically insulating indenter
Resultant force: P / P_ECMII
Total electric charge: Q / Q_ECMII
1.5
1
0.5
0
10^-6
10^-5
10^-4
10^-3
10^-2
10^-1
κ*_e

Figure(s)

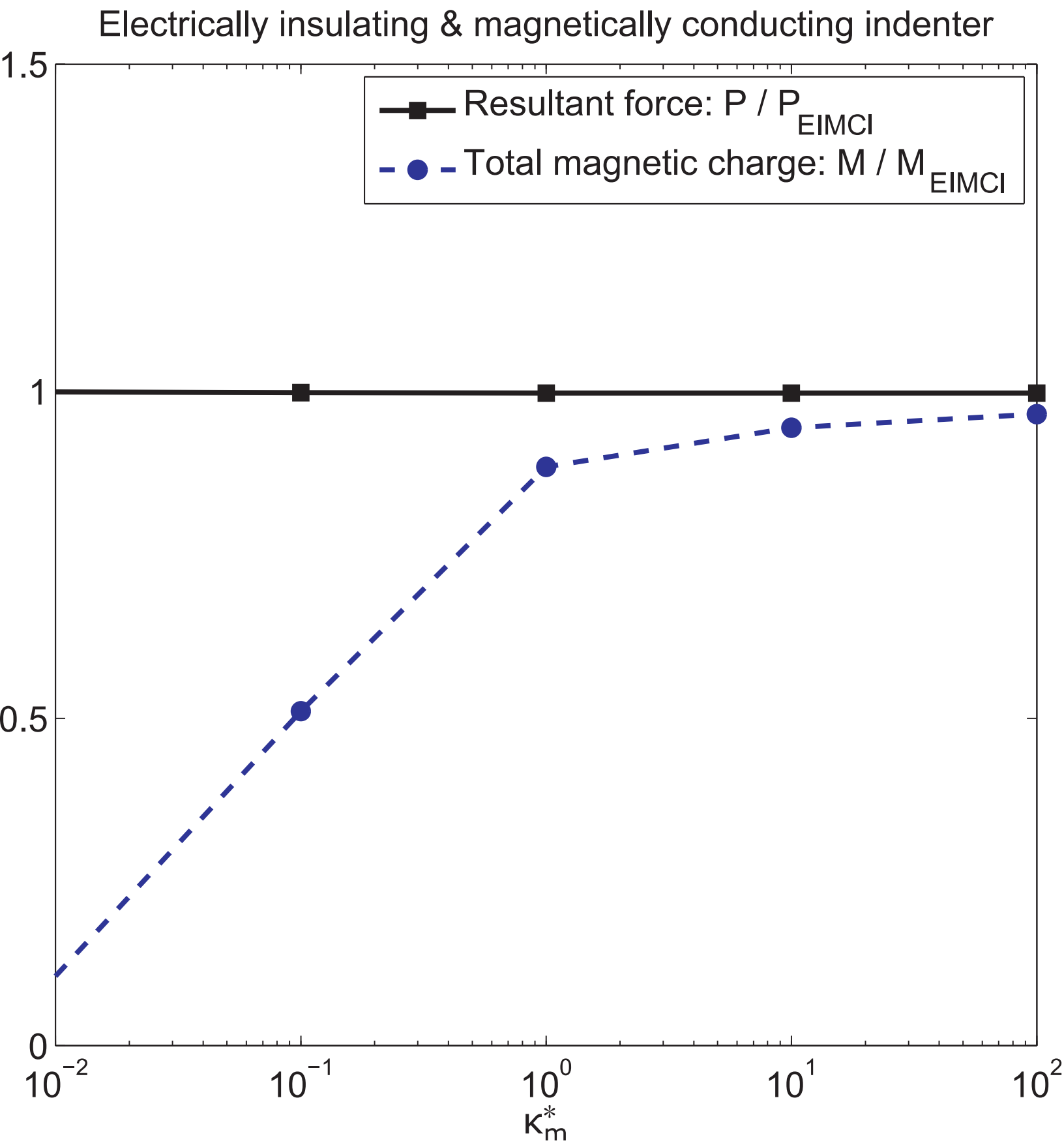
Electrically insulating & magnetically conducting indenter
Resultant force: P / P EIMCI
Total magnetic charge: M / M EIMCI
1.5
1
0.5
0
10^-2
10^-1
10^0
10^1
10^2
K*m

Figure(s)

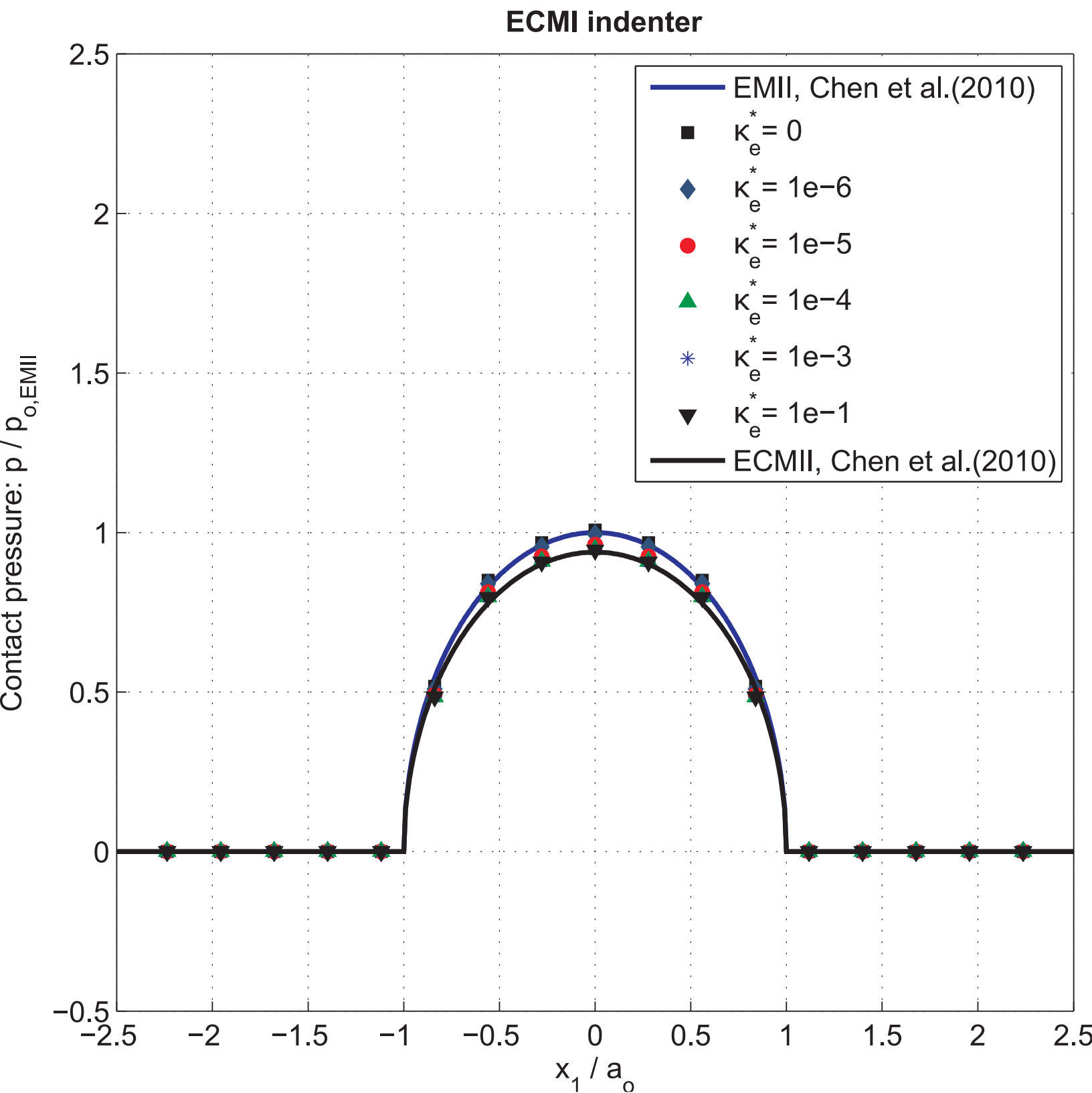
ECMI indenter
EMII, Chen et al.(2010)
κ*e = 0
κ*e = 1e−6
κ*e = 1e−5
κ*e = 1e−4
κ*e = 1e−3
κ*e = 1e−1
ECMII, Chen et al.(2010)
Contact pressure: p / po,EMII
x1 / ao
2.5
2
1.5
1
0.5
0
−0.5
−2.5
−2
−1.5
−1
−0.5
0
0.5
1
1.5
2
2.5

Figure(s)

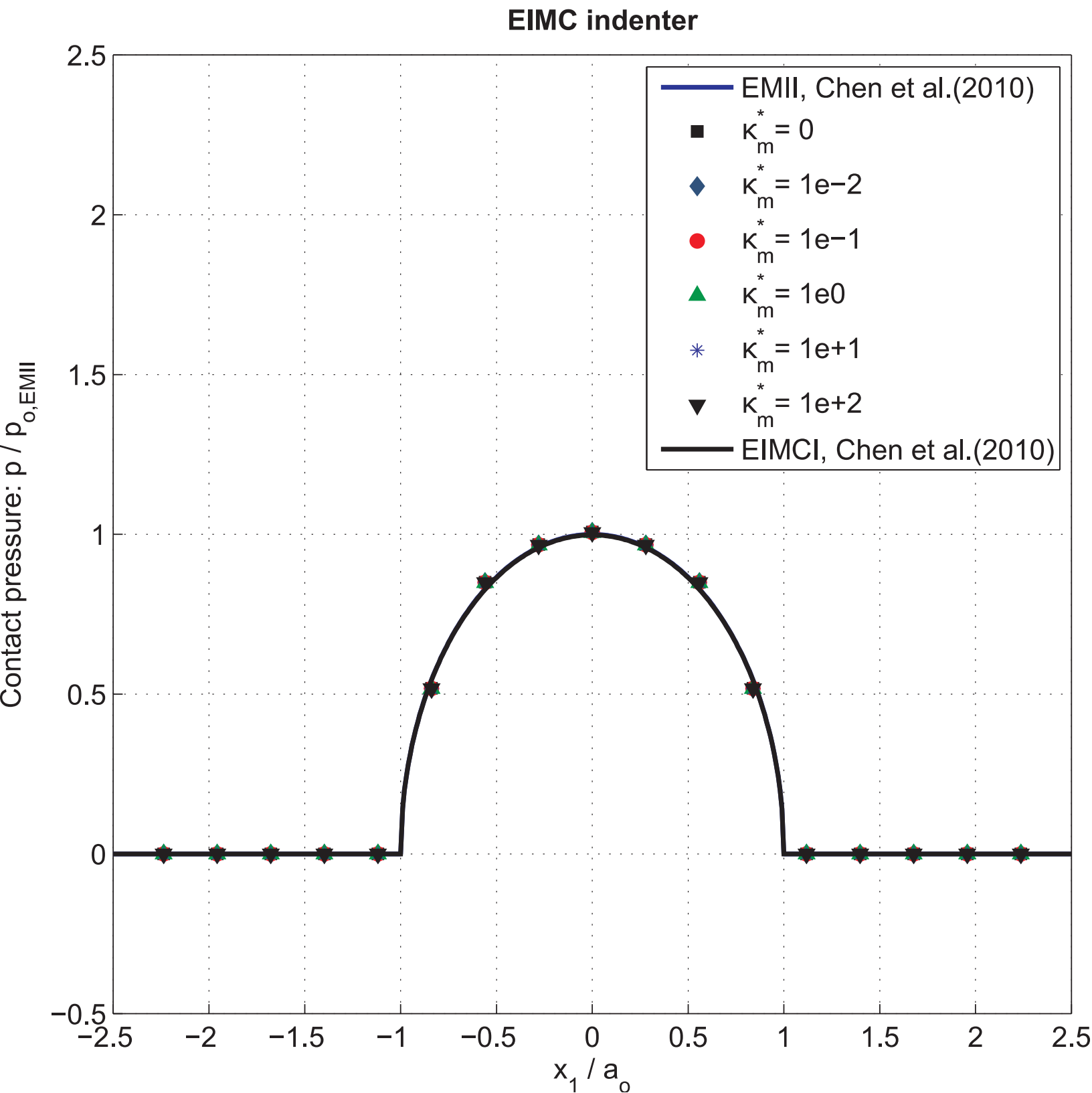
EIMC indenter
EMII, Chen et al.(2010)
κ*m = 0
κ*m = 1e−2
κ*m = 1e−1
κ*m = 1e0
κ*m = 1e+1
κ*m = 1e+2
EIMCI, Chen et al.(2010)
Contact pressure: p / po,EMII
x1 / ao
2.5
2
1.5
1
0.5
0
−0.5
−2.5
−2
−1.5
−1
−0.5
0
0.5
1
1.5
2
2.5

Figure(s)

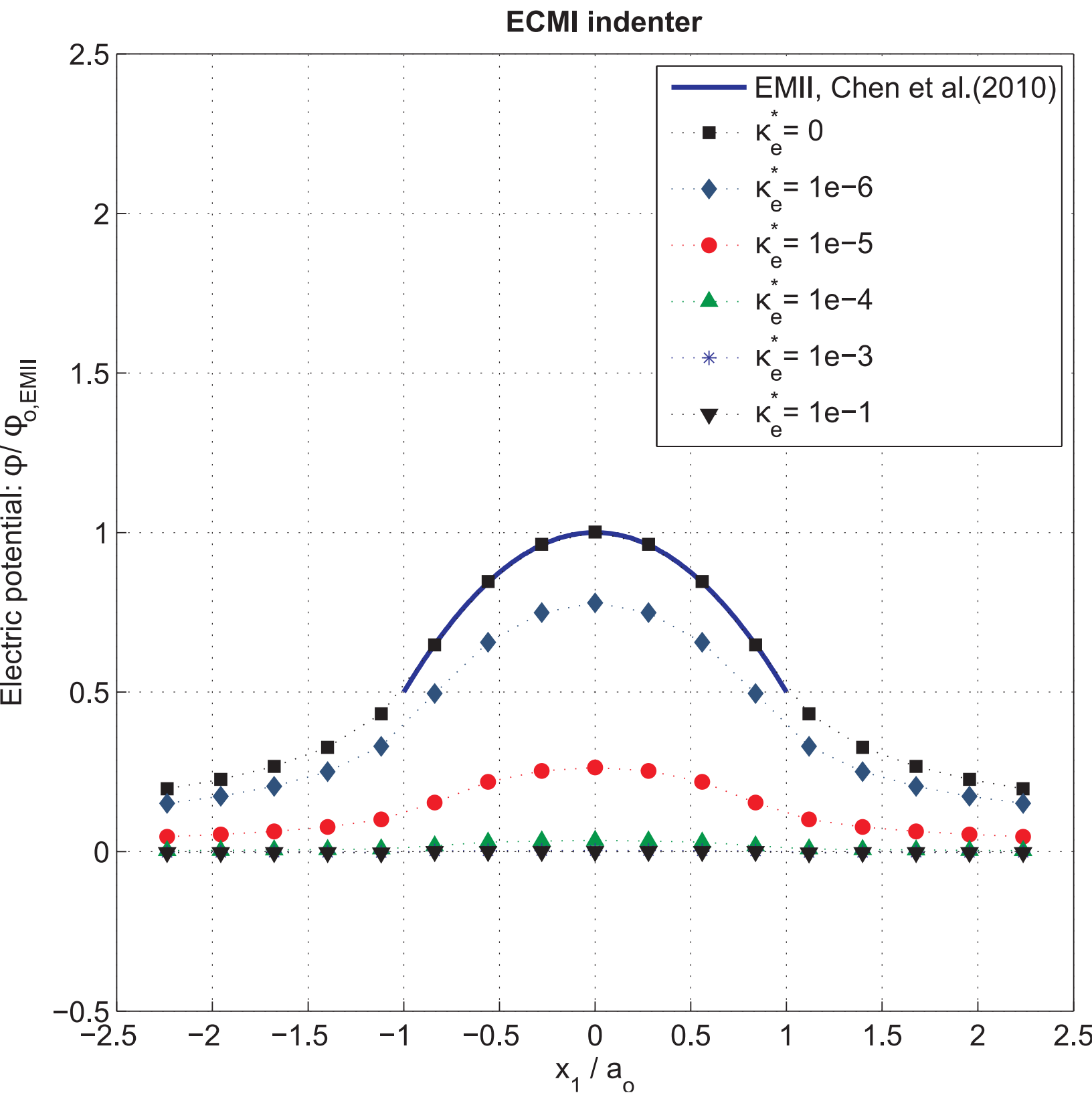
ECMI indenter
EMII, Chen et al.(2010)
κ*e = 0
κ*e = 1e−6
κ*e = 1e−5
κ*e = 1e−4
κ*e = 1e−3
κ*e = 1e−1
Electric potential: Φ/ Φo,EMII
x1 / ao
2.5
2
1.5
1
0.5
0
−0.5
−2.5
−2
−1.5
−1
−0.5
0
0.5
1
1.5
2
2.5

Figure(s)

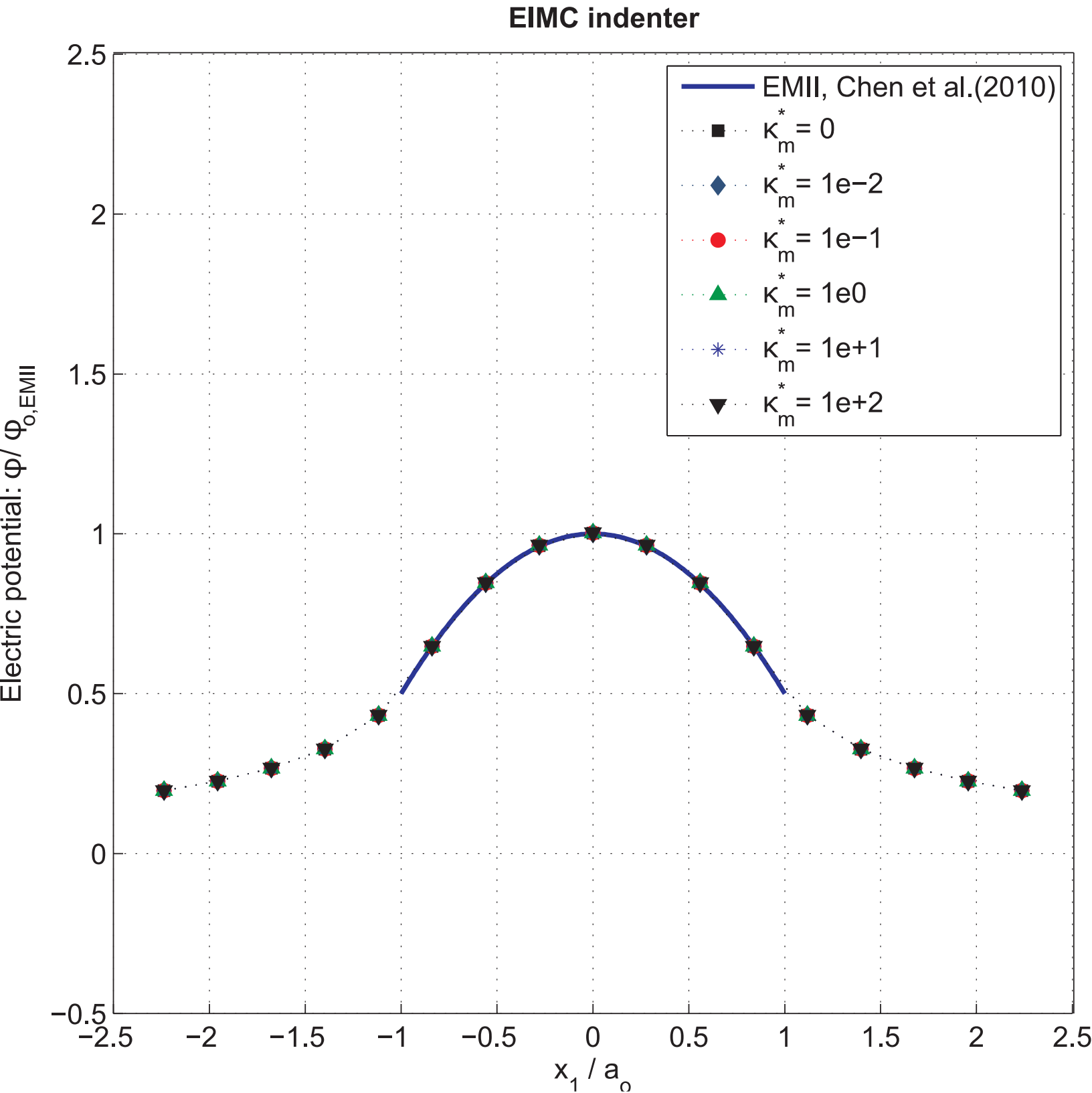
EIMC indenter
EMII, Chen et al.(2010)
κ*m = 0
κ*m = 1e−2
κ*m = 1e−1
κ*m = 1e0
κ*m = 1e+1
κ*m = 1e+2
Electric potential: φ/ φo,EMII
x1 / ao
2.5
2
1.5
1
0.5
0
−0.5
−2.5
−2
−1.5
−1
−0.5
0
0.5
1
1.5
2
2.5

Figure(s)

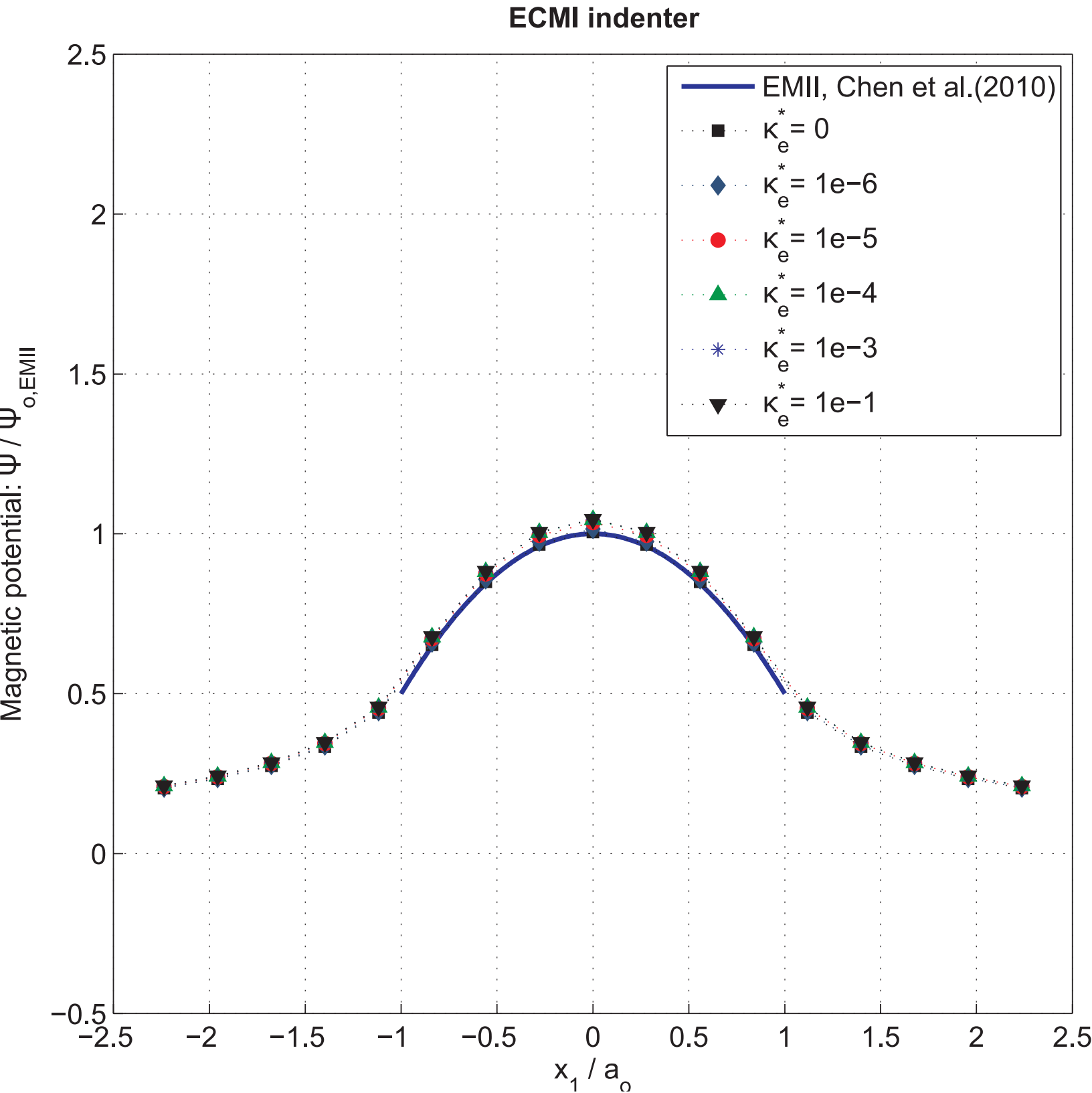
ECMI indenter
EMII, Chen et al.(2010)
κ_e^* = 0
κ_e^* = 1e−6
κ_e^* = 1e−5
κ_e^* = 1e−4
κ_e^* = 1e−3
κ_e^* = 1e−1
Magnetic potential: ψ / $\psi_{o,EMII}$
x_1 / a_o
2.5
2
1.5
1
0.5
0
−0.5
−2.5
−2
−1.5
−1
−0.5
0
0.5
1
1.5
2
2.5

Figure(s)

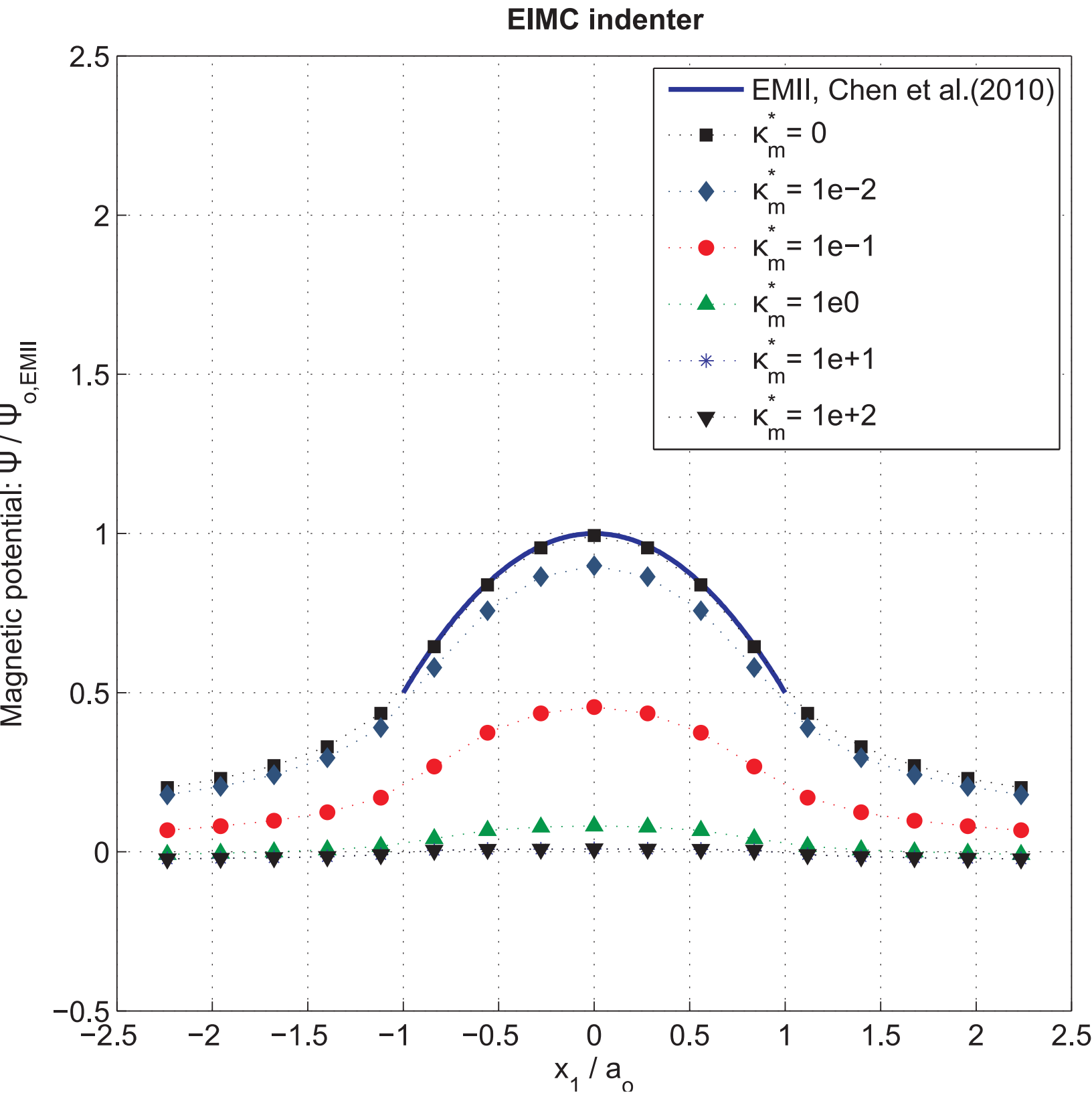
EIMC indenter
EMII, Chen et al.(2010)
$\kappa_m^* = 0$
$\kappa_m^* = 1e{-}2$
$\kappa_m^* = 1e{-}1$
$\kappa_m^* = 1e0$
$\kappa_m^* = 1e{+}1$
$\kappa_m^* = 1e{+}2$
Magnetic potential: $\Psi / \Psi_{o,EMII}$
x_1 / a_o
2.5
2
1.5
1
0.5
0
−0.5
−2.5
−2
−1.5
−1
−0.5
0
0.5
1
1.5
2
2.5

Figure(s)

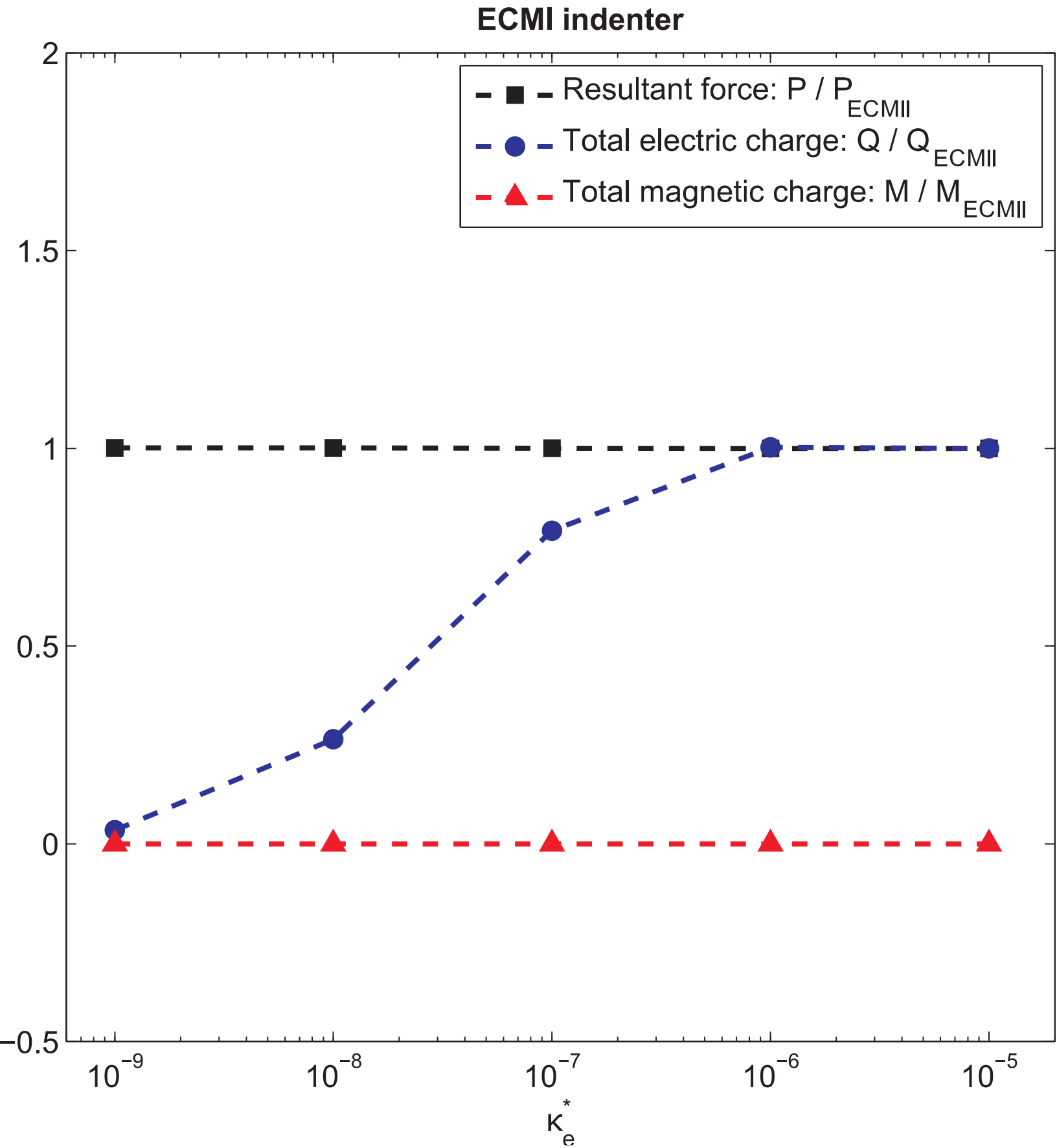
ECMI indenter
Resultant force: P / P_ECMII
Total electric charge: Q / Q_ECMII
Total magnetic charge: M / M_ECMII
2
1.5
1
0.5
0
−0.5
10^−9
10^−8
10^−7
10^−6
10^−5
κ*_e

Figure(s)

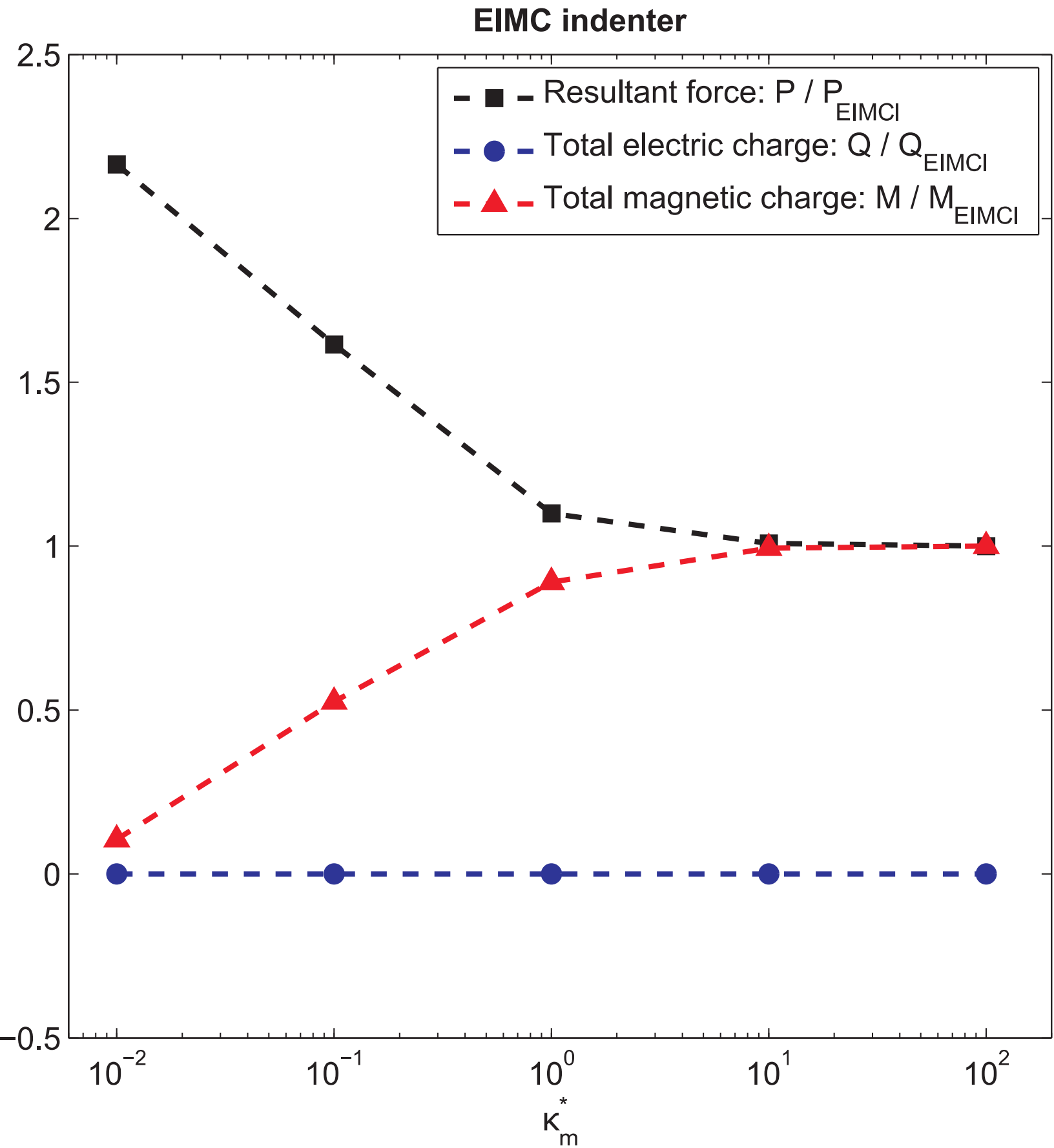
EIMC indenter
Resultant force: P / P_EIMCI
Total electric charge: Q / Q_EIMCI
Total magnetic charge: M / M_EIMCI
2.5
2
1.5
1
0.5
0
−0.5
10^−2
10^−1
10^0
10^1
10^2
K*_m

Figure(s)

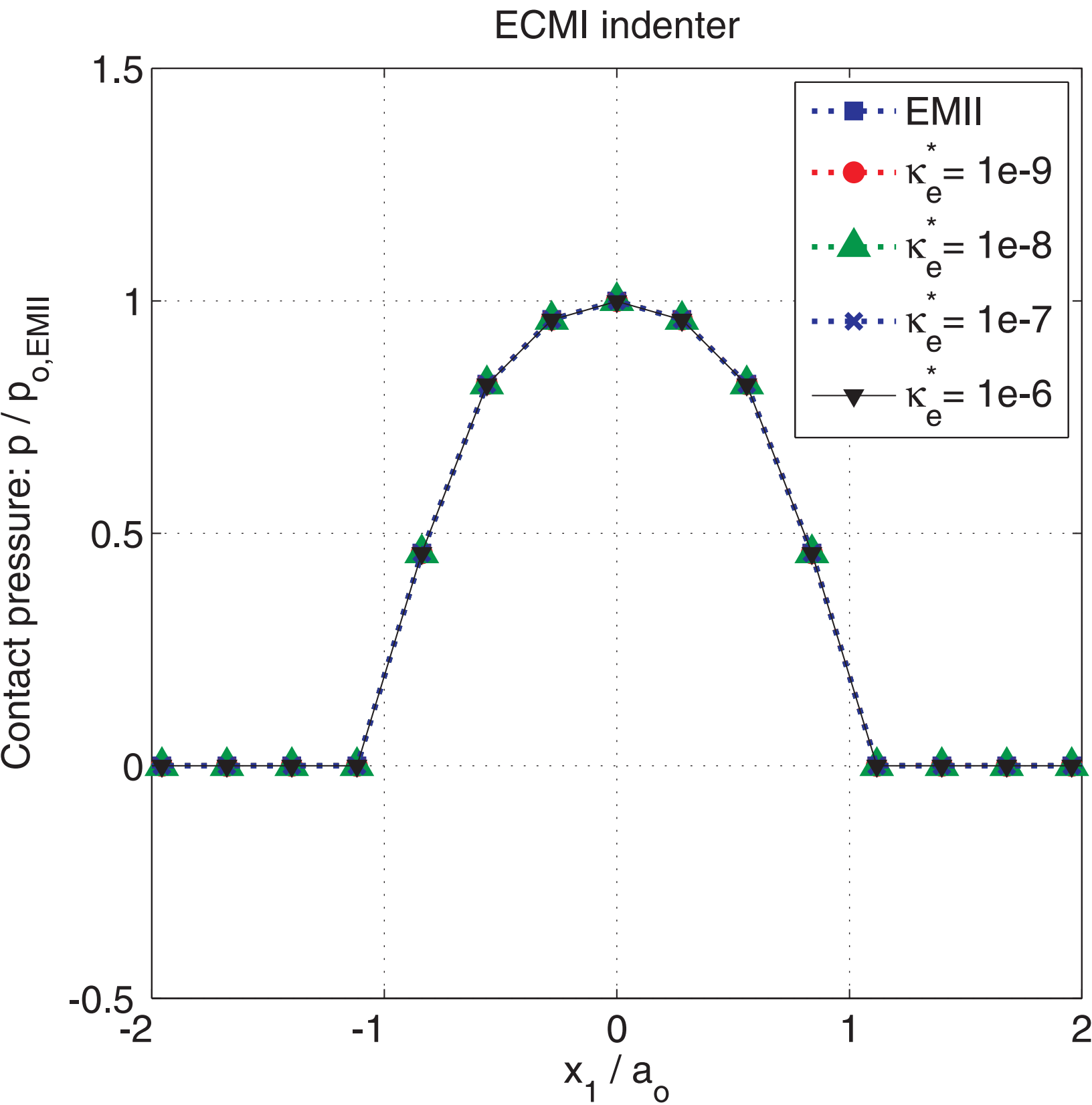
ECMI indenter
EMII
κ_e^*= 1e-9
κ_e^*= 1e-8
κ_e^*= 1e-7
κ_e^*= 1e-6
Contact pressure: p / $p_{o,EMII}$
x_1 / a_o
1.5
1
0.5
0
-0.5
-2
-1
0
1
2

Figure(s)

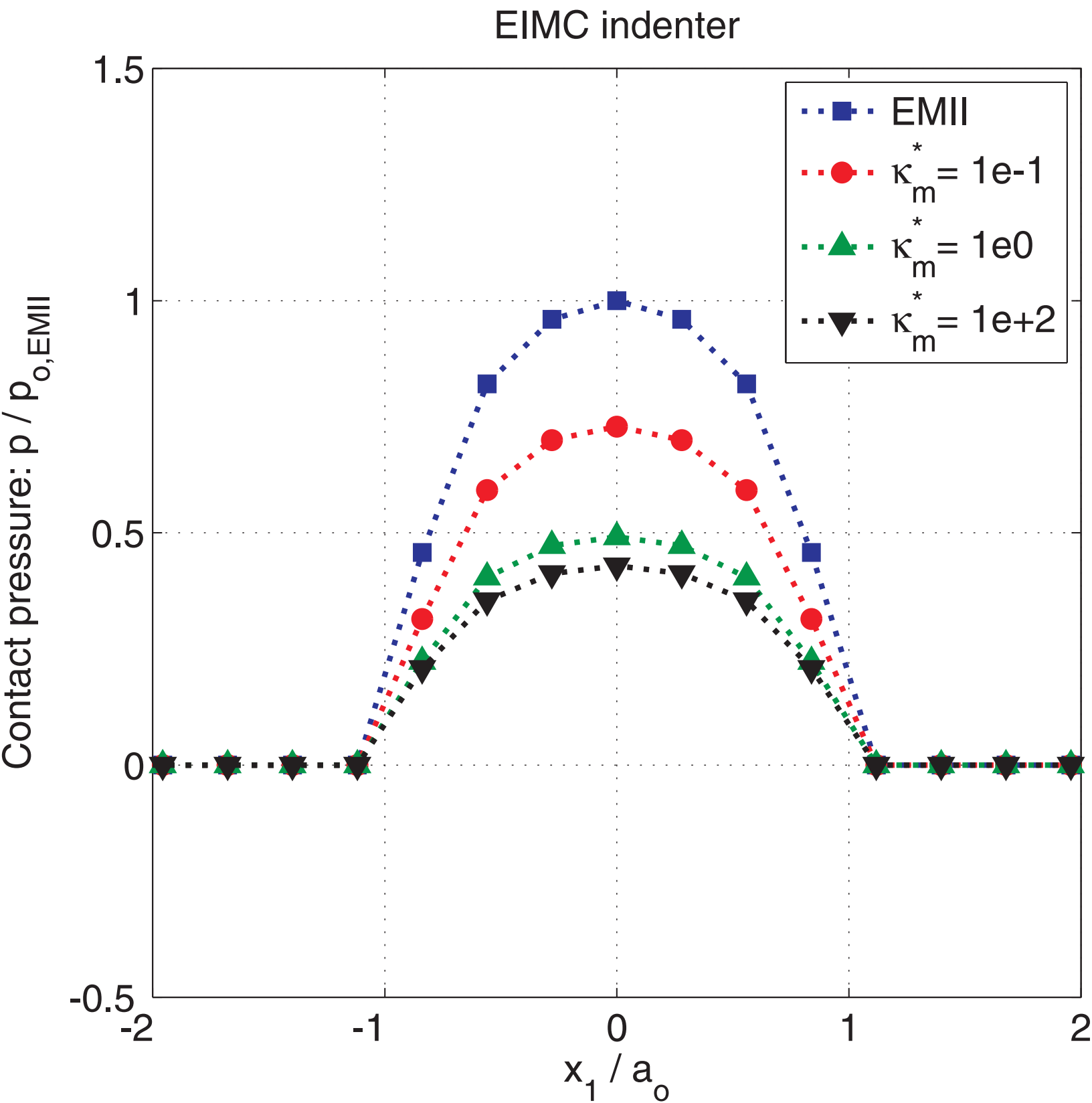
EIMC indenter
EMII
κ^*_m= 1e-1
κ^*_m= 1e0
κ^*_m= 1e+2
Contact pressure: p / $p_{o,EMII}$
x_1 / a_o
1.5
1
0.5
0
-0.5
-2
-1
0
1
2

Figure(s)

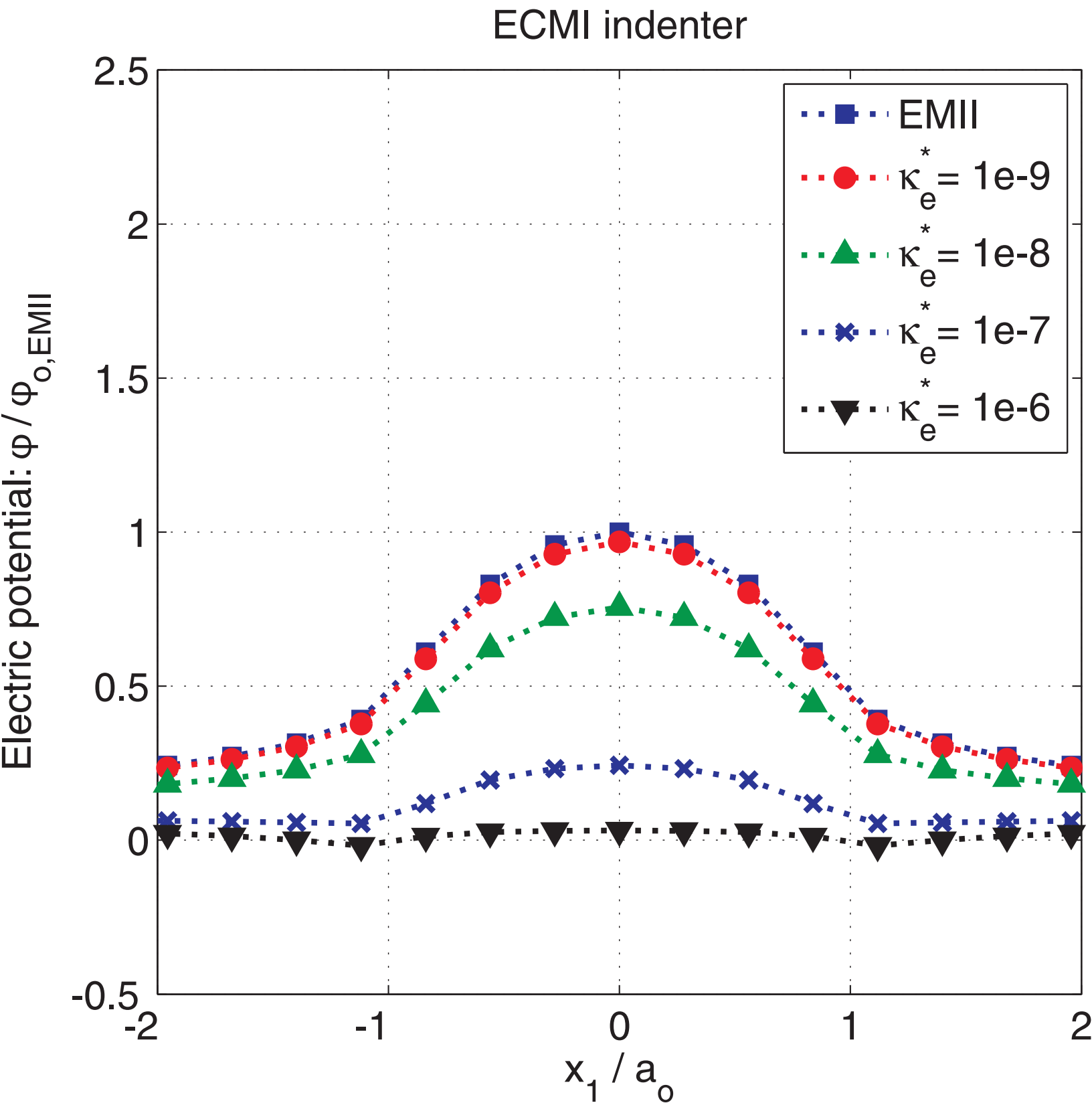
ECMI indenter
EMII
$\kappa_e^* = 1e\text{-}9$
$\kappa_e^* = 1e\text{-}8$
$\kappa_e^* = 1e\text{-}7$
$\kappa_e^* = 1e\text{-}6$
Electric potential: $\varphi / \varphi_{o,EMII}$
x_1 / a_o
2.5
2
1.5
1
0.5
0
-0.5
-2
-1
0
1
2

Figure(s)

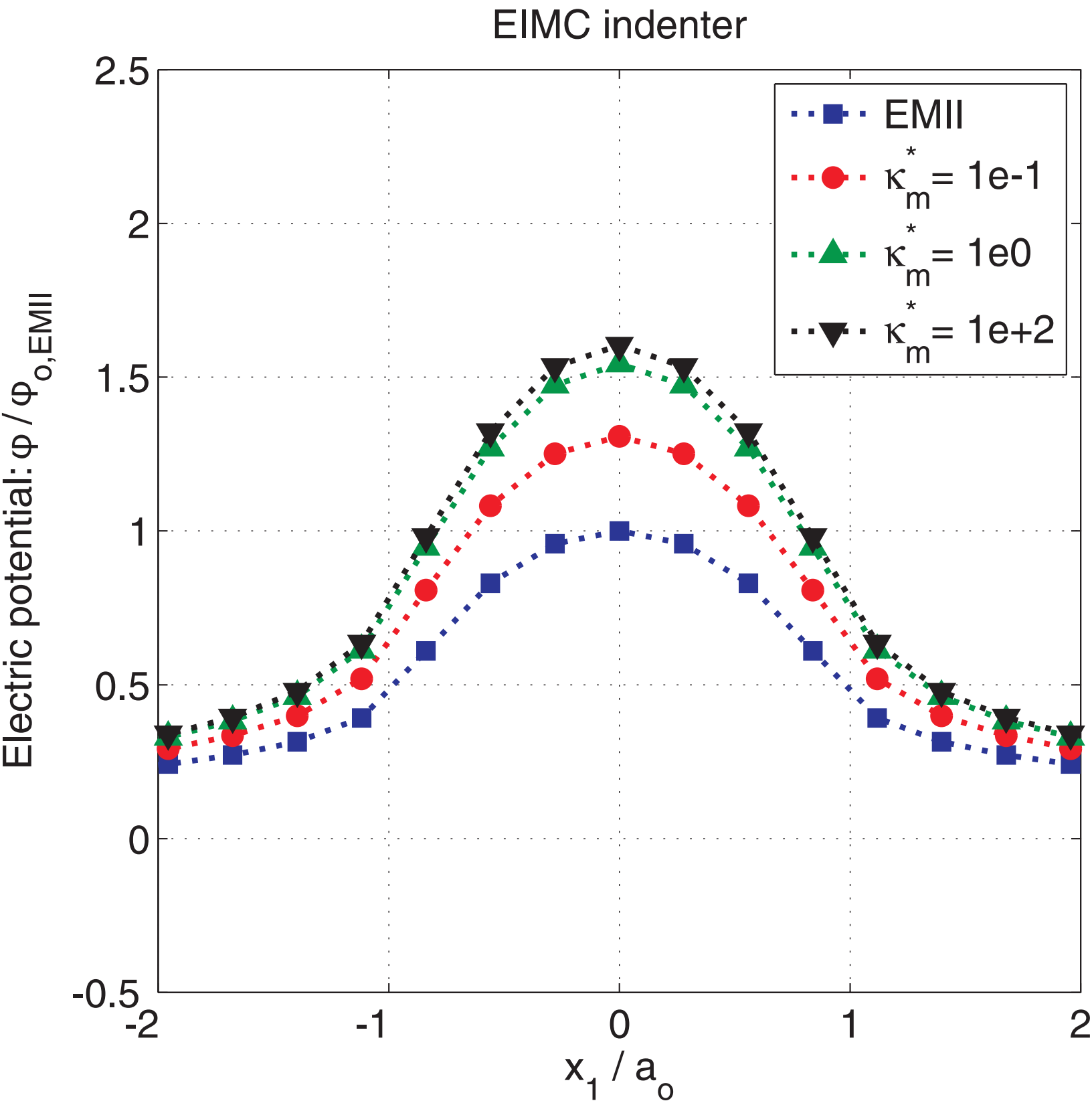
EIMC indenter
EMII
κ_m^* = 1e-1
κ_m^* = 1e0
κ_m^* = 1e+2
Electric potential: $\varphi / \varphi_{o,EMII}$
x_1 / a_o
2.5
2
1.5
1
0.5
0
-0.5
-2
-1
0
1
2

Figure(s)

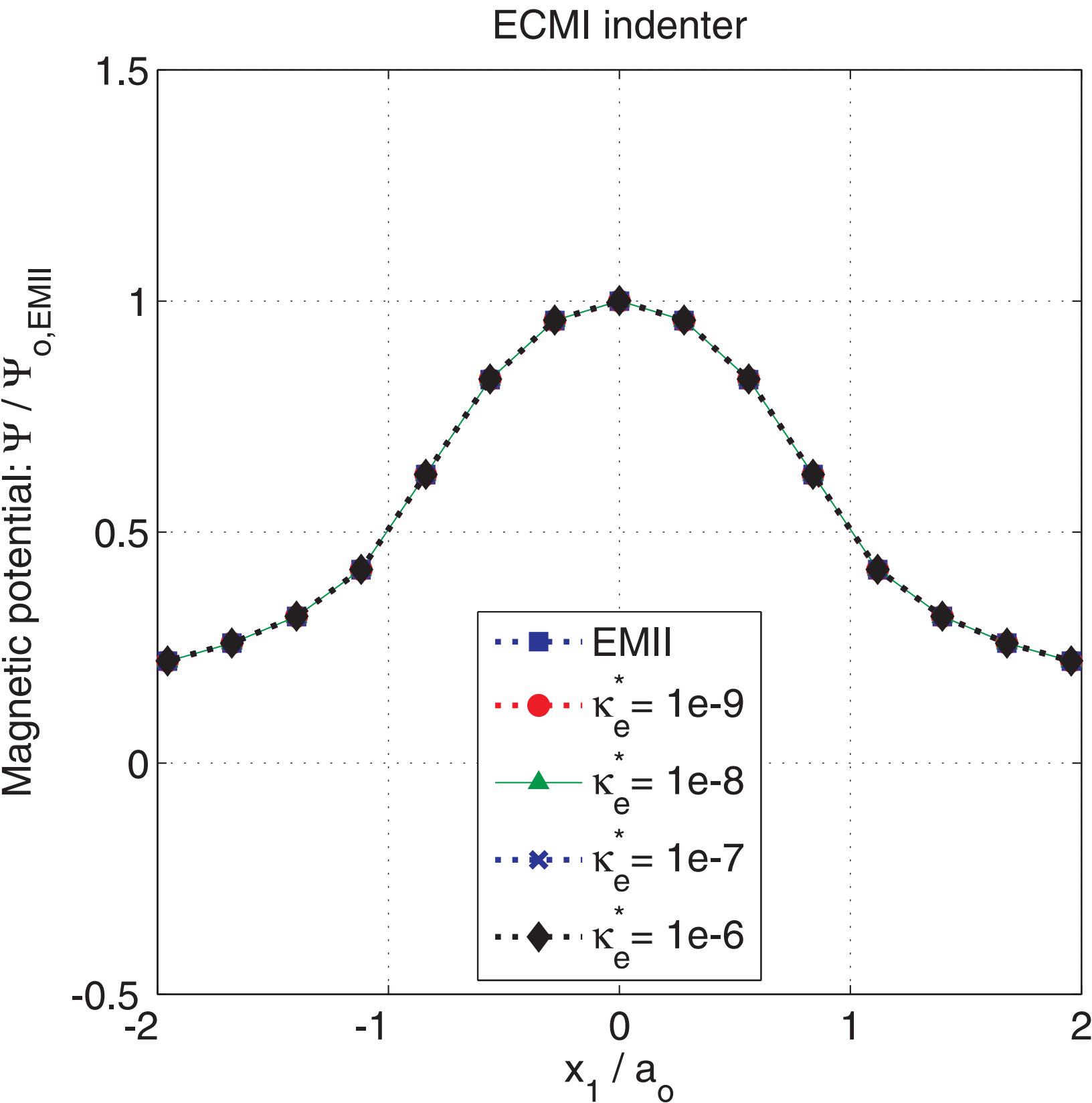
ECMI indenter
1.5
1
0.5
0
-0.5
-2
-1
0
1
2
Magnetic potential: Ψ / Ψ o,EMII
x1 / ao
EMII
κ*e = 1e-9
κ*e = 1e-8
κ*e = 1e-7
κ*e = 1e-6

Figure(s)

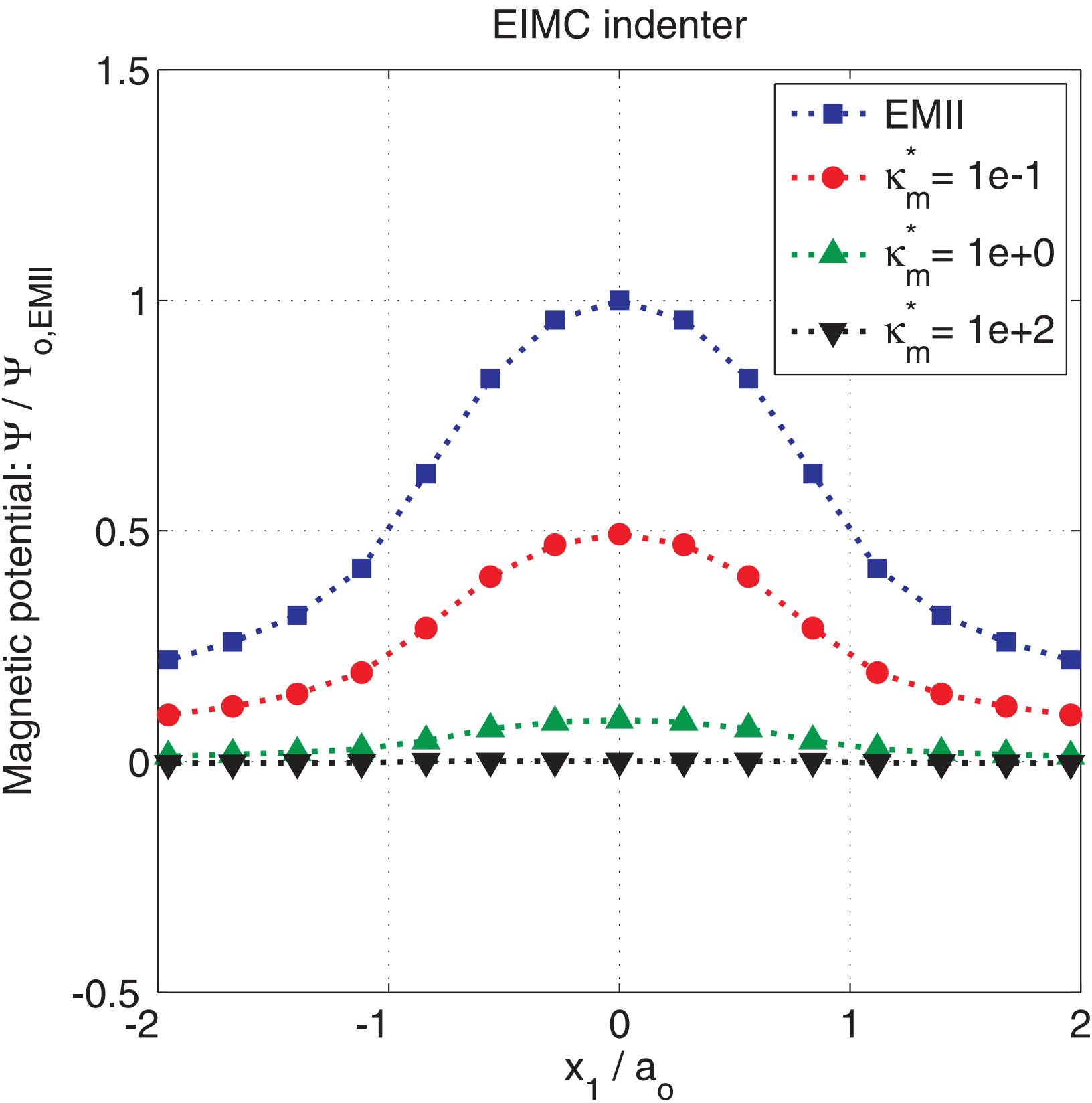
EIMC indenter
EMII
$\kappa_m^* = 1e\text{-}1$
$\kappa_m^* = 1e+0$
$\kappa_m^* = 1e+2$
Magnetic potential: $\Psi / \Psi_{o,EMII}$
x_1 / a_o
1.5
1
0.5
0
-0.5
-2
-1
0
1
2

Figure(s)

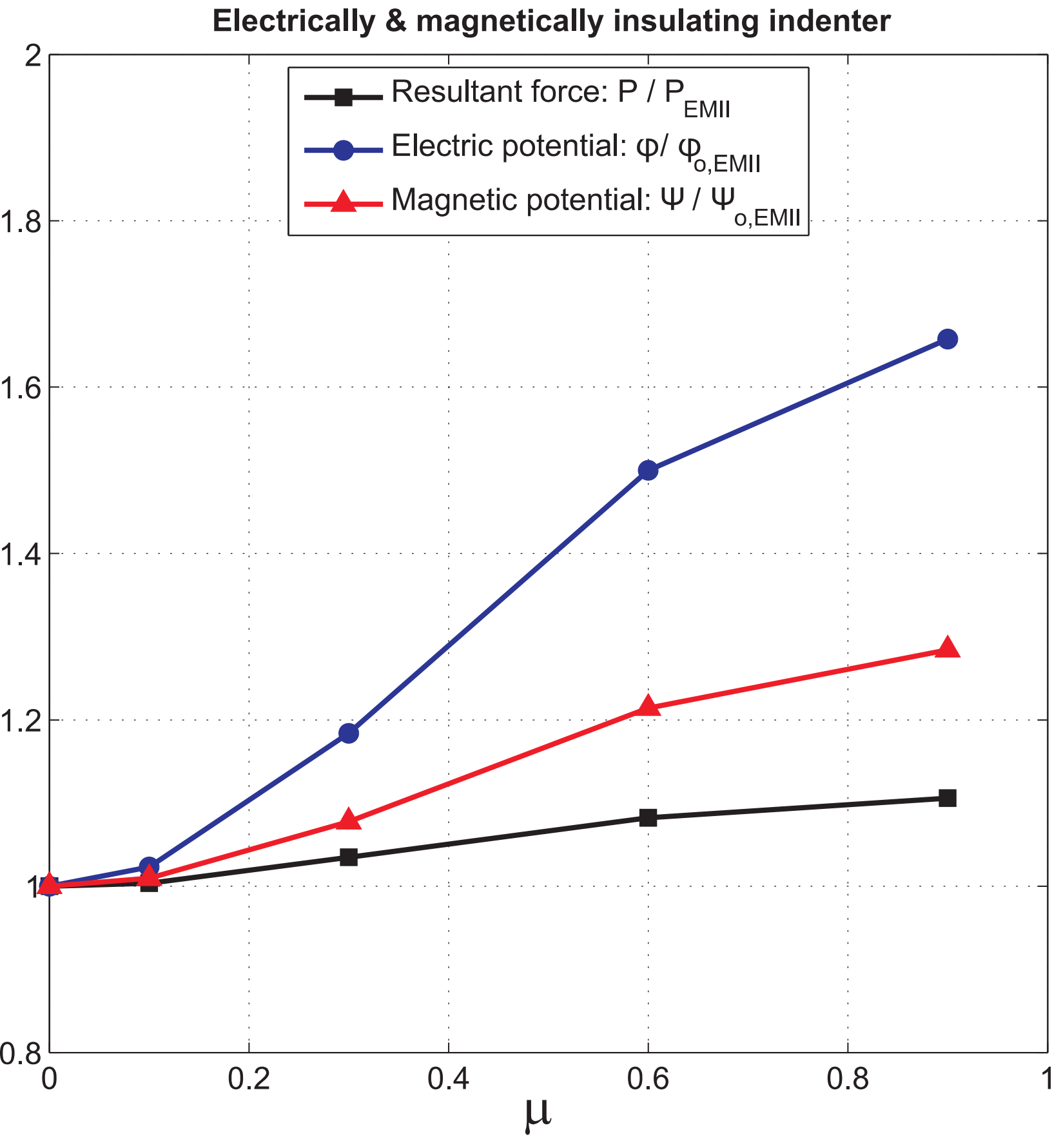
Electrically & magnetically insulating indenter
Resultant force: P / P EMII
Electric potential: φ/ φ o,EMII
Magnetic potential: Ψ / Ψ o,EMII
2
1.8
1.6
1.4
1.2
1
0.8
0
0.2
0.4
0.6
0.8
1
μ

Figure(s)

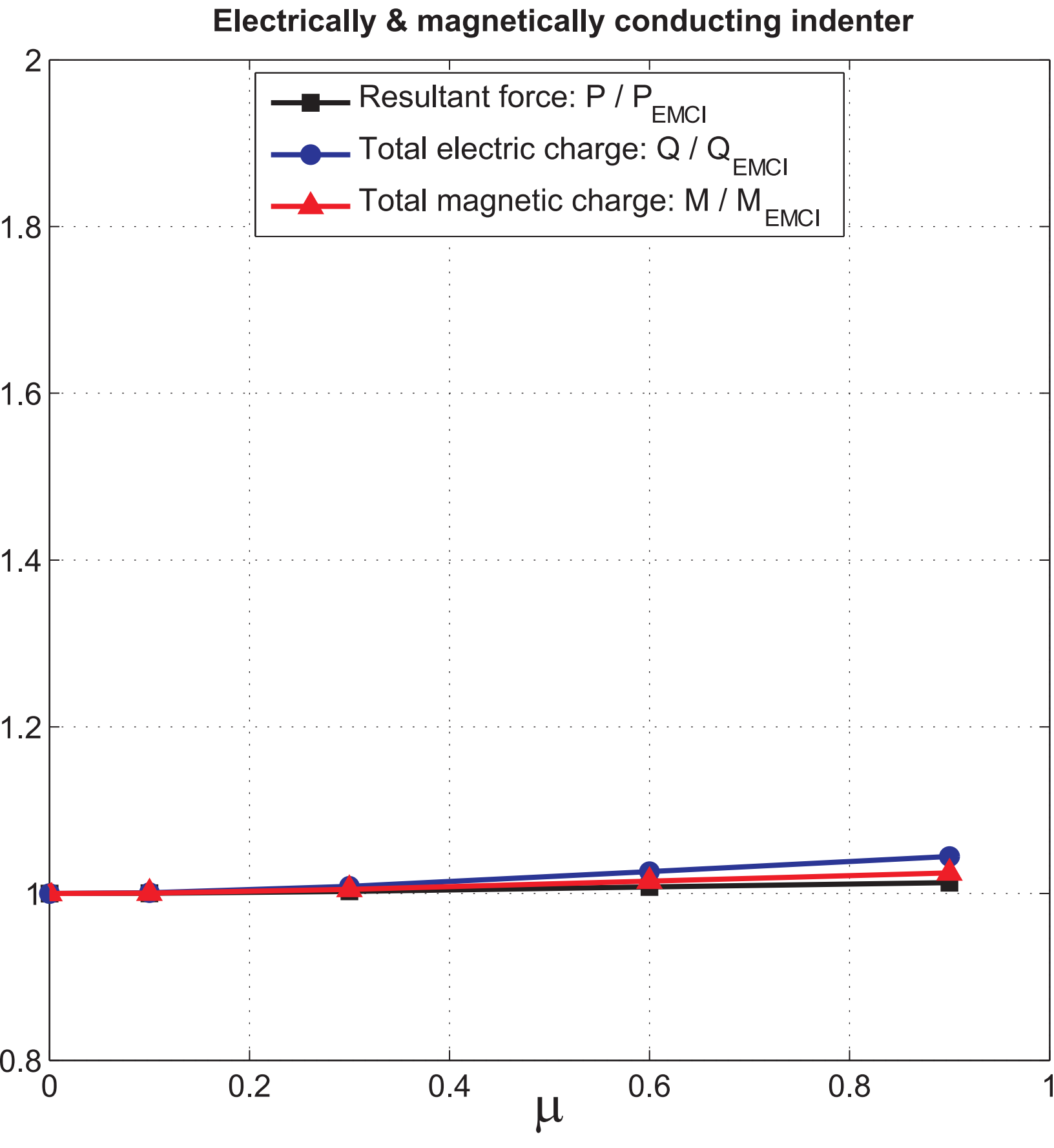
Electrically & magnetically conducting indenter
Resultant force: P / P EMCI
Total electric charge: Q / Q EMCI
Total magnetic charge: M / M EMCI
2
1.8
1.6
1.4
1.2
1
0.8
0
0.2
0.4
0.6
0.8
1
μ

Figure(s)

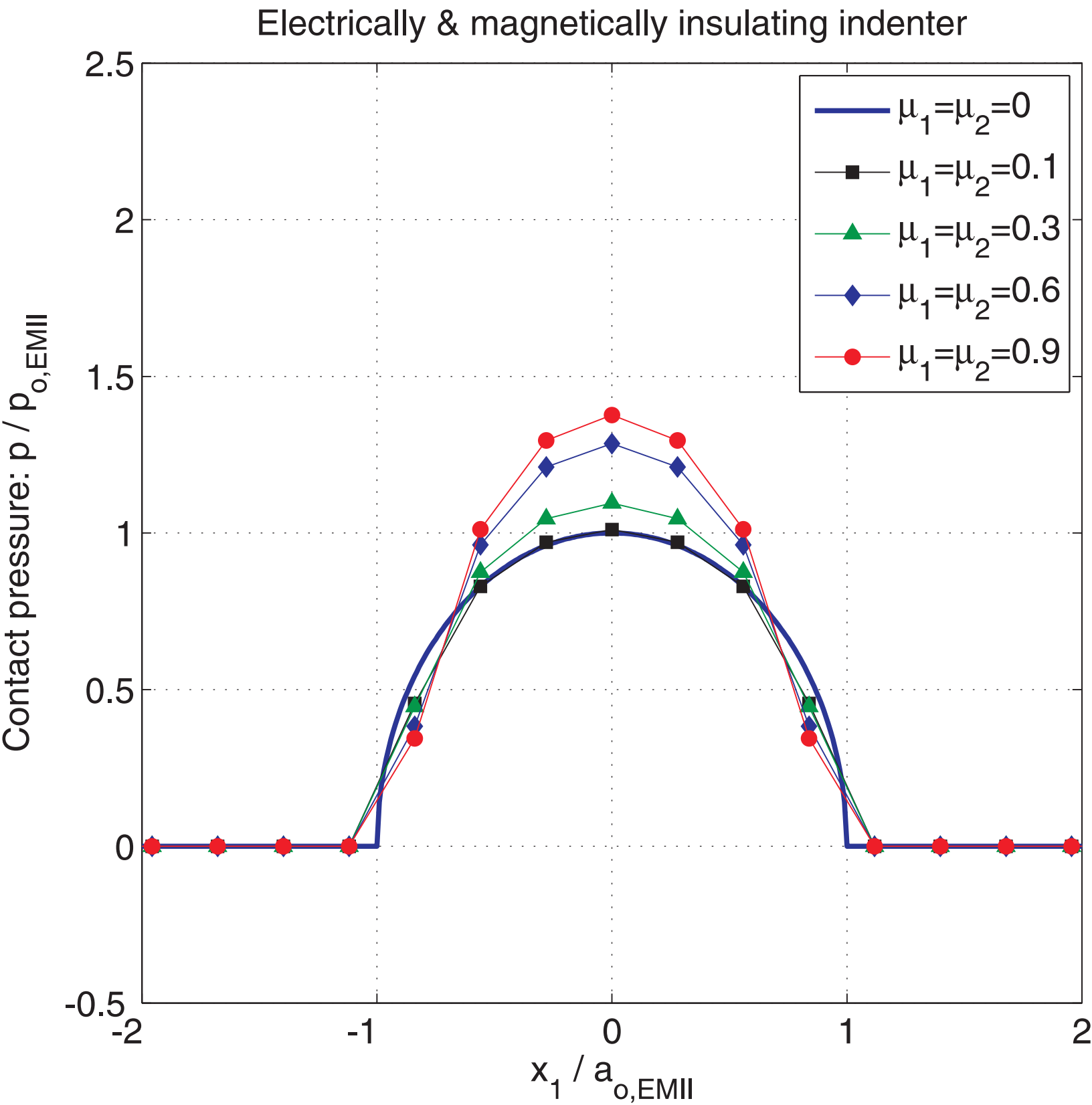
Electrically & magnetically insulating indenter
Contact pressure: p / p_o,EMII
x_1 / a_o,EMII
μ_1=μ_2=0
μ_1=μ_2=0.1
μ_1=μ_2=0.3
μ_1=μ_2=0.6
μ_1=μ_2=0.9
2.5
2
1.5
1
0.5
0
-0.5
-2
-1
0
1
2

Figure(s)

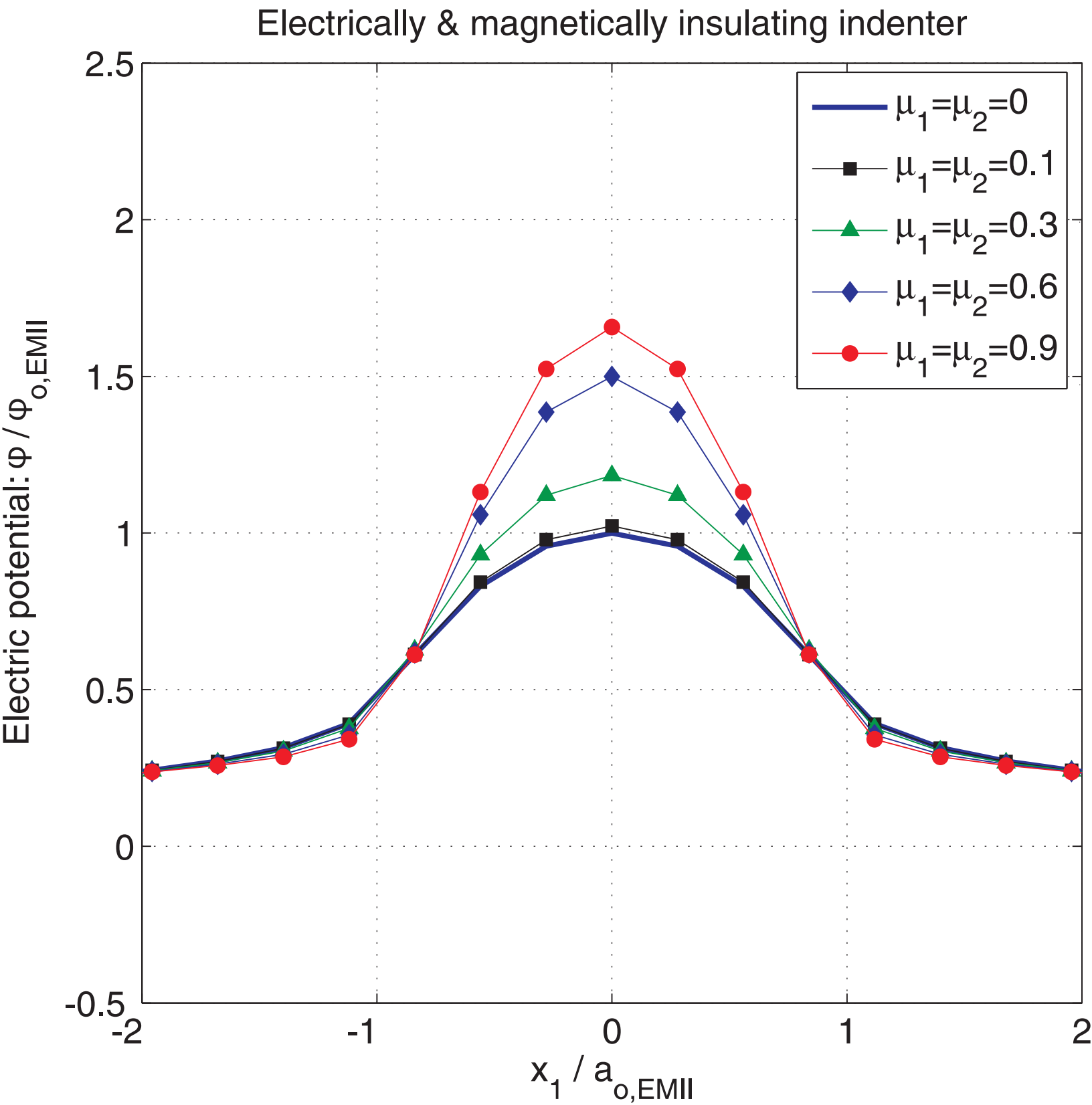
Electrically & magnetically insulating indenter
2.5
2
1.5
1
0.5
0
-0.5
-2
-1
0
1
2
Electric potential: φ / φo,EMII
x1 / ao,EMII
μ1=μ2=0
μ1=μ2=0.1
μ1=μ2=0.3
μ1=μ2=0.6
μ1=μ2=0.9

Figure(s)

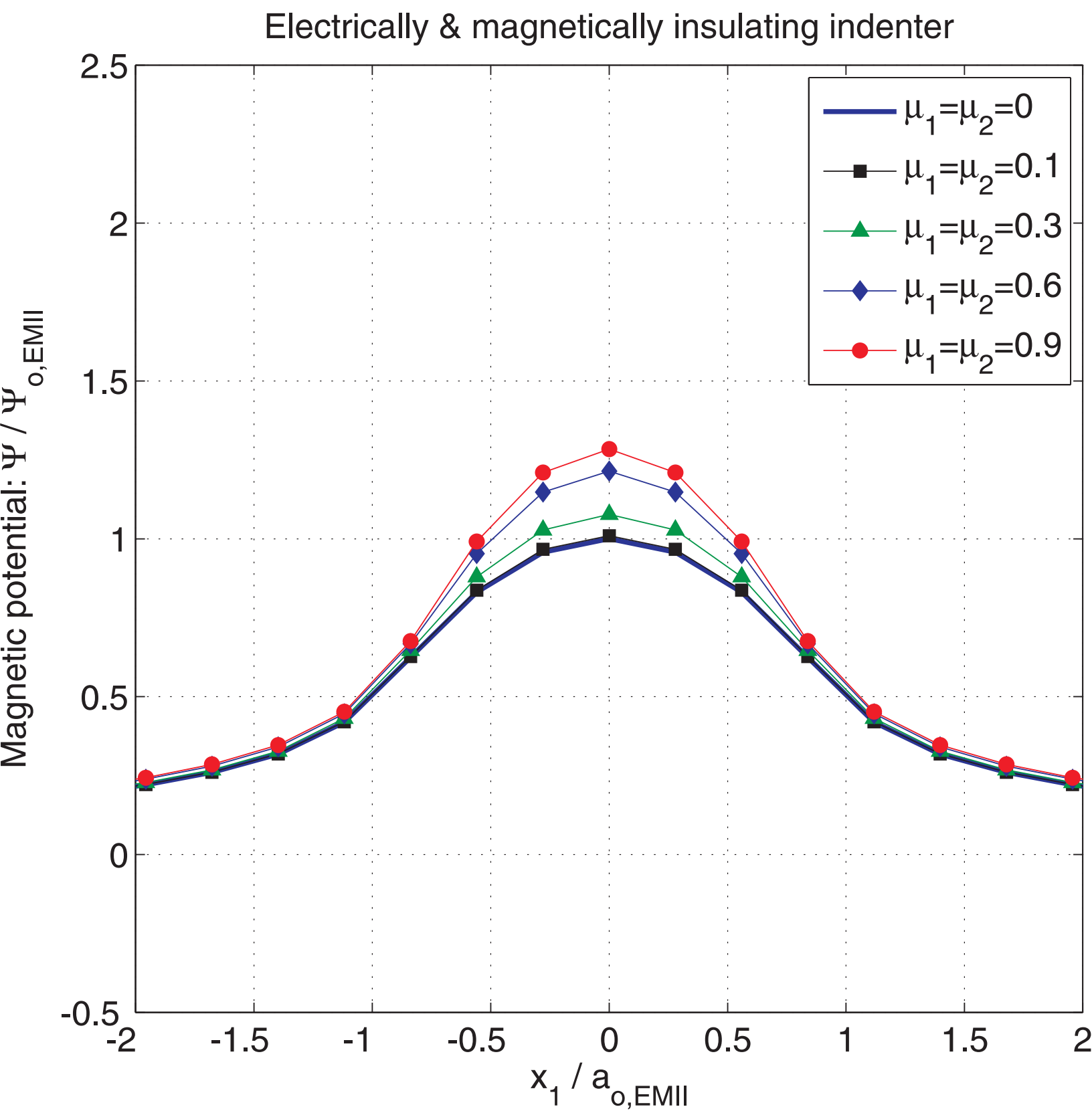
Electrically & magnetically insulating indenter
Magnetic potential: Ψ / Ψ o,EMII
x1 / a o,EMII
μ1=μ2=0
μ1=μ2=0.1
μ1=μ2=0.3
μ1=μ2=0.6
μ1=μ2=0.9
2.5
2
1.5
1
0.5
0
-0.5
-2
-1.5
-1
-0.5
0
0.5
1
1.5
2

Figure(s)

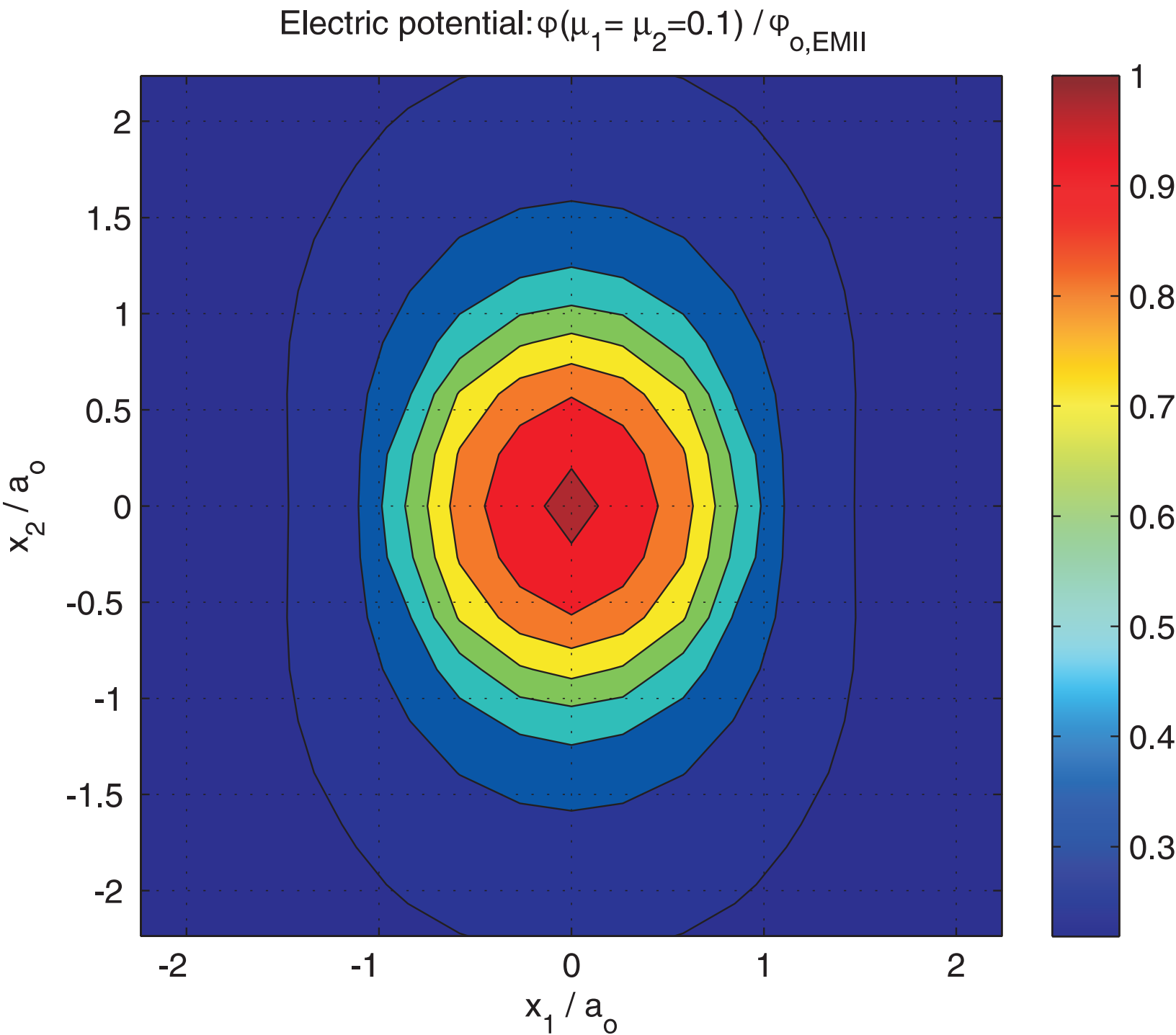
Electric potential: φ(μ1= μ2=0.1) / φo,EMII
x2 / ao
x1 / ao
2
1.5
1
0.5
0
-0.5
-1
-1.5
-2
-2
-1
0
1
2
1
0.9
0.8
0.7
0.6
0.5
0.4
0.3

Figure(s)

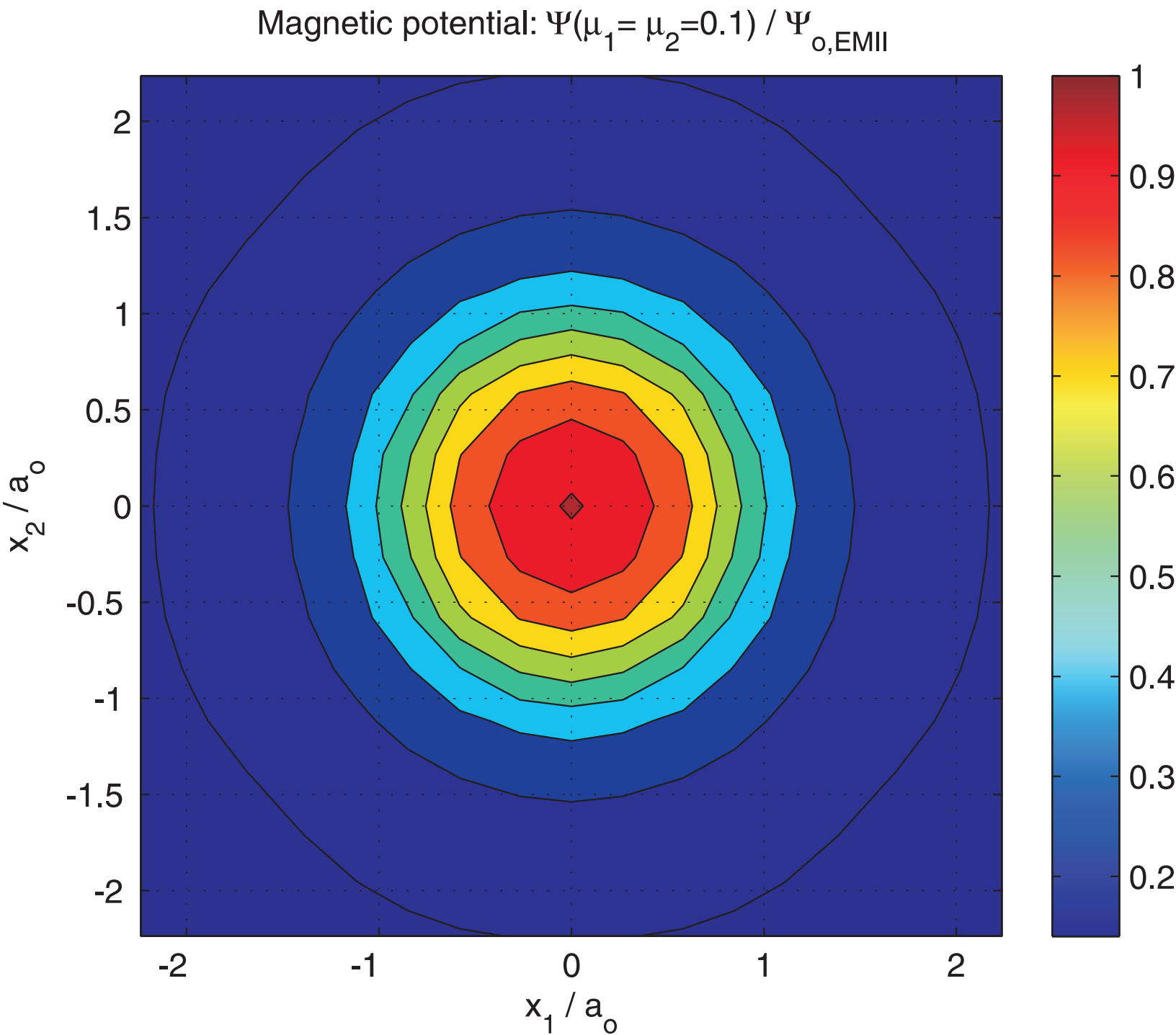
Magnetic potential: Ψ(μ1= μ2=0.1) / Ψo,EMII
x2 / ao
x1 / ao
2
1.5
1
0.5
0
-0.5
-1
-1.5
-2
-2
-1
0
1
2
1
0.9
0.8
0.7
0.6
0.5
0.4
0.3
0.2

Figure(s)

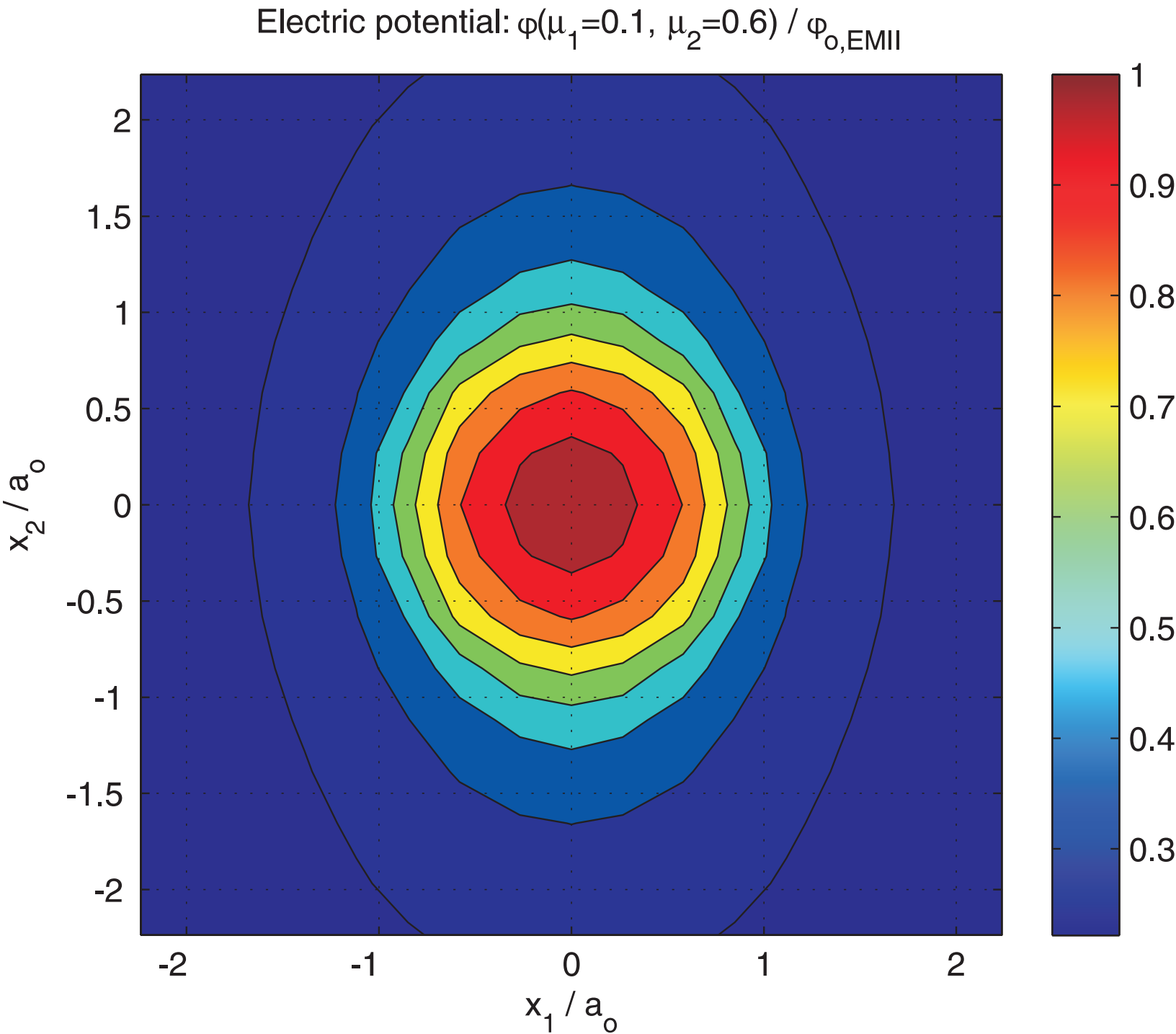
Electric potential: φ(μ1=0.1, μ2=0.6) / φo,EMII
x2 / ao
x1 / ao
2
1.5
1
0.5
0
-0.5
-1
-1.5
-2
-2
-1
0
1
2
1
0.9
0.8
0.7
0.6
0.5
0.4
0.3

Figure(s)

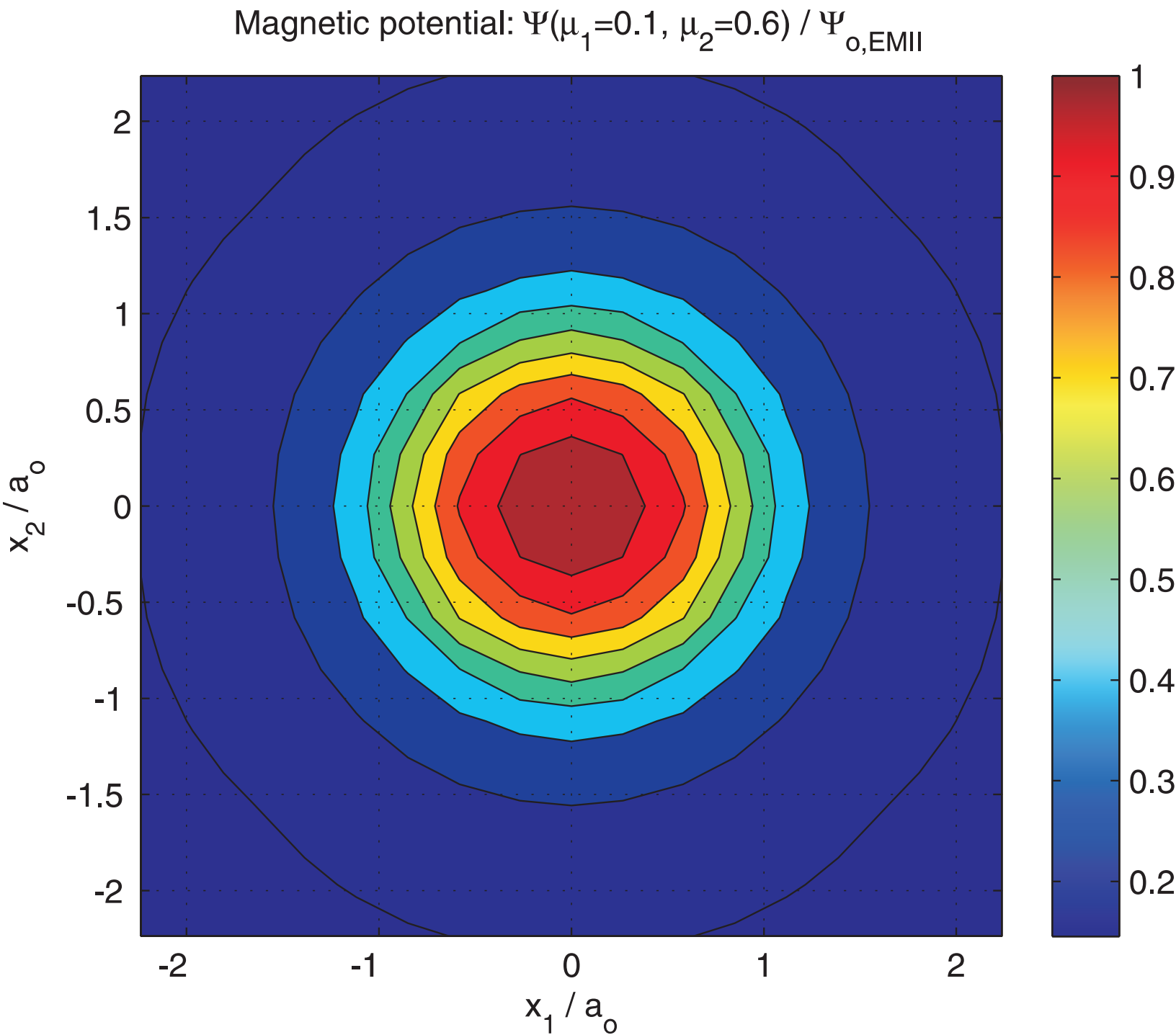
Magnetic potential: Ψ(μ1=0.1, μ2=0.6) / Ψo,EMII
x2 / ao
x1 / ao
2
1.5
1
0.5
0
-0.5
-1
-1.5
-2
-2
-1
0
1
2
1
0.9
0.8
0.7
0.6
0.5
0.4
0.3
0.2

Figure(s)

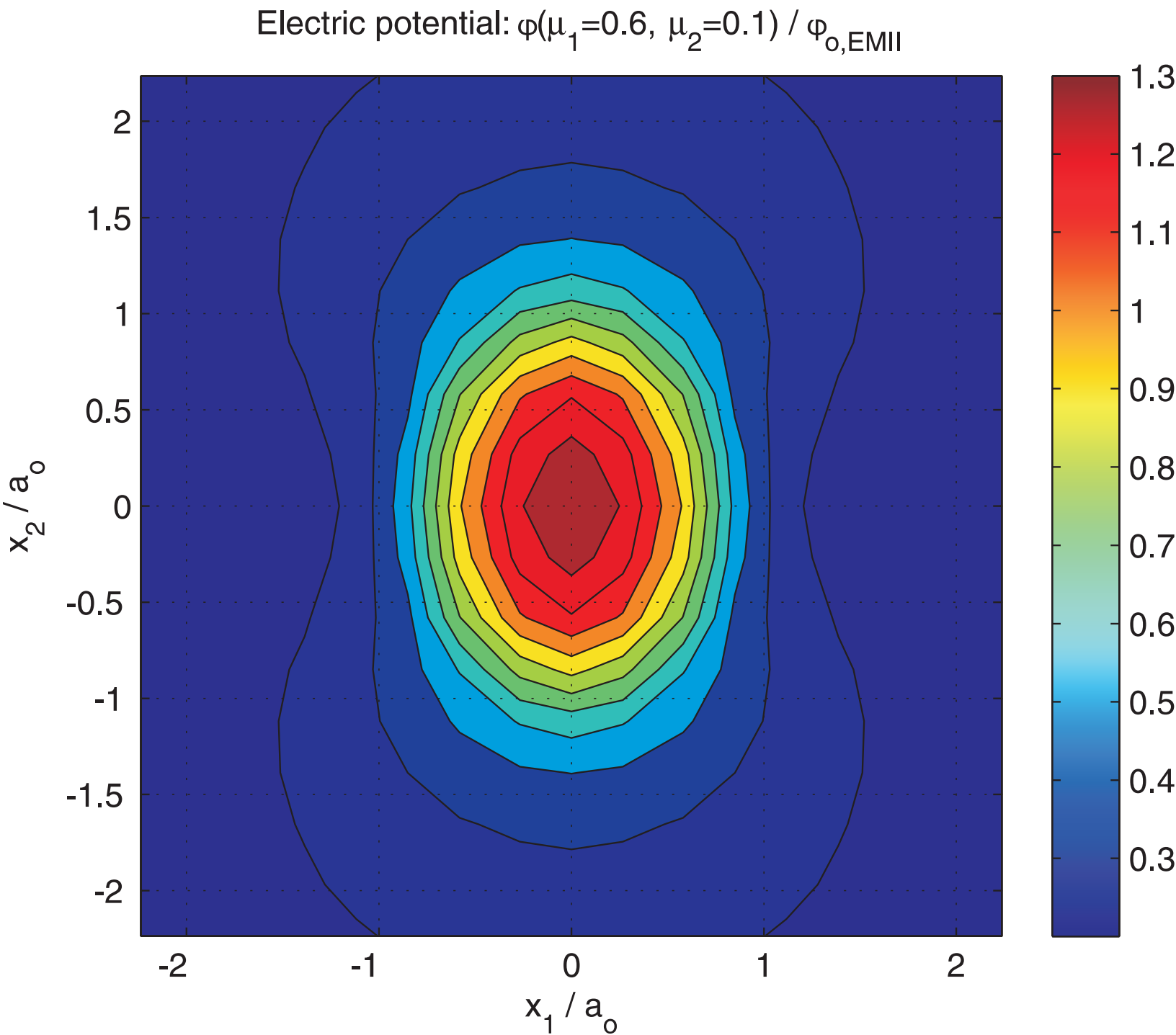
Electric potential: φ(μ1=0.6, μ2=0.1) / φo,EMII
x2 / ao
x1 / ao
2
1.5
1
0.5
0
-0.5
-1
-1.5
-2
-2
-1
0
1
2
1.3
1.2
1.1
1
0.9
0.8
0.7
0.6
0.5
0.4
0.3

Figure(s)

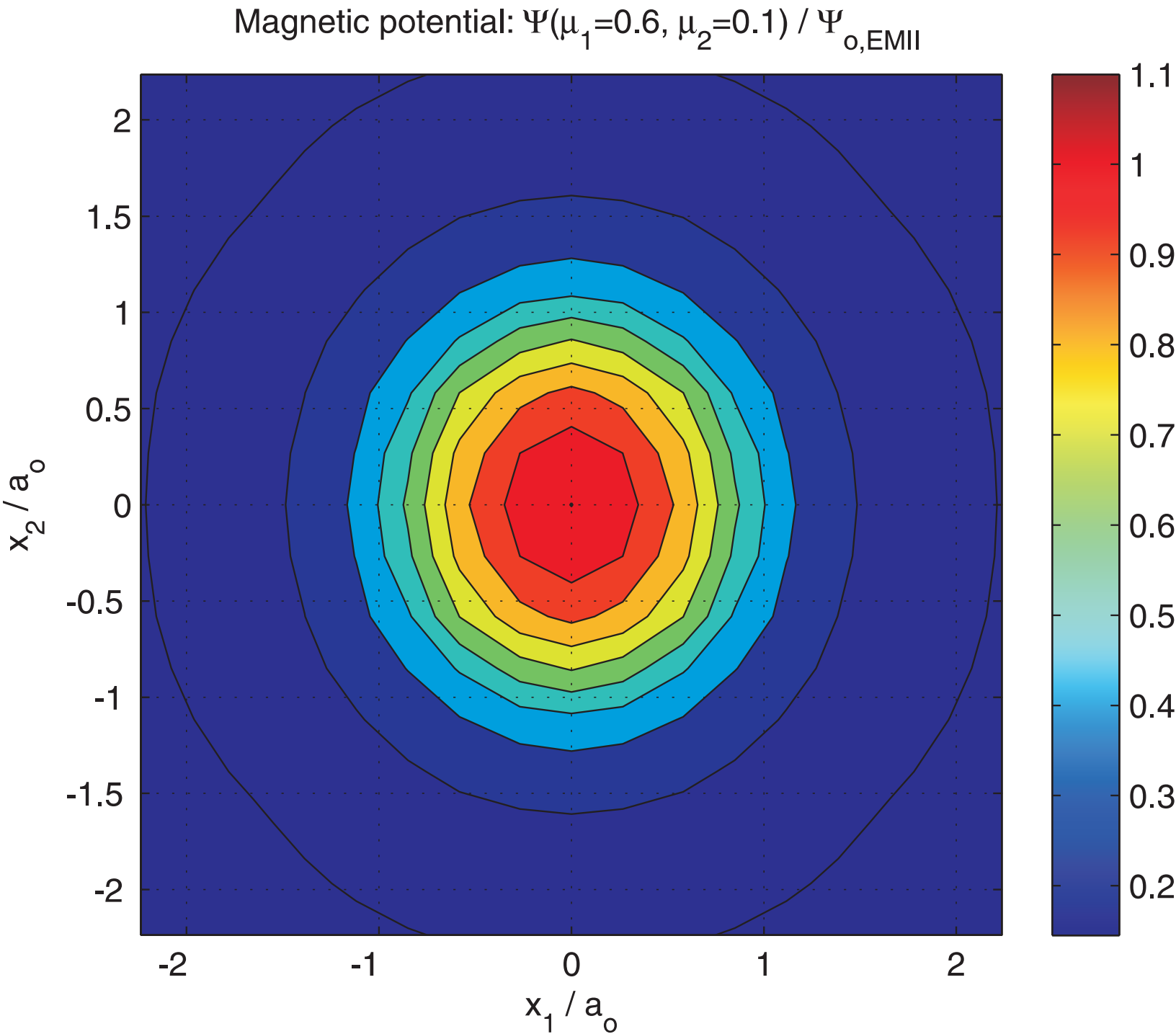
Magnetic potential: Ψ(μ1=0.6, μ2=0.1) / Ψo,EMII
x2 / ao
x1 / ao
2
1.5
1
0.5
0
-0.5
-1
-1.5
-2
-2
-1
0
1
2
1.1
1
0.9
0.8
0.7
0.6
0.5
0.4
0.3
0.2

Figure(s)

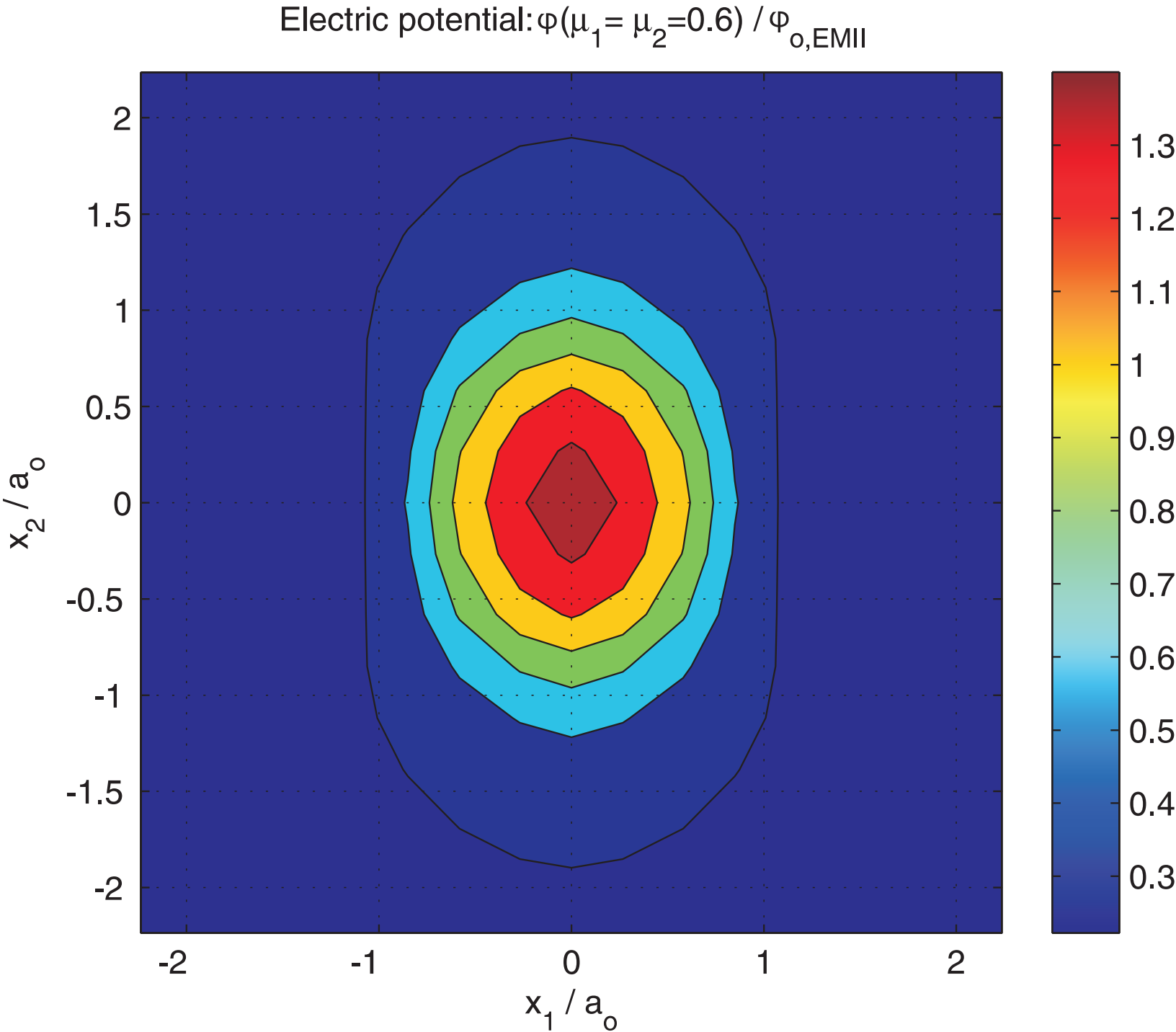
Electric potential: φ(μ1= μ2=0.6) / φo,EMII
2
1.5
1
0.5
0
-0.5
-1
-1.5
-2
x2 / ao
-2
-1
0
1
2
x1 / ao
1.3
1.2
1.1
1
0.9
0.8
0.7
0.6
0.5
0.4
0.3

Figure(s)

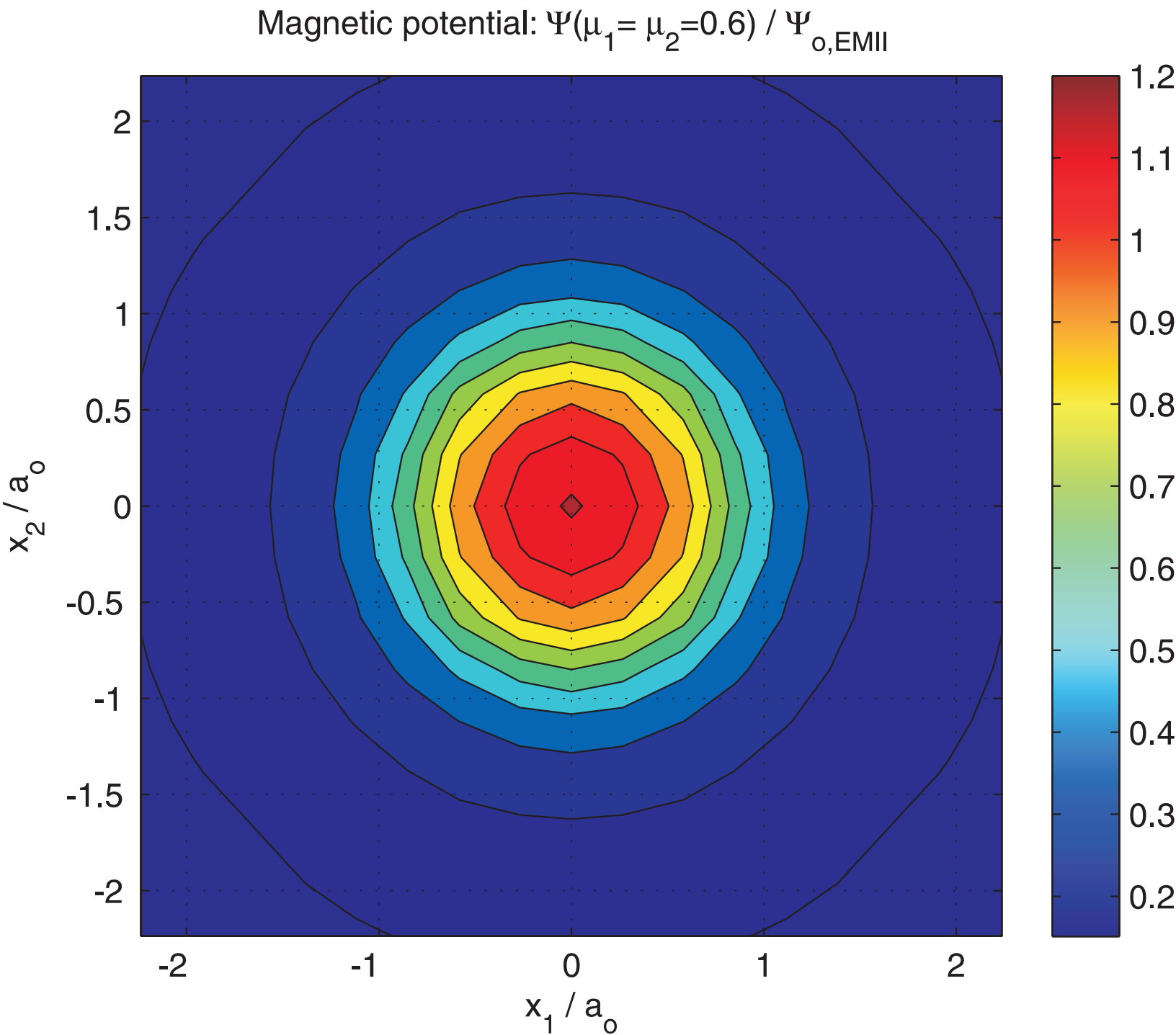
Magnetic potential: Ψ(μ1= μ2=0.6) / Ψo,EMII
x2 / ao
x1 / ao
2
1.5
1
0.5
0
-0.5
-1
-1.5
-2
-2
-1
0
1
2
1.2
1.1
1
0.9
0.8
0.7
0.6
0.5
0.4
0.3
0.2

Figure(s)

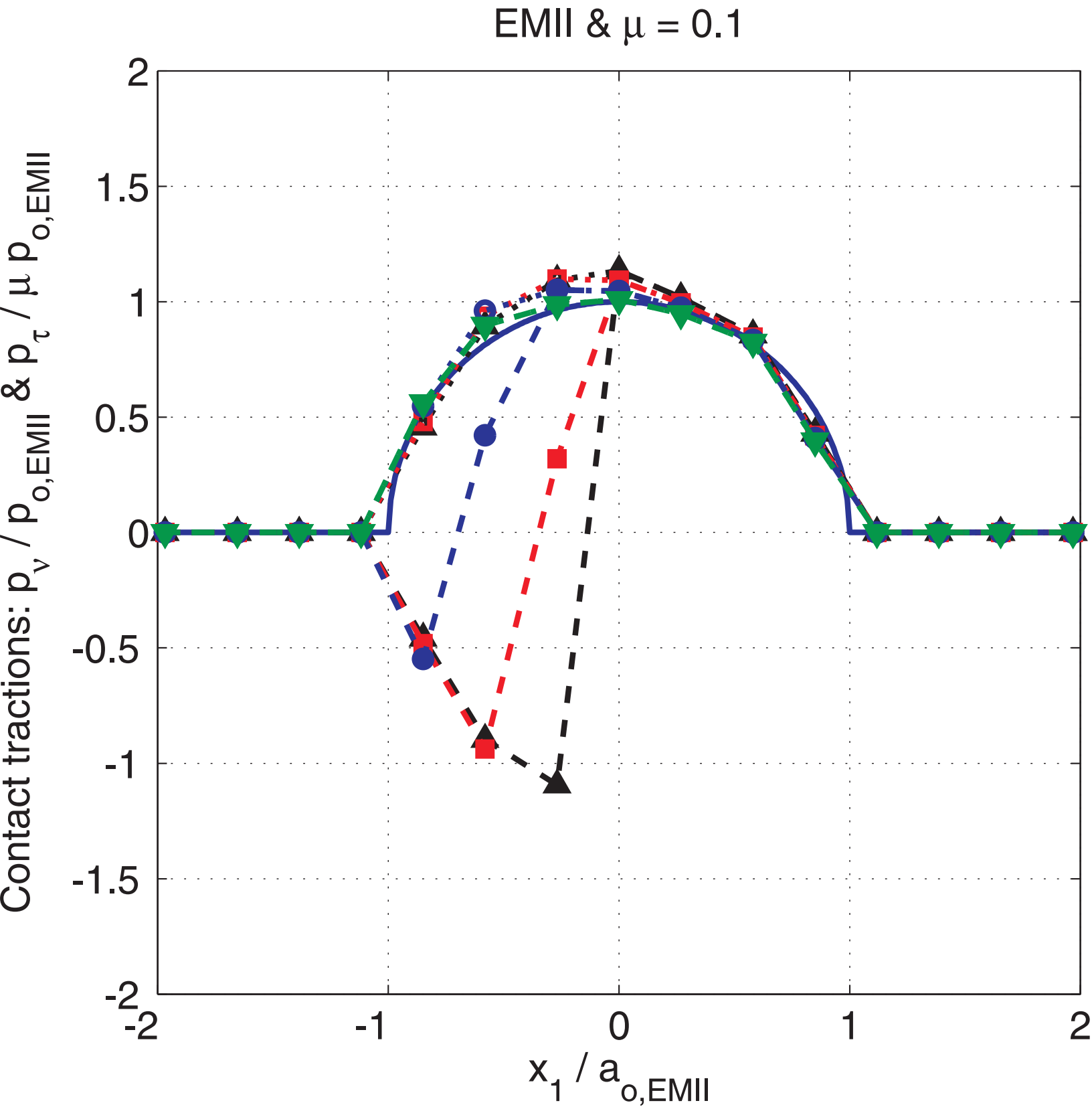
EMII & μ = 0.1
Contact tractions: $p_\nu / p_{o,EMII}$ & $p_\tau / \mu\, p_{o,EMII}$
$x_1 / a_{o,EMII}$
2
1.5
1
0.5
0
-0.5
-1
-1.5
-2
-2
-1
0
1
2

Figure(s)

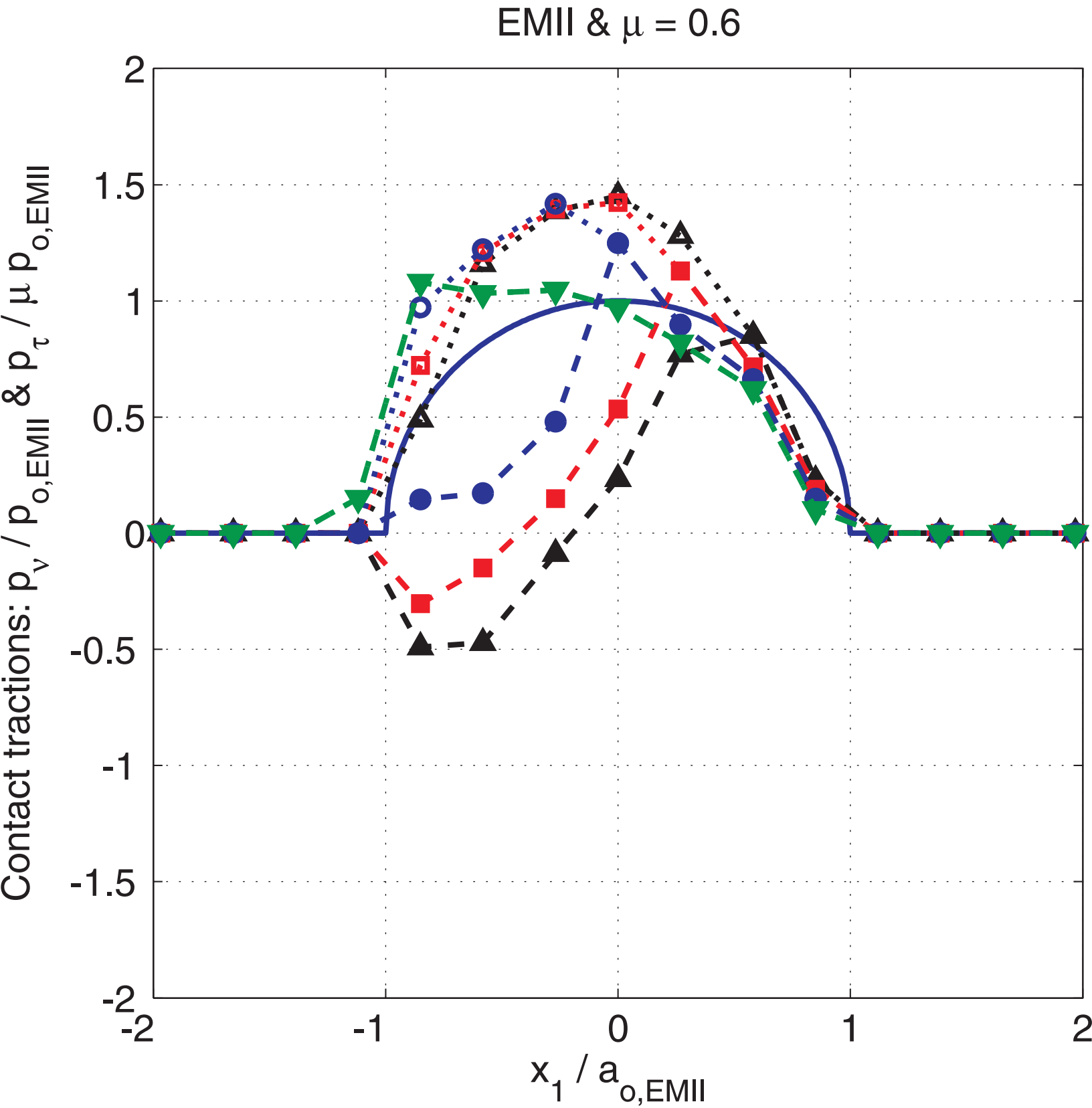
EMII & μ = 0.6
Contact tractions: p_ν / $p_{o,EMII}$ & p_τ / μ $p_{o,EMII}$
x_1 / $a_{o,EMII}$
2
1.5
1
0.5
0
-0.5
-1
-1.5
-2
-2
-1
0
1
2

Figure(s)

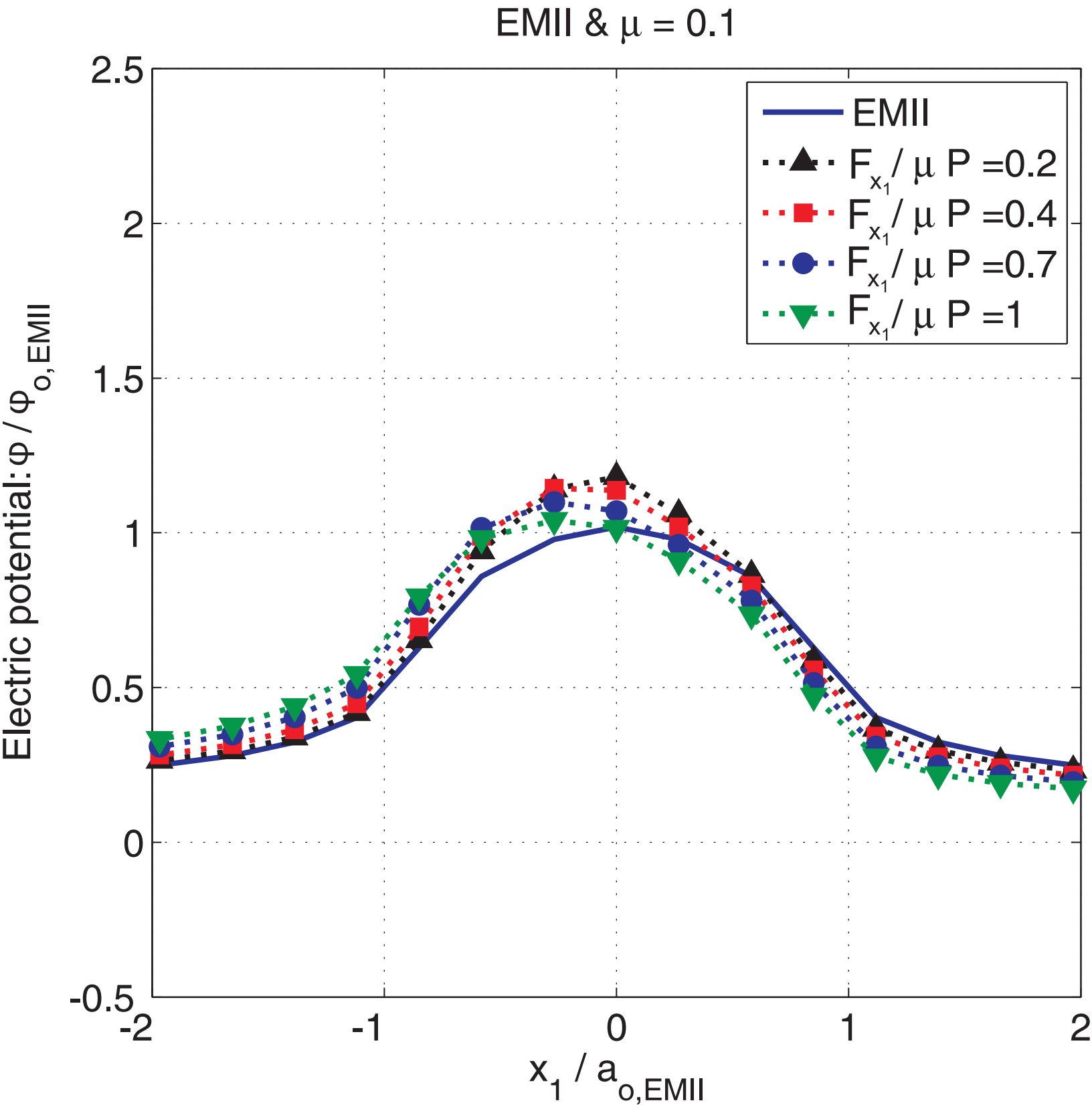
EMII & μ = 0.1
EMII
F x1 / μ P =0.2
F x1 / μ P =0.4
F x1 / μ P =0.7
F x1 / μ P =1
Electric potential: φ / φ o,EMII
x 1 / a o,EMII
2.5
2
1.5
1
0.5
0
-0.5
-2
-1
0
1
2

Figure(s)

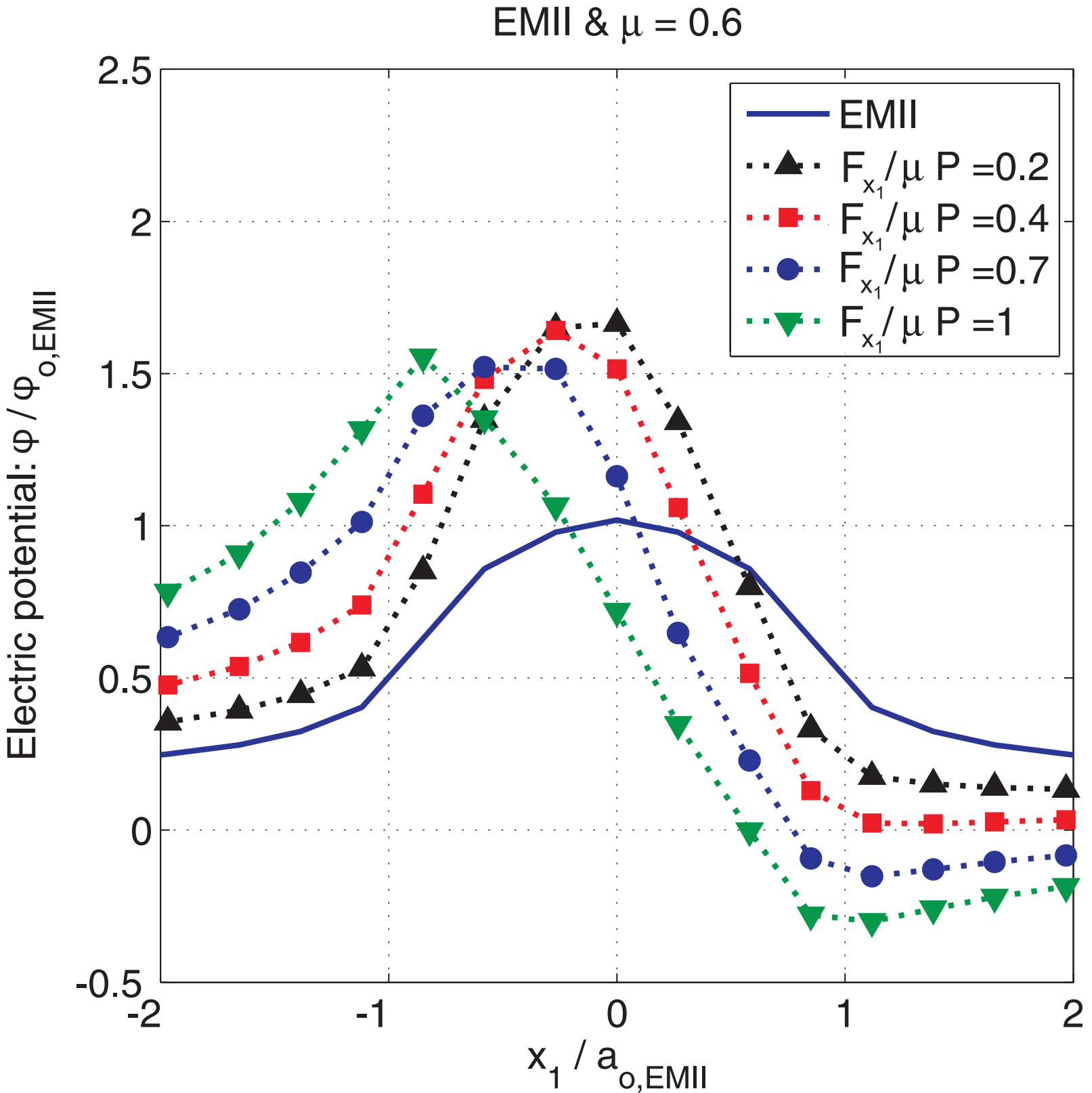
EMII & μ = 0.6
EMII
F_x1/μ P =0.2
F_x1/μ P =0.4
F_x1/μ P =0.7
F_x1/μ P =1
Electric potential: φ / φ_o,EMII
x_1 / a_o,EMII
2.5
2
1.5
1
0.5
0
-0.5
-2
-1
0
1
2

Figure(s)

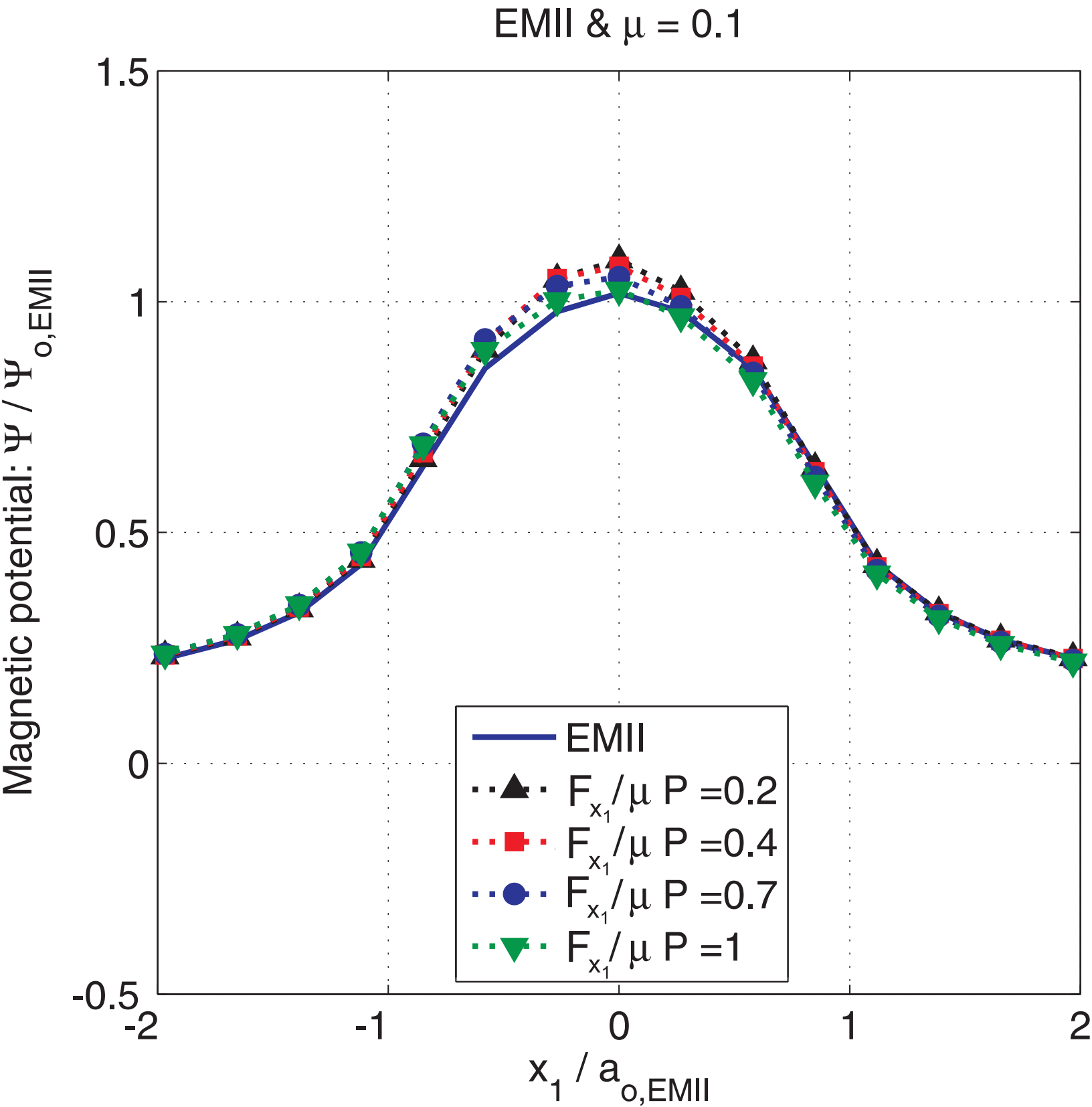
EMII & μ = 0.1
1.5
1
0.5
0
-0.5
-2
-1
0
1
2
Magnetic potential: Ψ / Ψ o,EMII
x1 / a o,EMII
EMII
Fx1/μ P =0.2
Fx1/μ P =0.4
Fx1/μ P =0.7
Fx1/μ P =1

Figure(s)

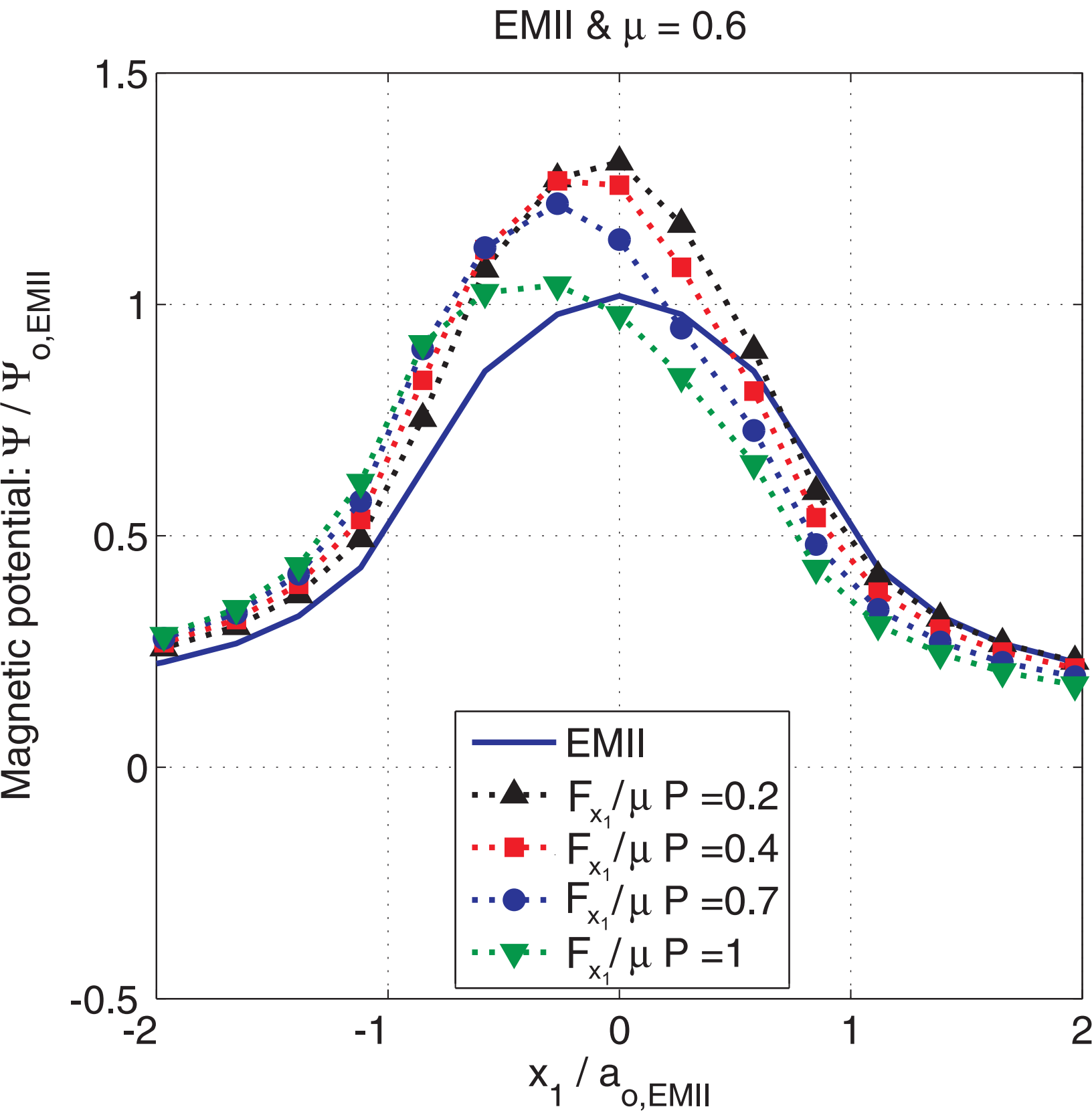
EMII & μ = 0.6
1.5
1
0.5
0
-0.5
-2
-1
0
1
2
Magnetic potential: Ψ / Ψ o,EMII
x1 / a o,EMII
EMII
Fx1/μ P =0.2
Fx1/μ P =0.4
Fx1/μ P =0.7
Fx1/μ P =1

Figure(s)

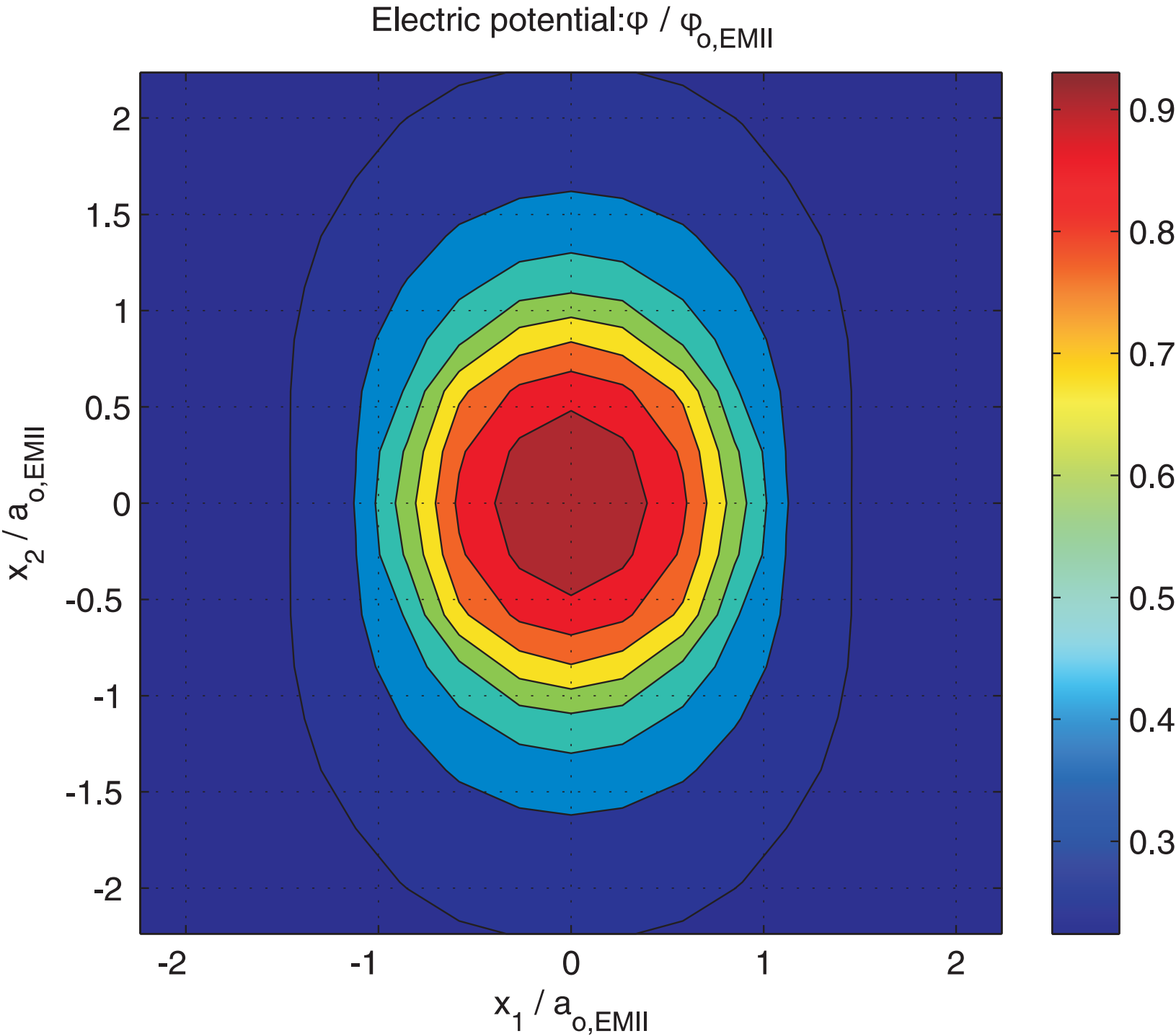
Electric potential:φ / φo,EMII
2
1.5
1
0.5
0
-0.5
-1
-1.5
-2
x2 / ao,EMII
-2
-1
0
1
2
x1 / ao,EMII
0.9
0.8
0.7
0.6
0.5
0.4
0.3

Figure(s)

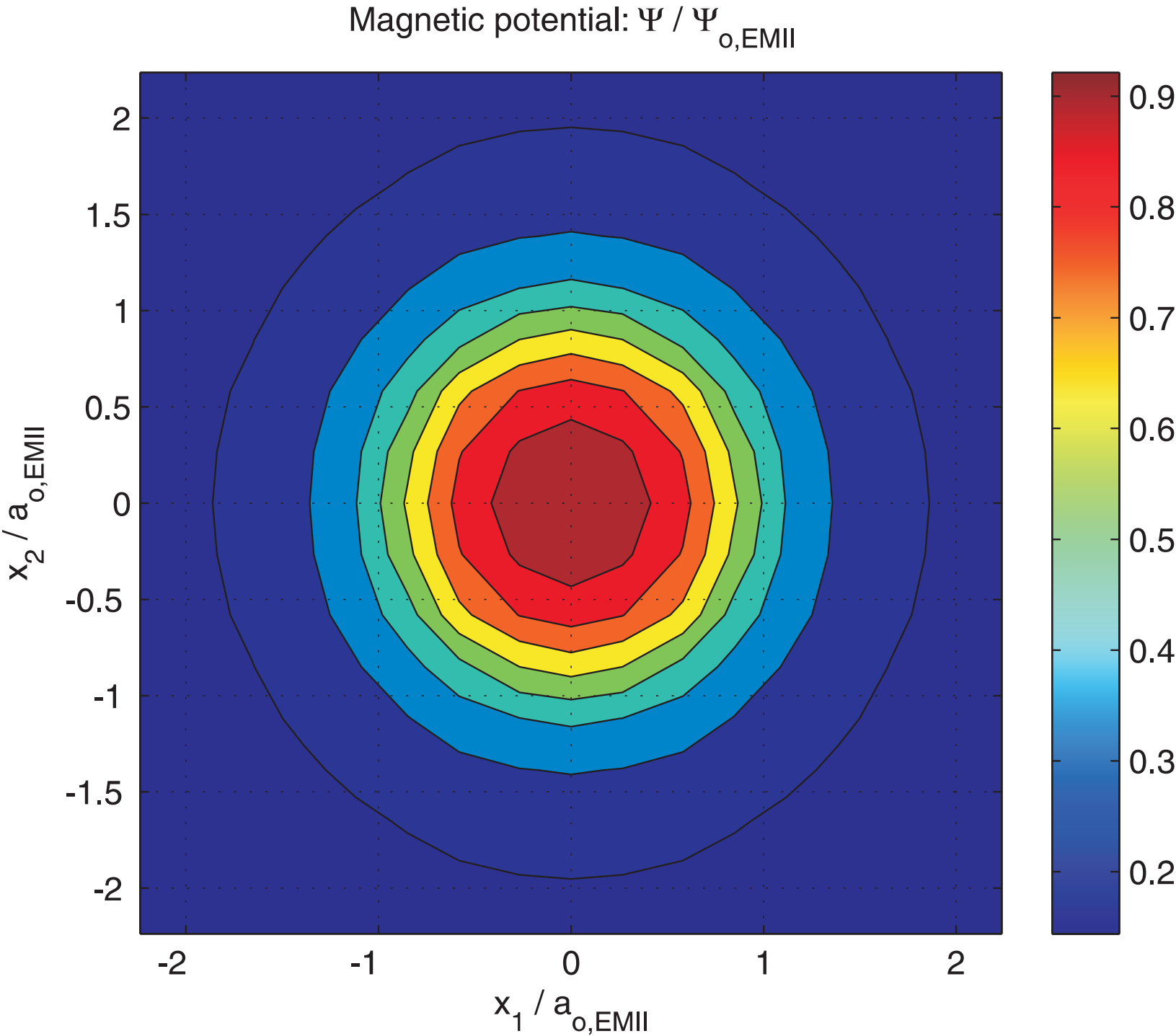
Magnetic potential: Ψ / Ψo,EMII
2
1.5
1
0.5
0
-0.5
-1
-1.5
-2
x2 / ao,EMII
-2
-1
0
1
2
x1 / ao,EMII
0.9
0.8
0.7
0.6
0.5
0.4
0.3
0.2

Figure(s)

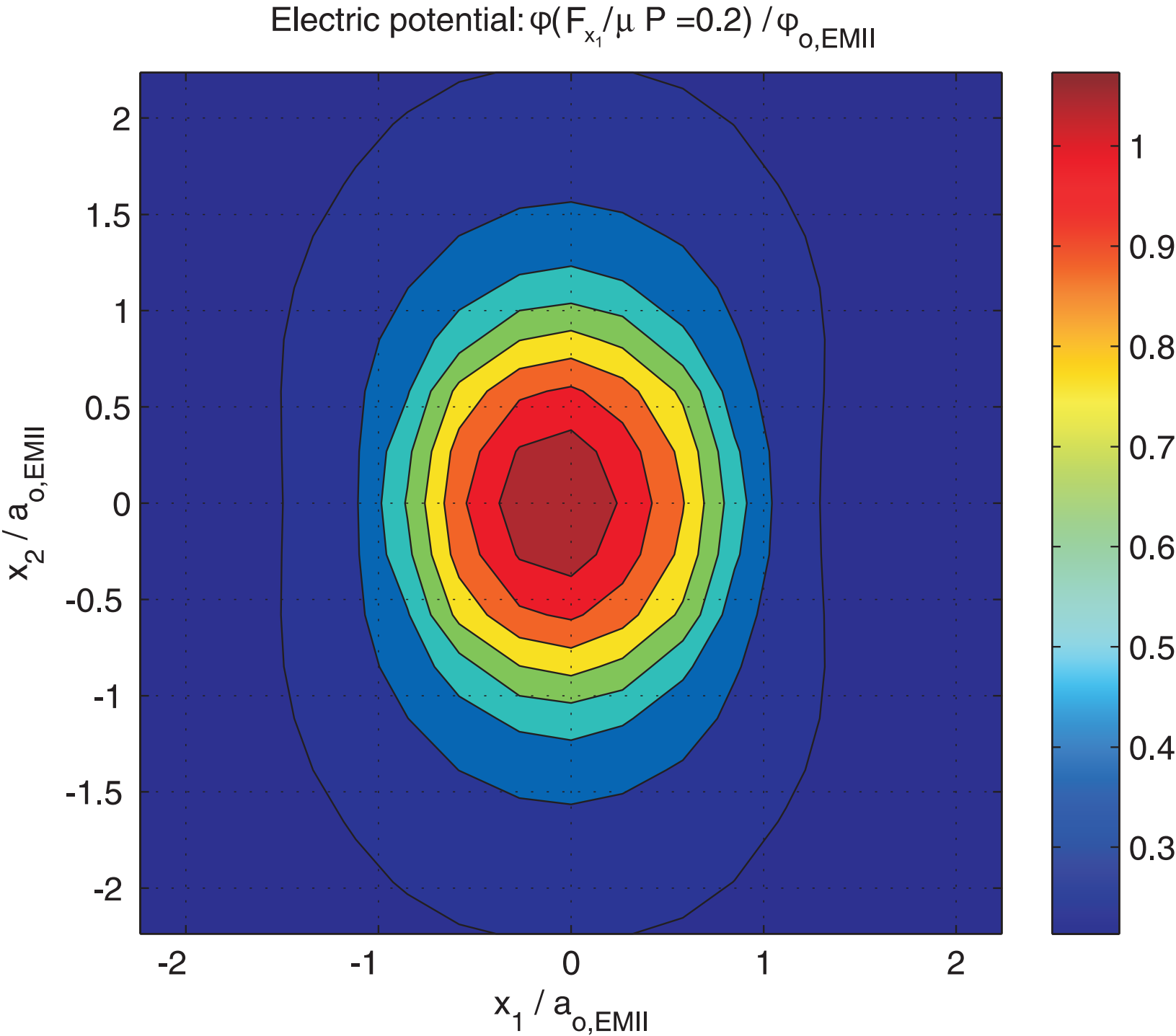
Electric potential: φ(F x1 /μ P =0.2) / φ o,EMII
2
1.5
1
0.5
0
-0.5
-1
-1.5
-2
x2 / ao,EMII
-2
-1
0
1
2
x1 / ao,EMII
1
0.9
0.8
0.7
0.6
0.5
0.4
0.3

Figure(s)

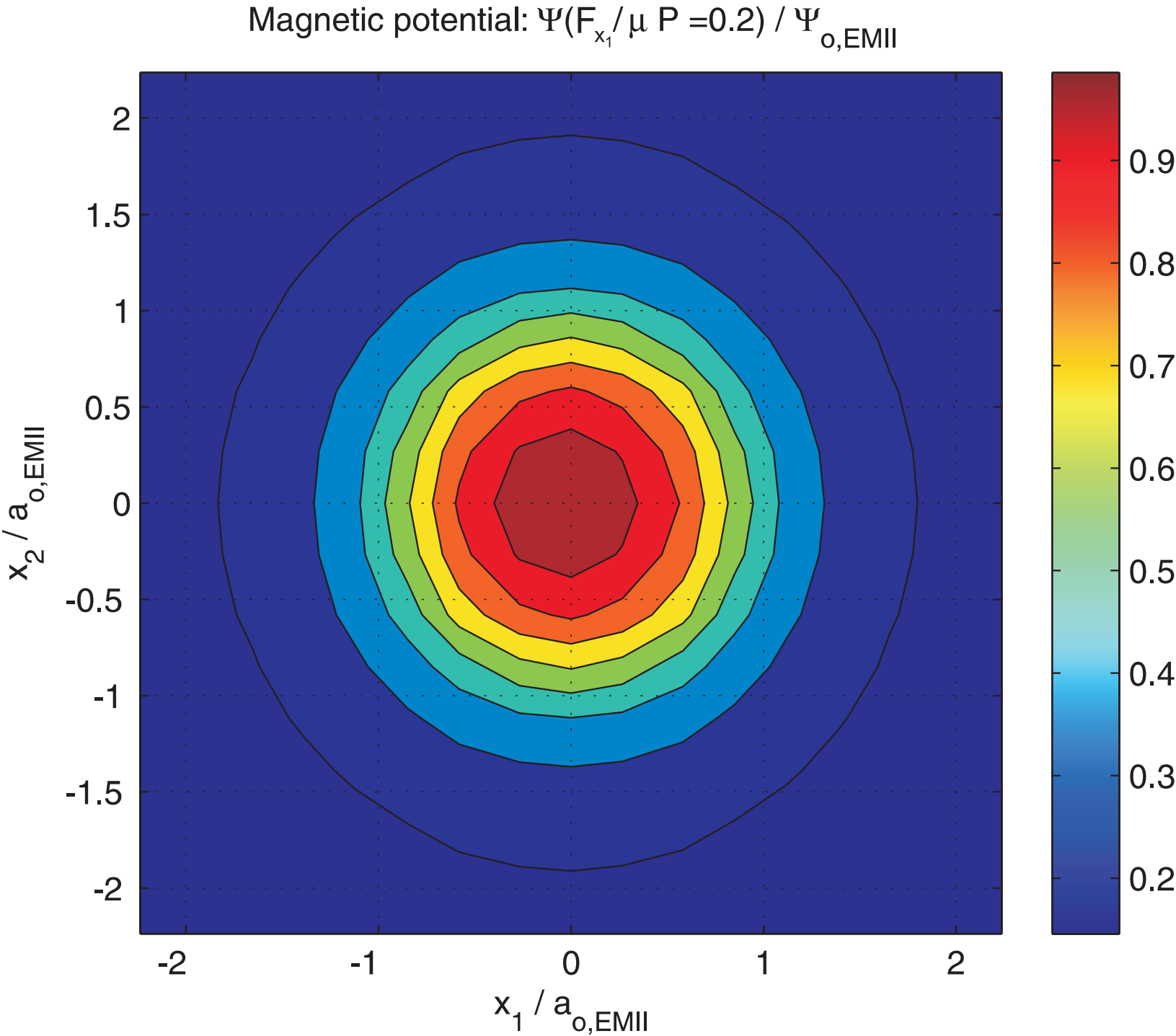
Magnetic potential: Ψ(F_x1 / μ P =0.2) / Ψ_o,EMII
2
1.5
1
0.5
0
-0.5
-1
-1.5
-2
x_2 / a_o,EMII
-2
-1
0
1
2
x_1 / a_o,EMII
0.9
0.8
0.7
0.6
0.5
0.4
0.3
0.2

Figure(s)

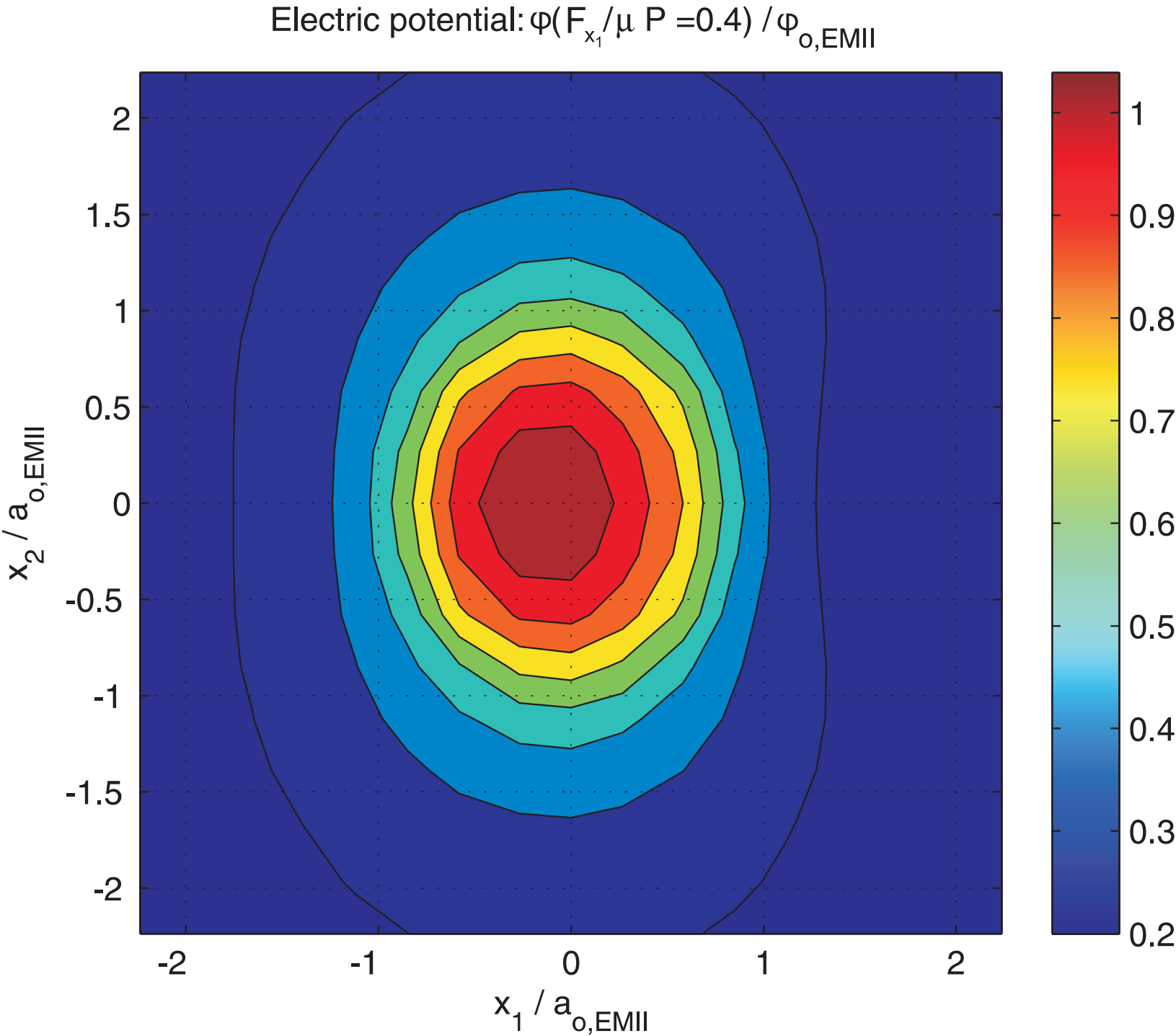
Electric potential: φ(F x1 /μ P =0.4) / φ o,EMII
2
1.5
1
0.5
0
-0.5
-1
-1.5
-2
x2 / ao,EMII
-2
-1
0
1
2
x1 / ao,EMII
1
0.9
0.8
0.7
0.6
0.5
0.4
0.3
0.2

Figure(s)

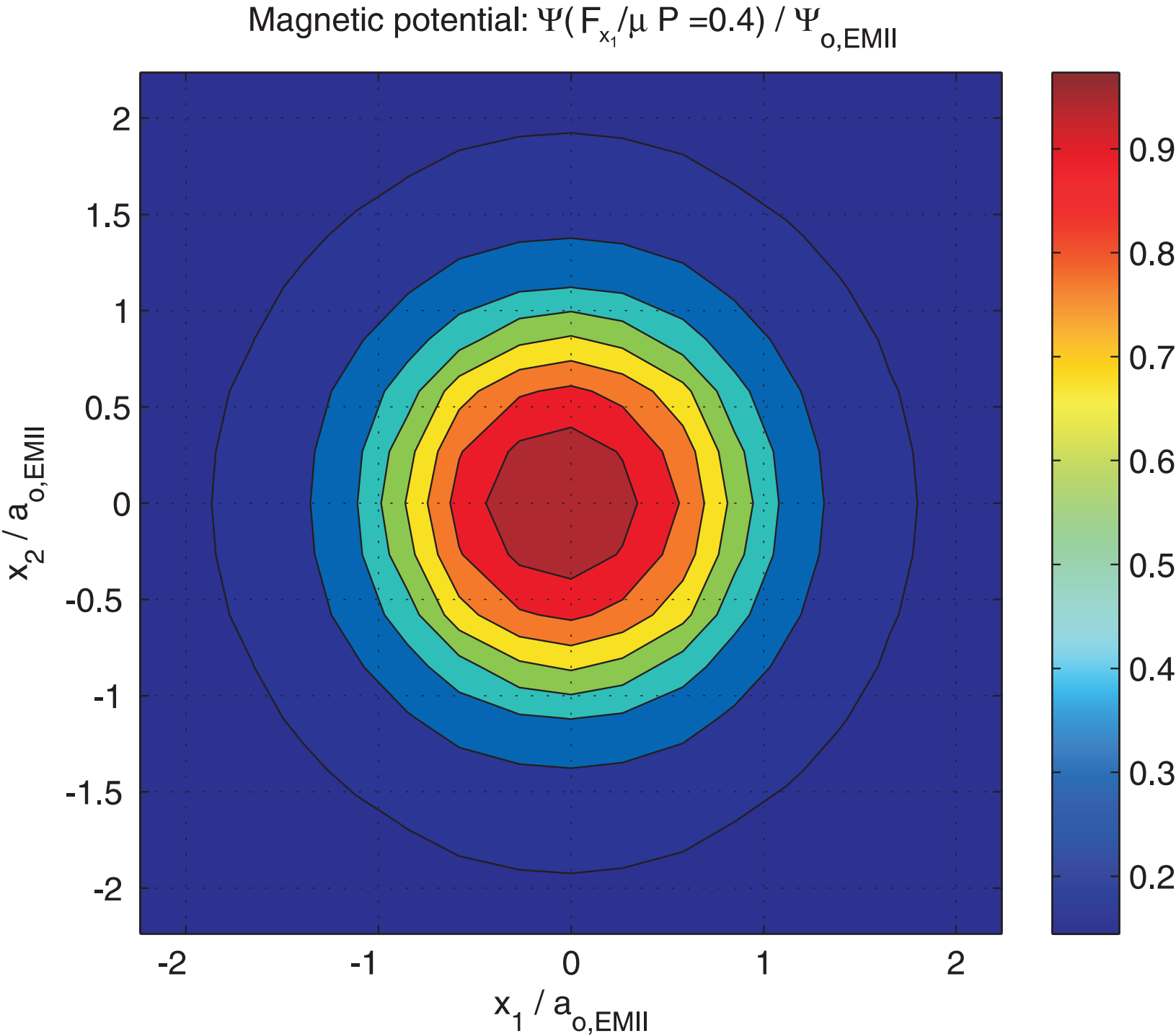
Magnetic potential: Ψ(F x1 /μ P =0.4) / Ψ o,EMII
2
1.5
1
0.5
0
-0.5
-1
-1.5
-2
x2 / ao,EMII
-2
-1
0
1
2
x1 / ao,EMII
0.9
0.8
0.7
0.6
0.5
0.4
0.3
0.2

Figure(s)

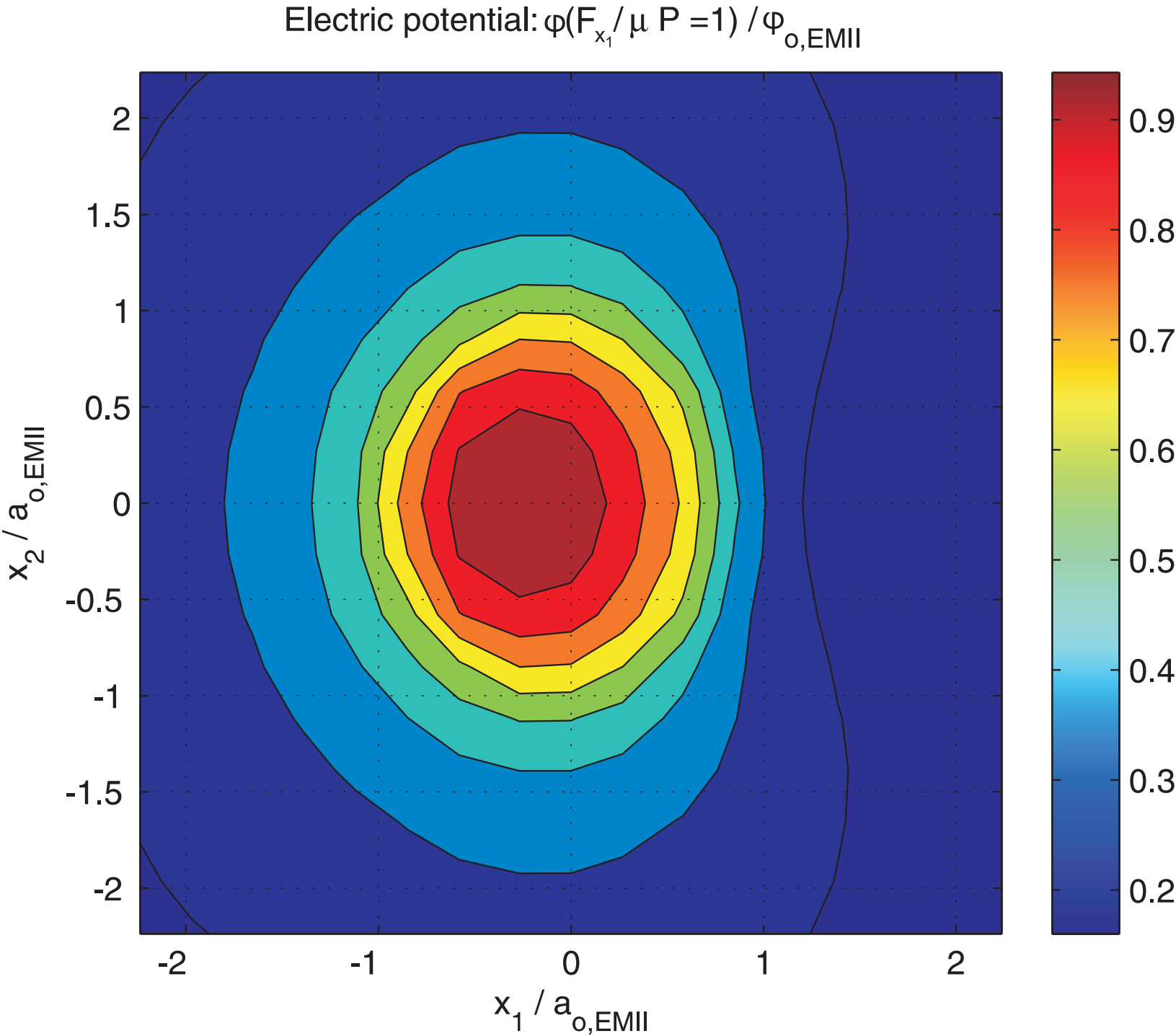
Electric potential: φ(F_x1 / μ P =1) / φ_o,EMII
2
1.5
1
0.5
0
-0.5
-1
-1.5
-2
x_2 / a_o,EMII
-2
-1
0
1
2
x_1 / a_o,EMII
0.9
0.8
0.7
0.6
0.5
0.4
0.3
0.2

Figure(s)

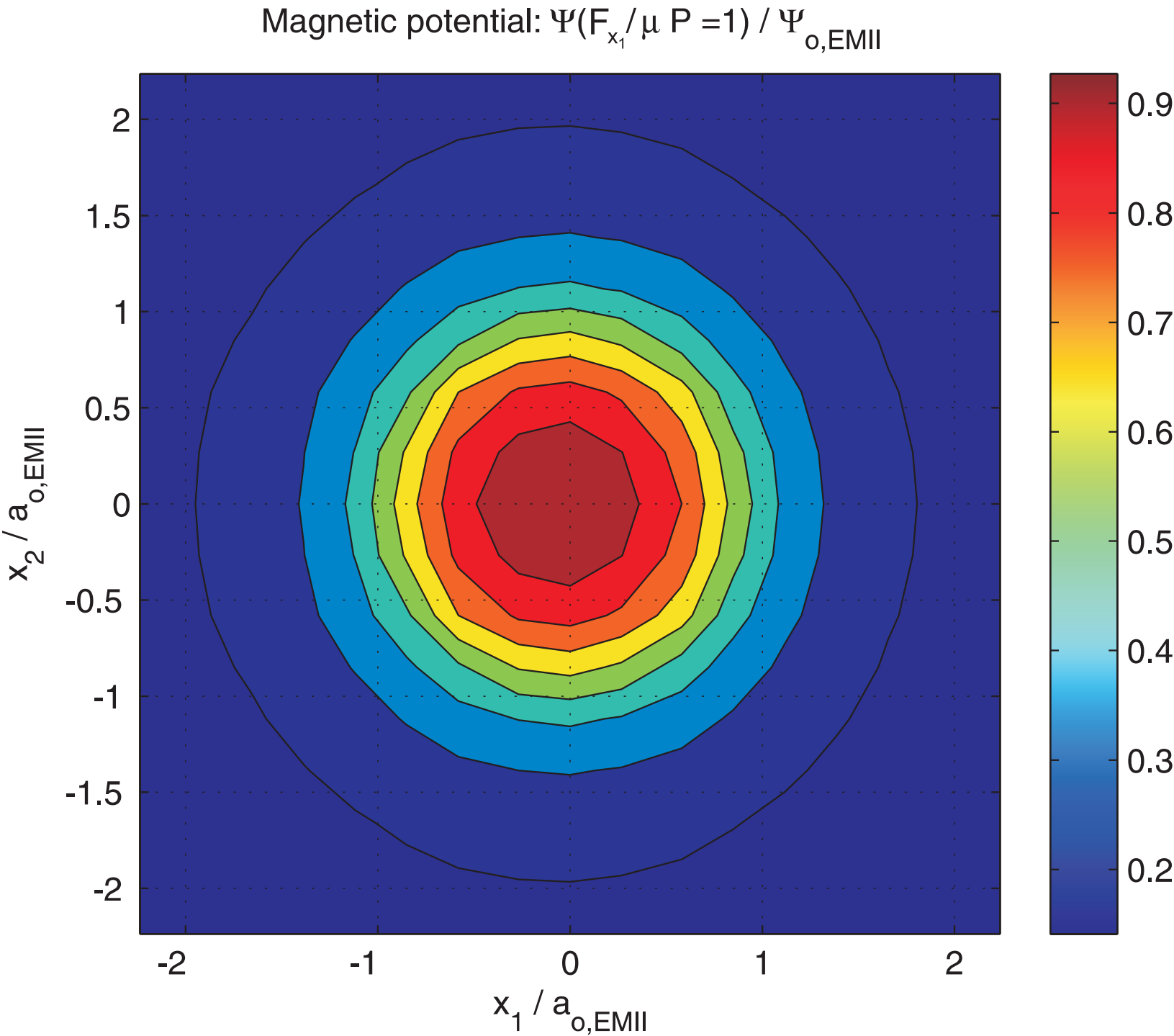
Magnetic potential: Ψ(F_x1 / μ P =1) / Ψ_o,EMII
2
1.5
1
0.5
0
-0.5
-1
-1.5
-2
x_2 / a_o,EMII
-2
-1
0
1
2
x_1 / a_o,EMII
0.9
0.8
0.7
0.6
0.5
0.4
0.3
0.2

Figure(s)

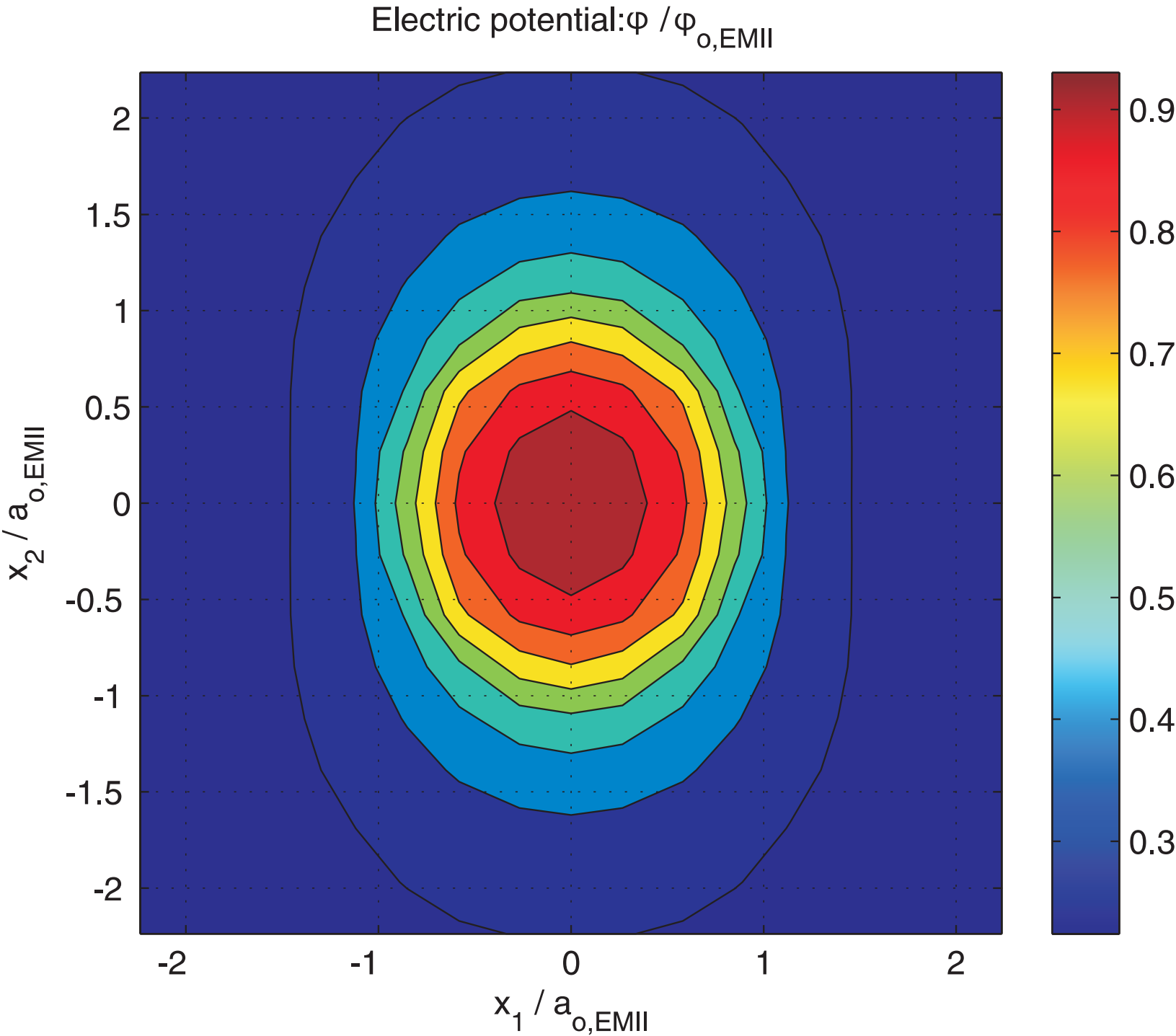
Electric potential:φ / φo,EMII
2
1.5
1
0.5
0
-0.5
-1
-1.5
-2
x2 / ao,EMII
-2
-1
0
1
2
x1 / ao,EMII
0.9
0.8
0.7
0.6
0.5
0.4
0.3

Figure(s)

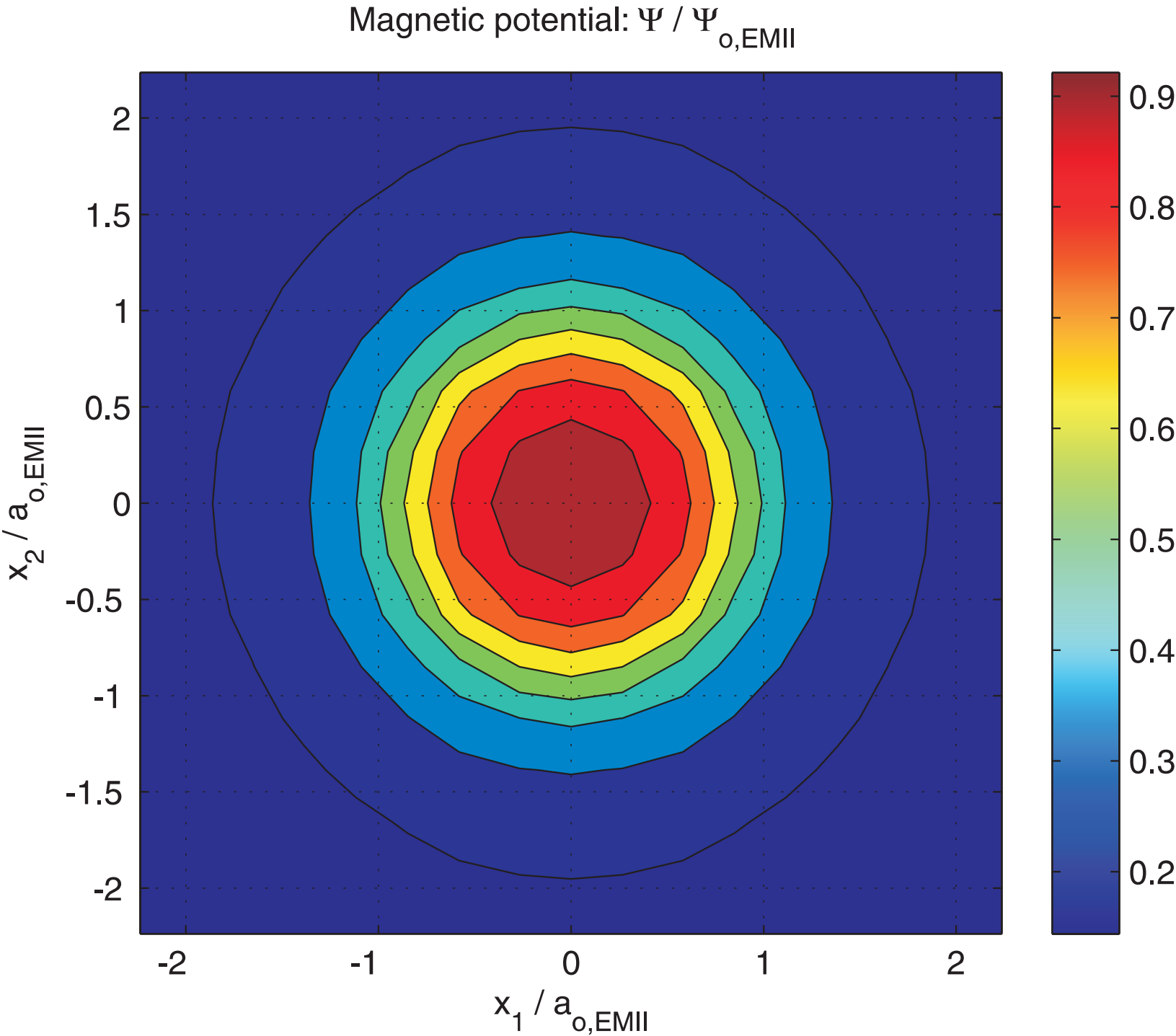
Magnetic potential: Ψ / Ψo,EMII
2
1.5
1
0.5
0
-0.5
-1
-1.5
-2
x2 / ao,EMII
-2
-1
0
1
2
x1 / ao,EMII
0.9
0.8
0.7
0.6
0.5
0.4
0.3
0.2

Figure(s)

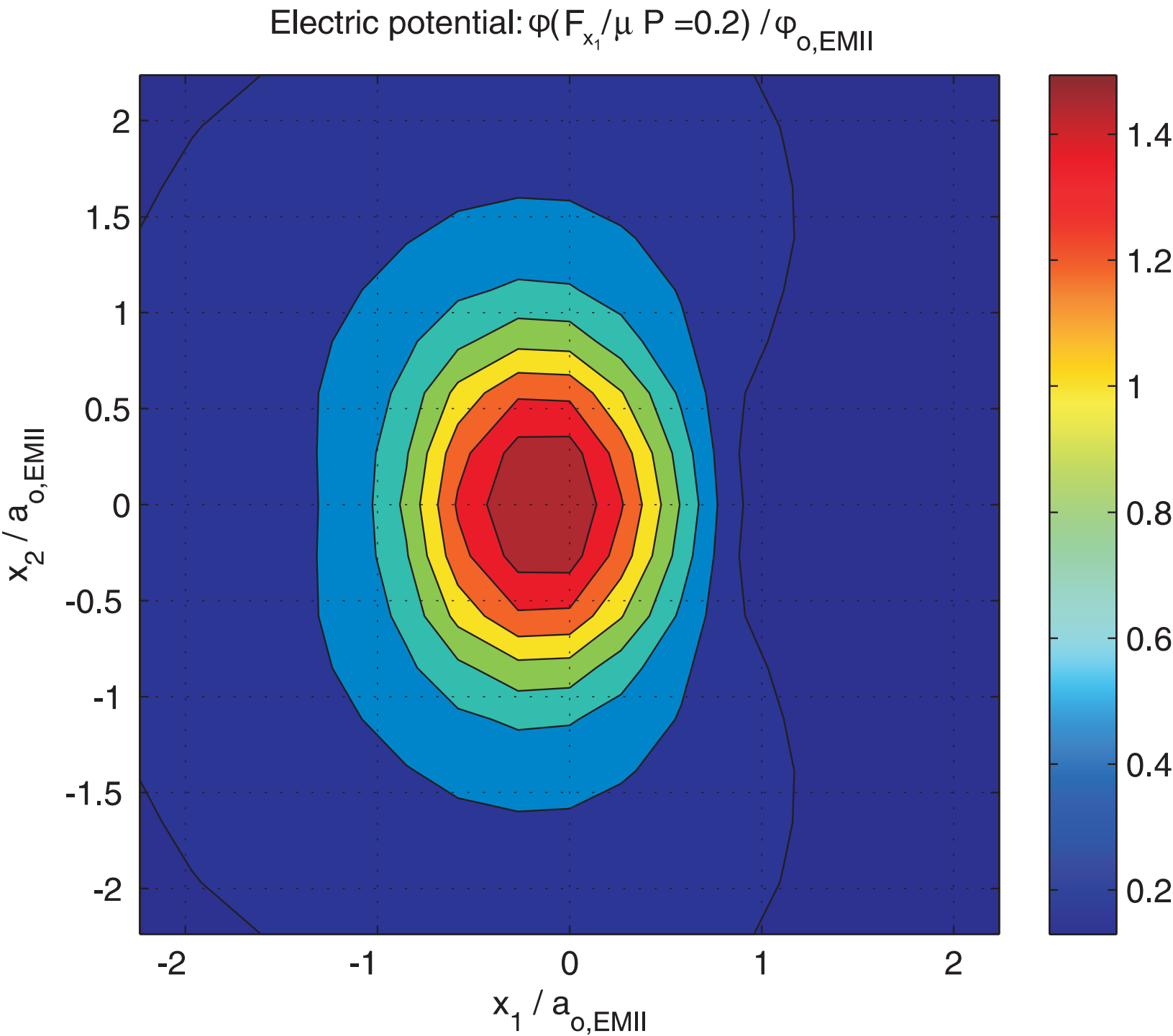
Electric potential: φ(F x1 /μ P =0.2) / φ o,EMII
2
1.5
1
0.5
0
-0.5
-1
-1.5
-2
x2 / ao,EMII
-2
-1
0
1
2
x1 / ao,EMII
1.4
1.2
1
0.8
0.6
0.4
0.2

Figure(s)

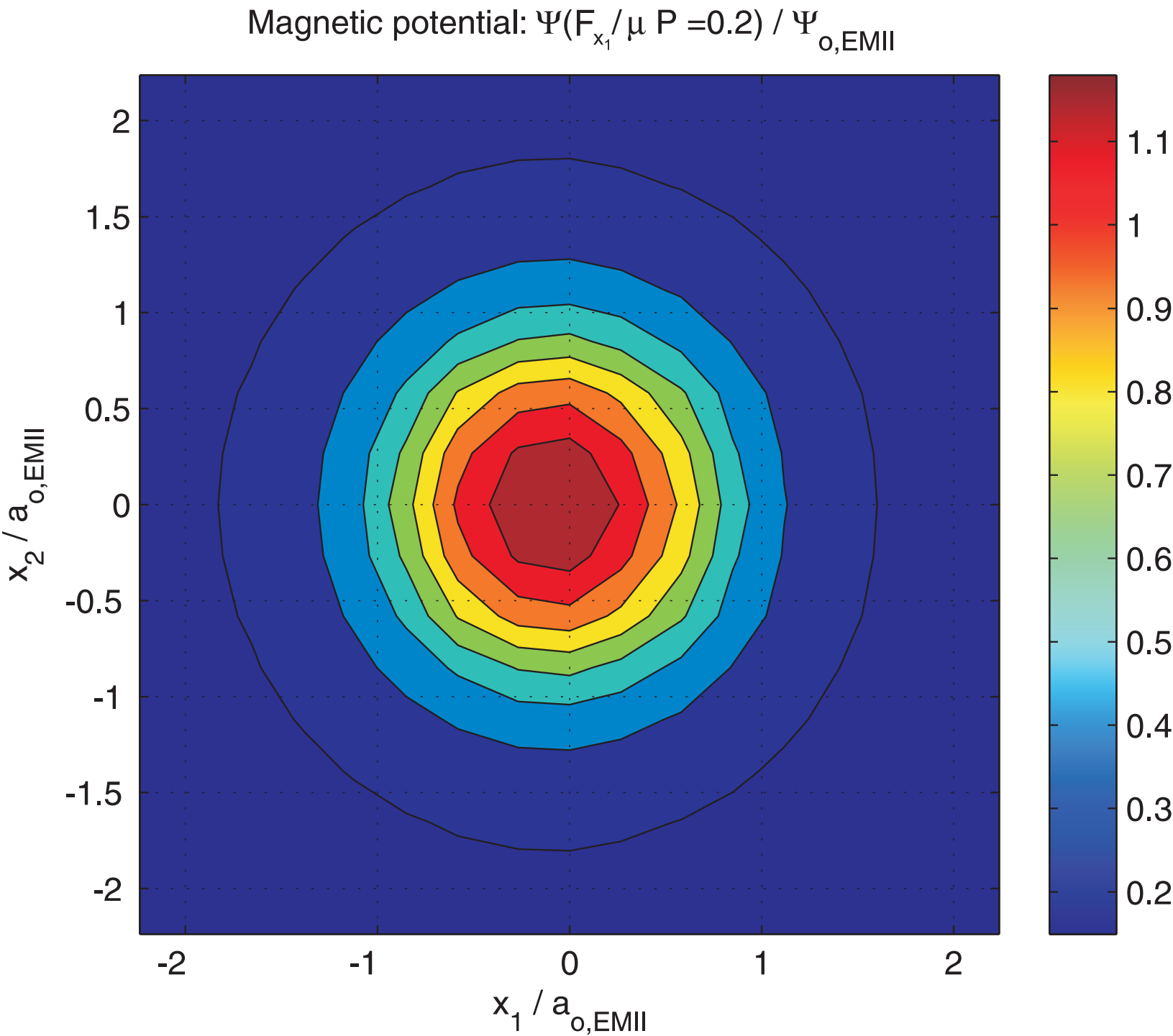
Magnetic potential: Ψ(F_x1 / μ P =0.2) / Ψ_o,EMII
x_2 / a_o,EMII
x_1 / a_o,EMII
2
1.5
1
0.5
0
-0.5
-1
-1.5
-2
-2
-1
0
1
2
1.1
1
0.9
0.8
0.7
0.6
0.5
0.4
0.3
0.2

Figure(s)

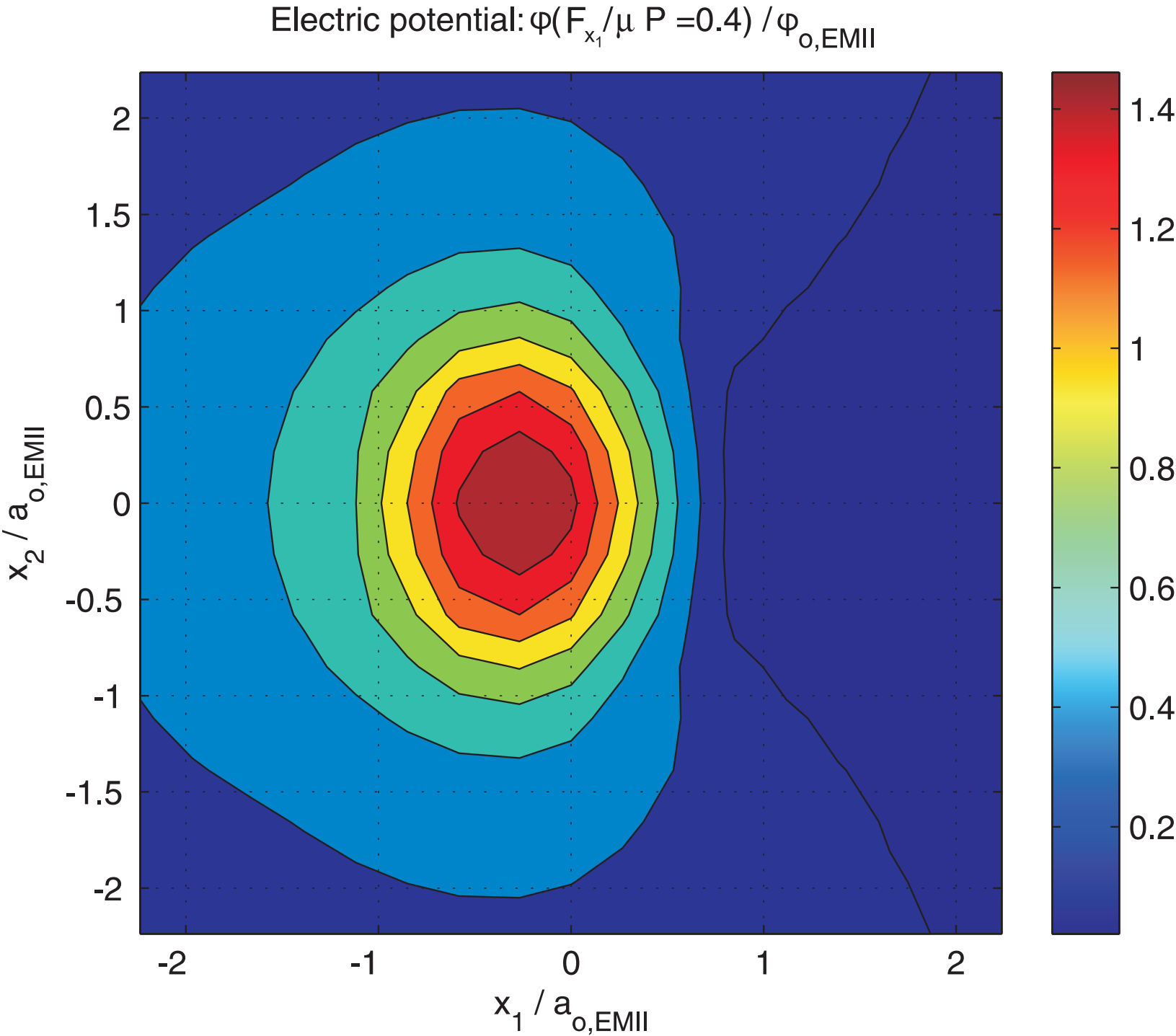
Electric potential: φ(F x1 /μ P =0.4) / φ o,EMII
2
1.5
1
0.5
0
-0.5
-1
-1.5
-2
x2 / ao,EMII
-2
-1
0
1
2
x1 / ao,EMII
1.4
1.2
1
0.8
0.6
0.4
0.2

Figure(s)

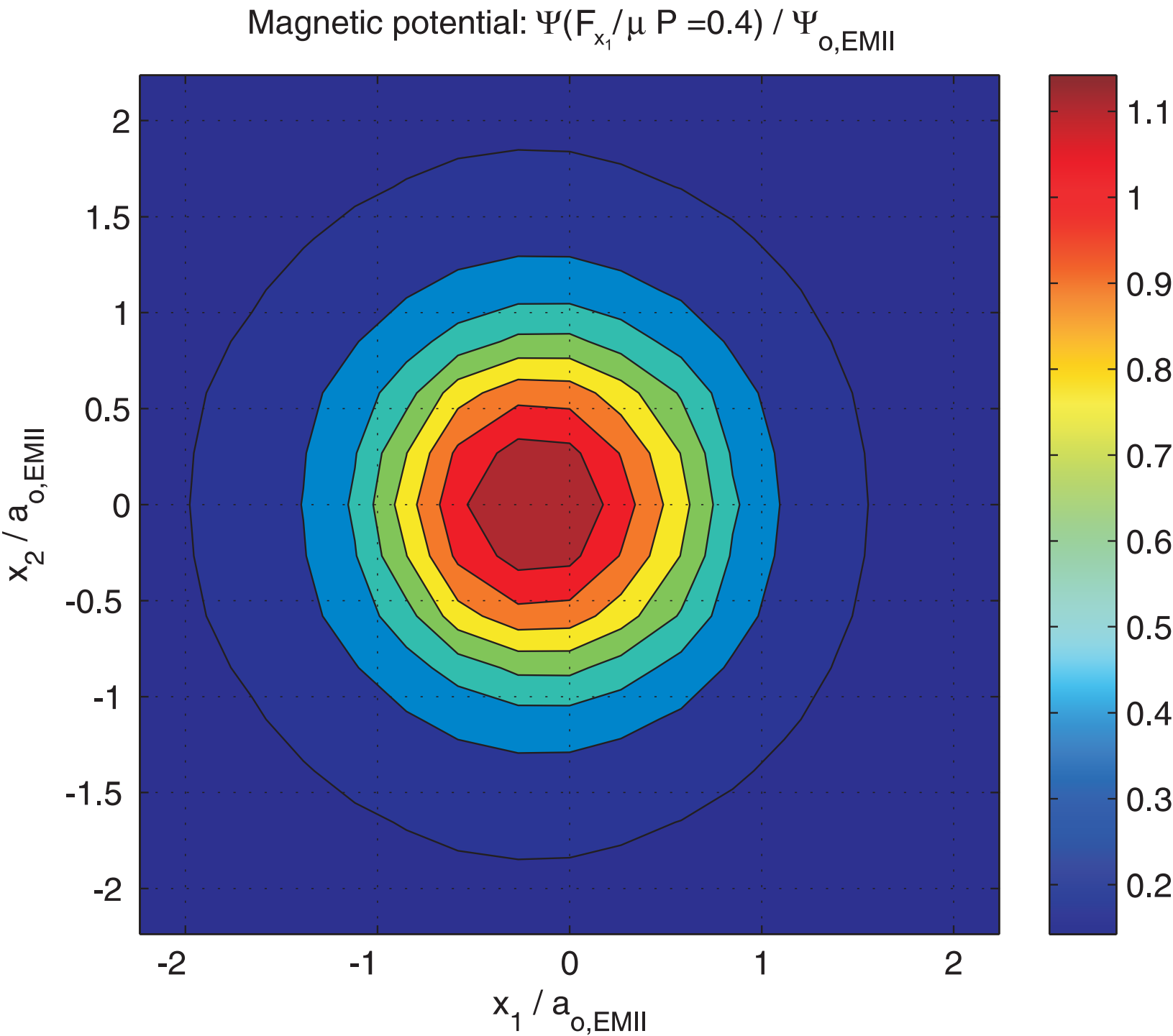
Magnetic potential: Ψ(F_x1/μ P =0.4) / Ψ_o,EMII
2
1.5
1
0.5
0
-0.5
-1
-1.5
-2
x_2 / a_o,EMII
-2
-1
0
1
2
x_1 / a_o,EMII
1.1
1
0.9
0.8
0.7
0.6
0.5
0.4
0.3
0.2

Figure(s)

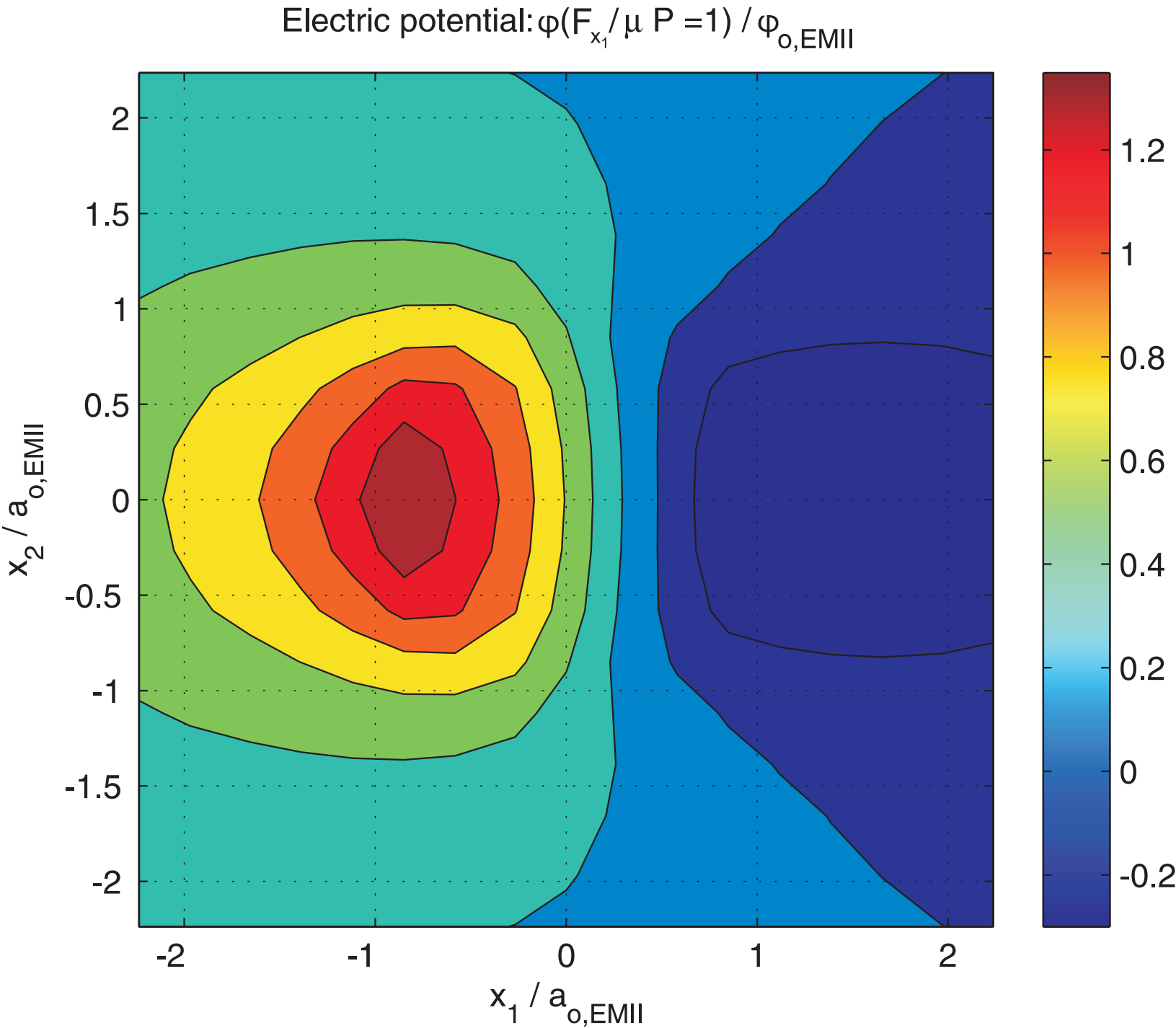
Electric potential: φ(F_x1 / μ P =1) / φ_o,EMII
2
1.5
1
0.5
0
-0.5
-1
-1.5
-2
x_2 / a_o,EMII
-2
-1
0
1
2
x_1 / a_o,EMII
1.2
1
0.8
0.6
0.4
0.2
0
-0.2

Figure(s)

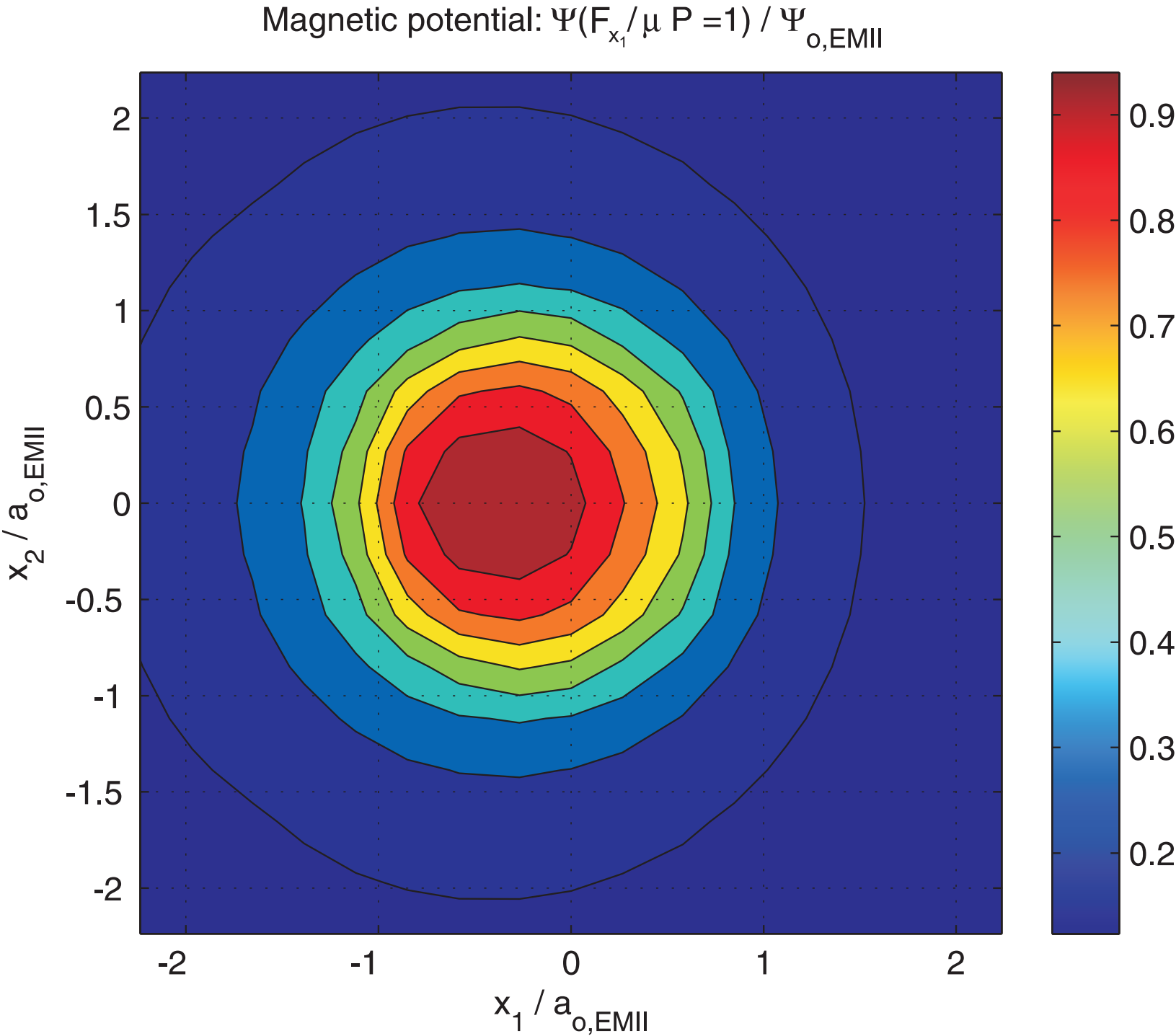
Magnetic potential: Ψ(F_x1 / μ P =1) / Ψ_o,EMII
2
1.5
1
0.5
0
-0.5
-1
-1.5
-2
x_2 / a_o,EMII
-2
-1
0
1
2
x_1 / a_o,EMII
0.9
0.8
0.7
0.6
0.5
0.4
0.3
0.2

Figure(s)

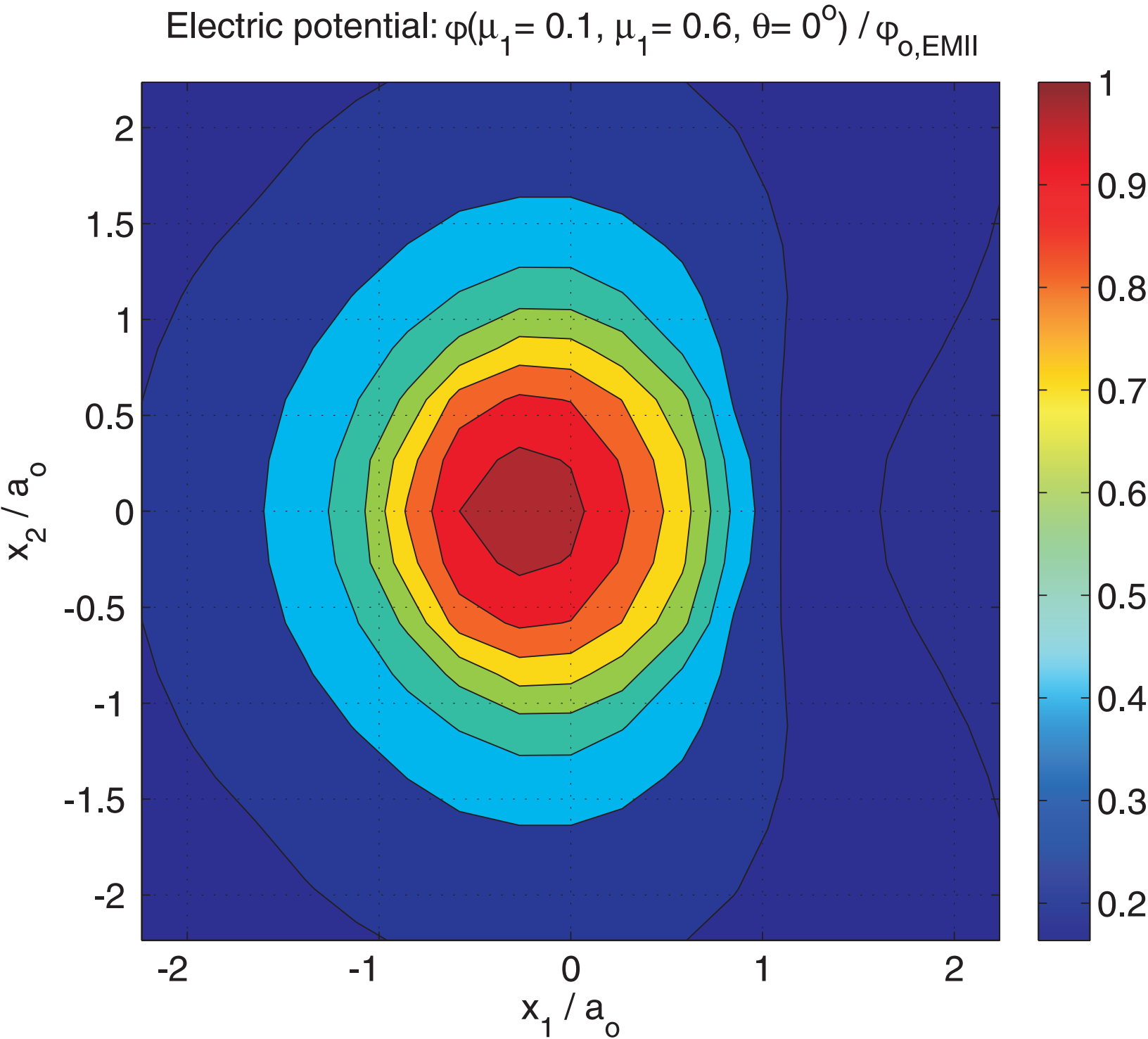
Electric potential: φ(μ1= 0.1, μ1= 0.6, θ= 0°) / φo,EMII
x2 / ao
x1 / ao
2
1.5
1
0.5
0
-0.5
-1
-1.5
-2
-2
-1
0
1
2
1
0.9
0.8
0.7
0.6
0.5
0.4
0.3
0.2

Figure(s)

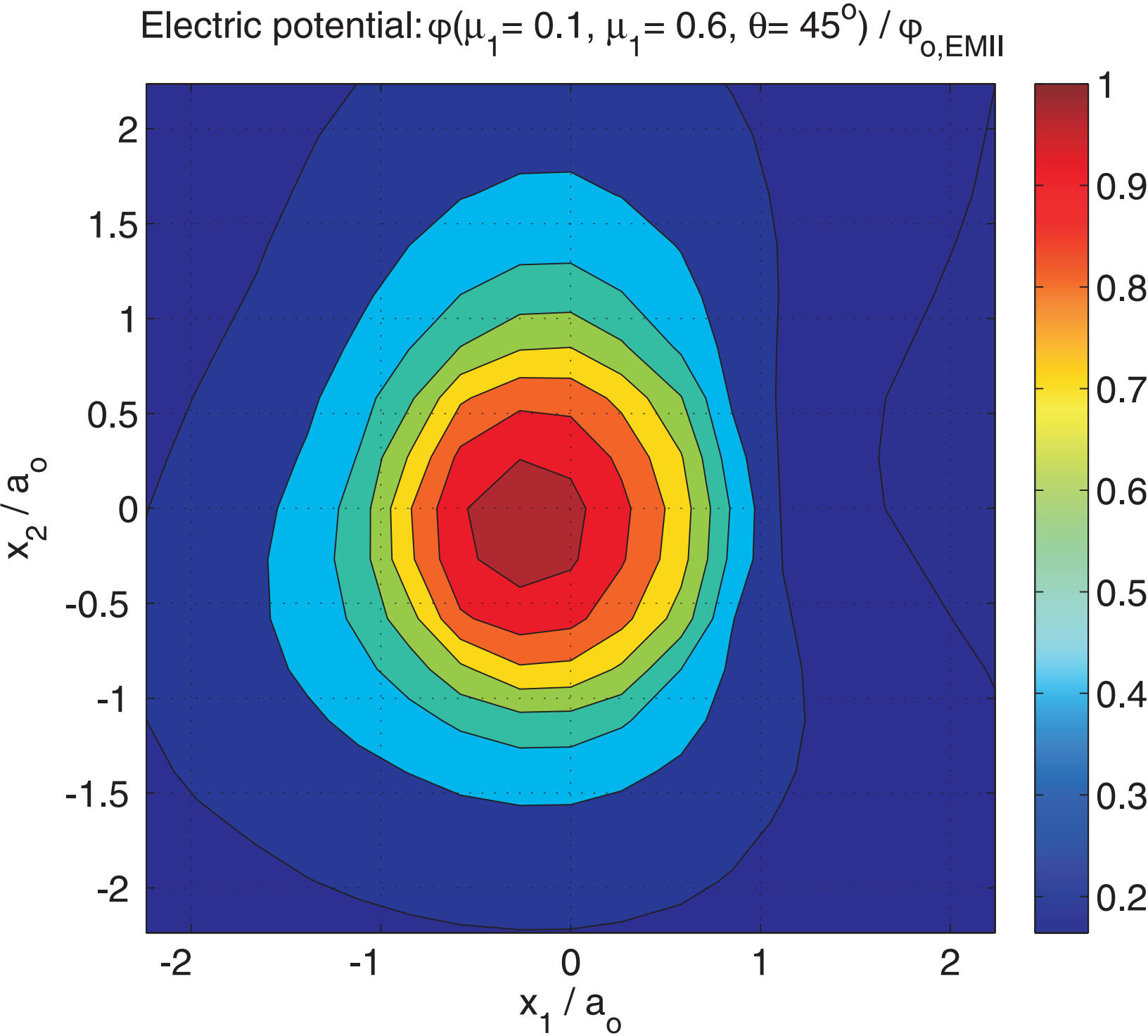
Electric potential: φ(μ1= 0.1, μ1= 0.6, θ= 45°) / φo,EMII
2
1.5
1
0.5
0
-0.5
-1
-1.5
-2
x2 / ao
-2
-1
0
1
2
x1 / ao
1
0.9
0.8
0.7
0.6
0.5
0.4
0.3
0.2

Figure(s)

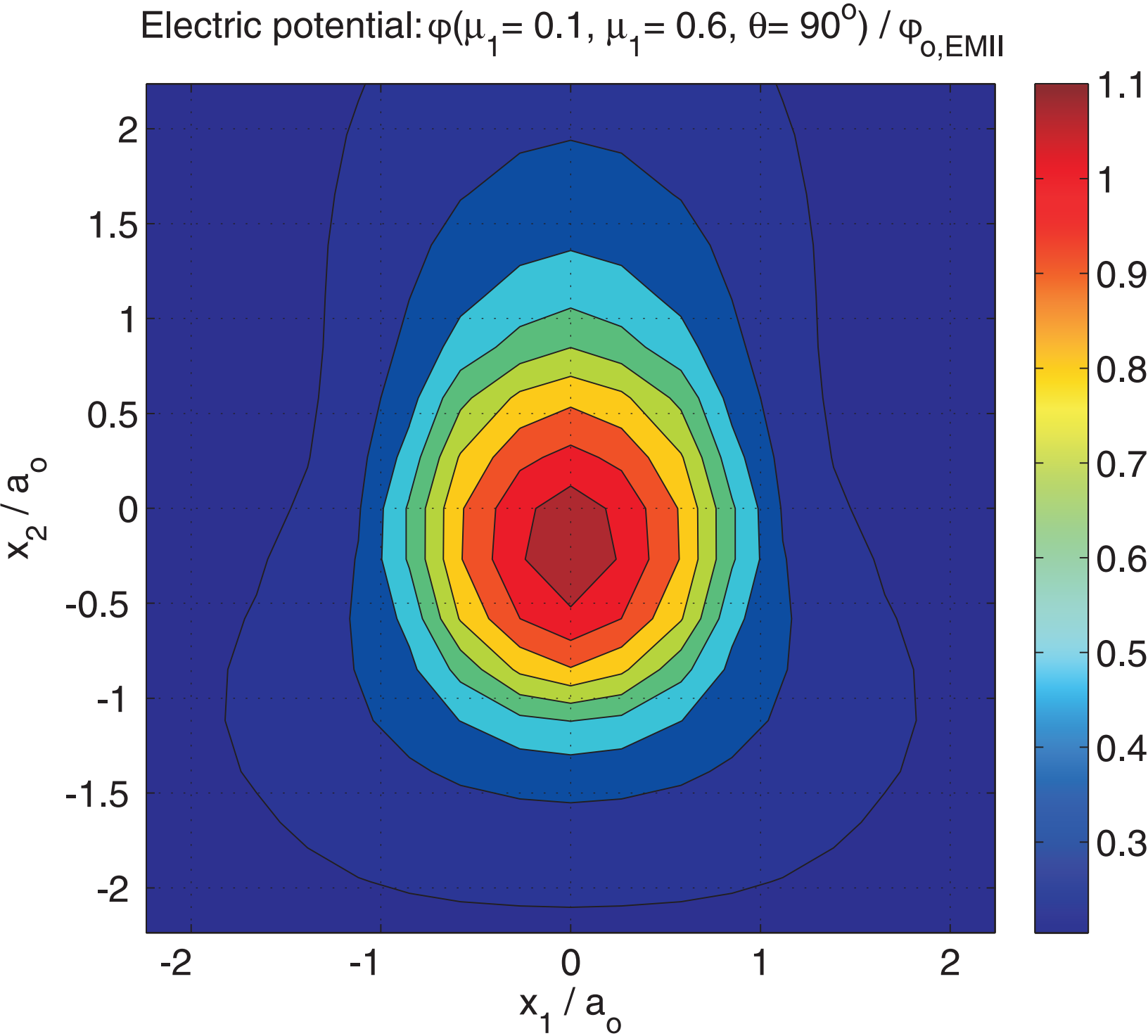
Electric potential: φ(μ1= 0.1, μ1= 0.6, θ= 90°) / φo,EMII
x2 / ao
x1 / ao
2
1.5
1
0.5
0
-0.5
-1
-1.5
-2
-2
-1
0
1
2
1.1
1
0.9
0.8
0.7
0.6
0.5
0.4
0.3

Figure(s)

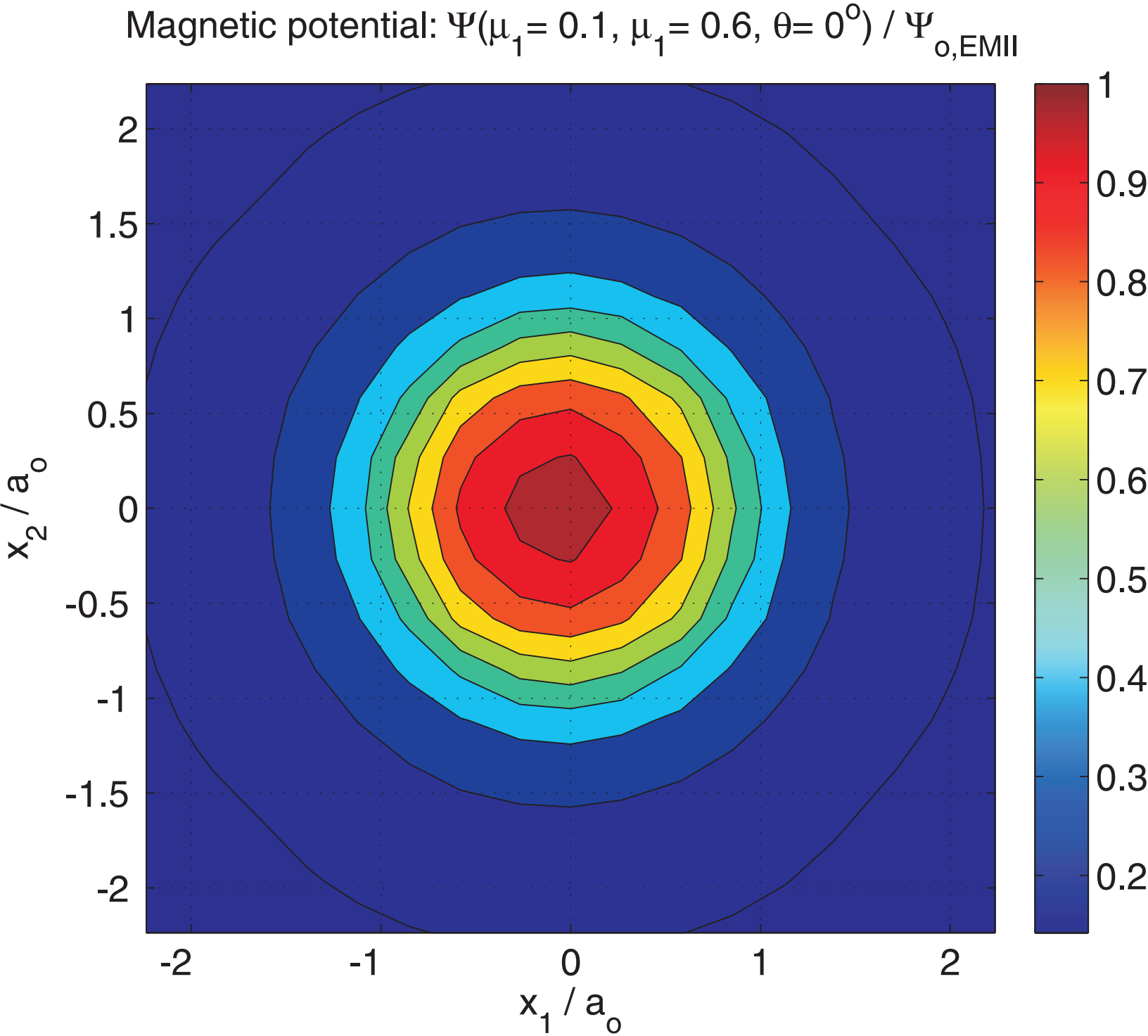
Magnetic potential: Ψ(μ1= 0.1, μ1= 0.6, θ= 0°) / Ψo,EMII
2
1.5
1
0.5
0
-0.5
-1
-1.5
-2
x2 / ao
-2
-1
0
1
2
x1 / ao
1
0.9
0.8
0.7
0.6
0.5
0.4
0.3
0.2

Figure(s)

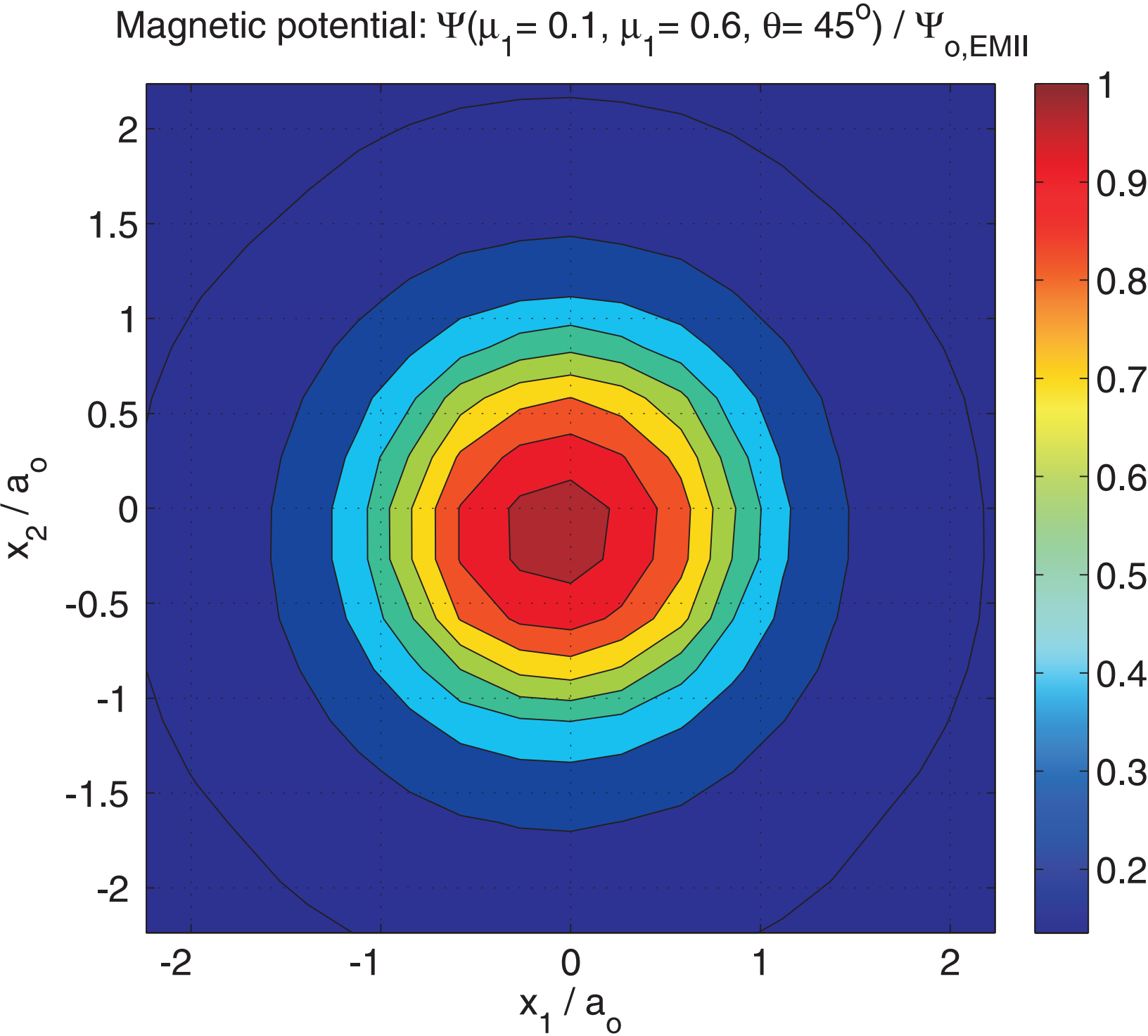
Magnetic potential: Ψ(μ1= 0.1, μ1= 0.6, θ= 45°) / Ψo,EMII
2
1.5
1
0.5
0
-0.5
-1
-1.5
-2
x2 / ao
-2
-1
0
1
2
x1 / ao
1
0.9
0.8
0.7
0.6
0.5
0.4
0.3
0.2

Figure(s)

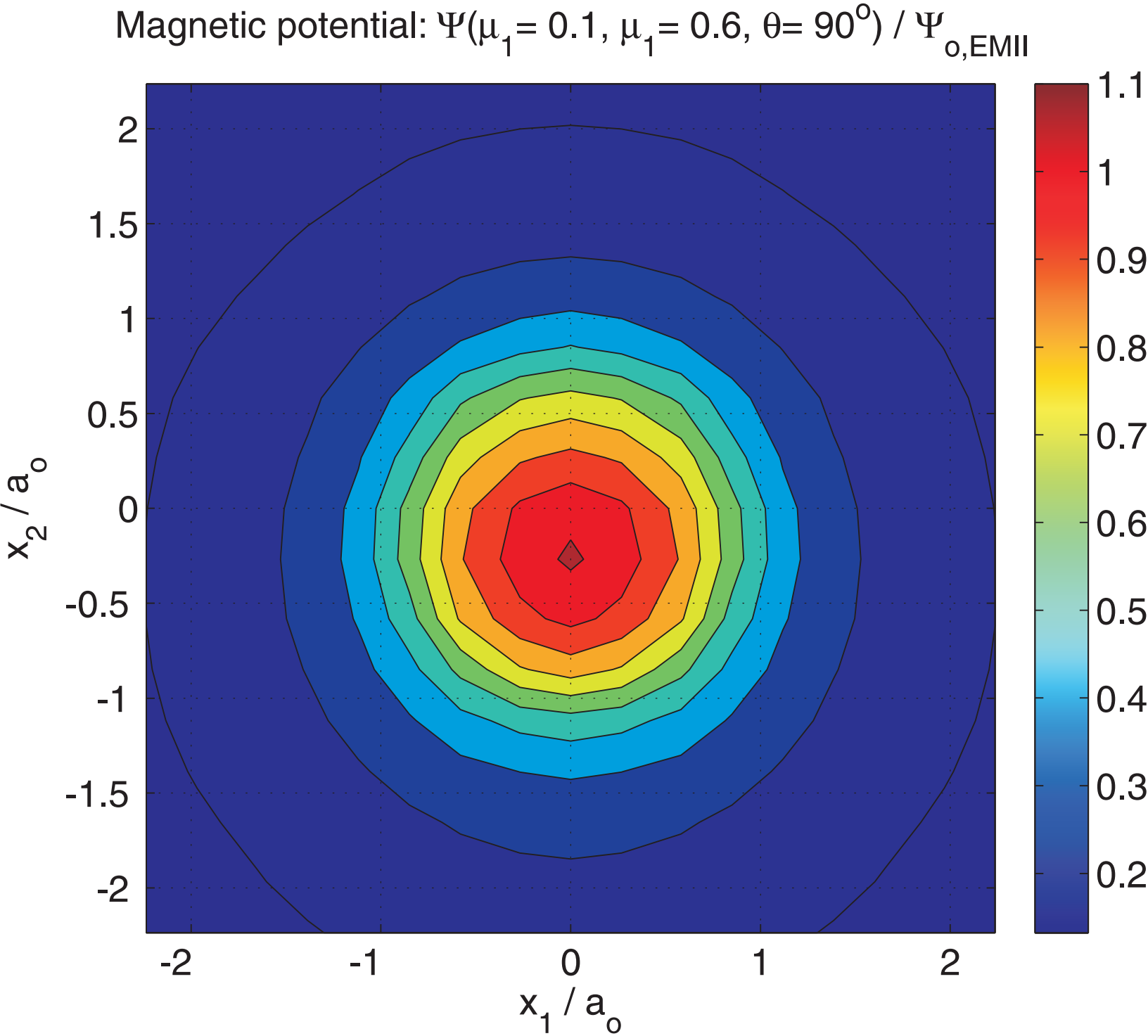
Magnetic potential: Ψ(μ1= 0.1, μ1= 0.6, θ= 90°) / Ψo,EMII
2
1.5
1
0.5
0
-0.5
-1
-1.5
-2
x2 / ao
-2
-1
0
1
2
x1 / ao
1.1
1
0.9
0.8
0.7
0.6
0.5
0.4
0.3
0.2

Figure(s)

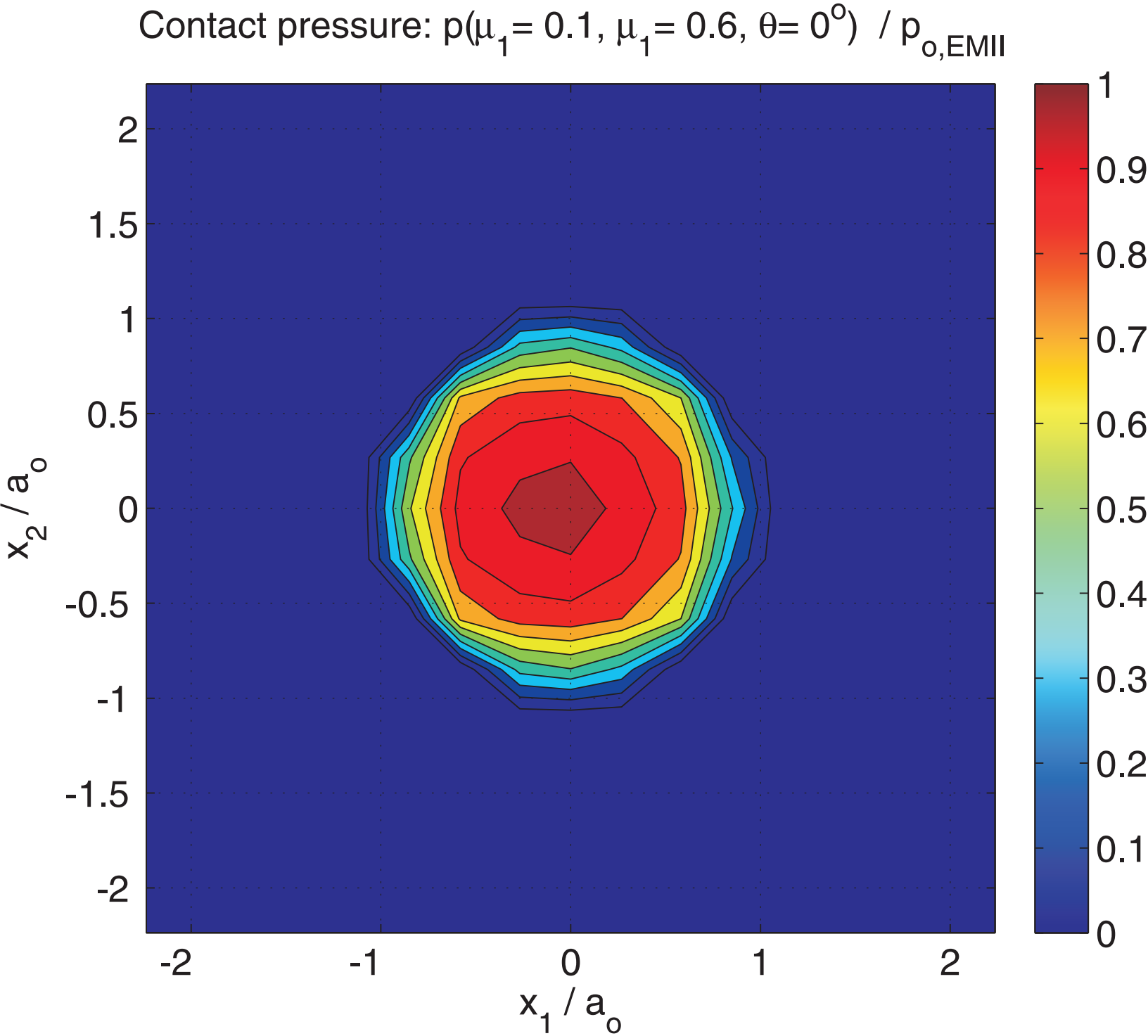
Contact pressure: p(μ1= 0.1, μ1= 0.6, θ= 0°) / po,EMII
x2 / ao
x1 / ao
2
1.5
1
0.5
0
-0.5
-1
-1.5
-2
-2
-1
0
1
2
1
0.9
0.8
0.7
0.6
0.5
0.4
0.3
0.2
0.1
0

Figure(s)

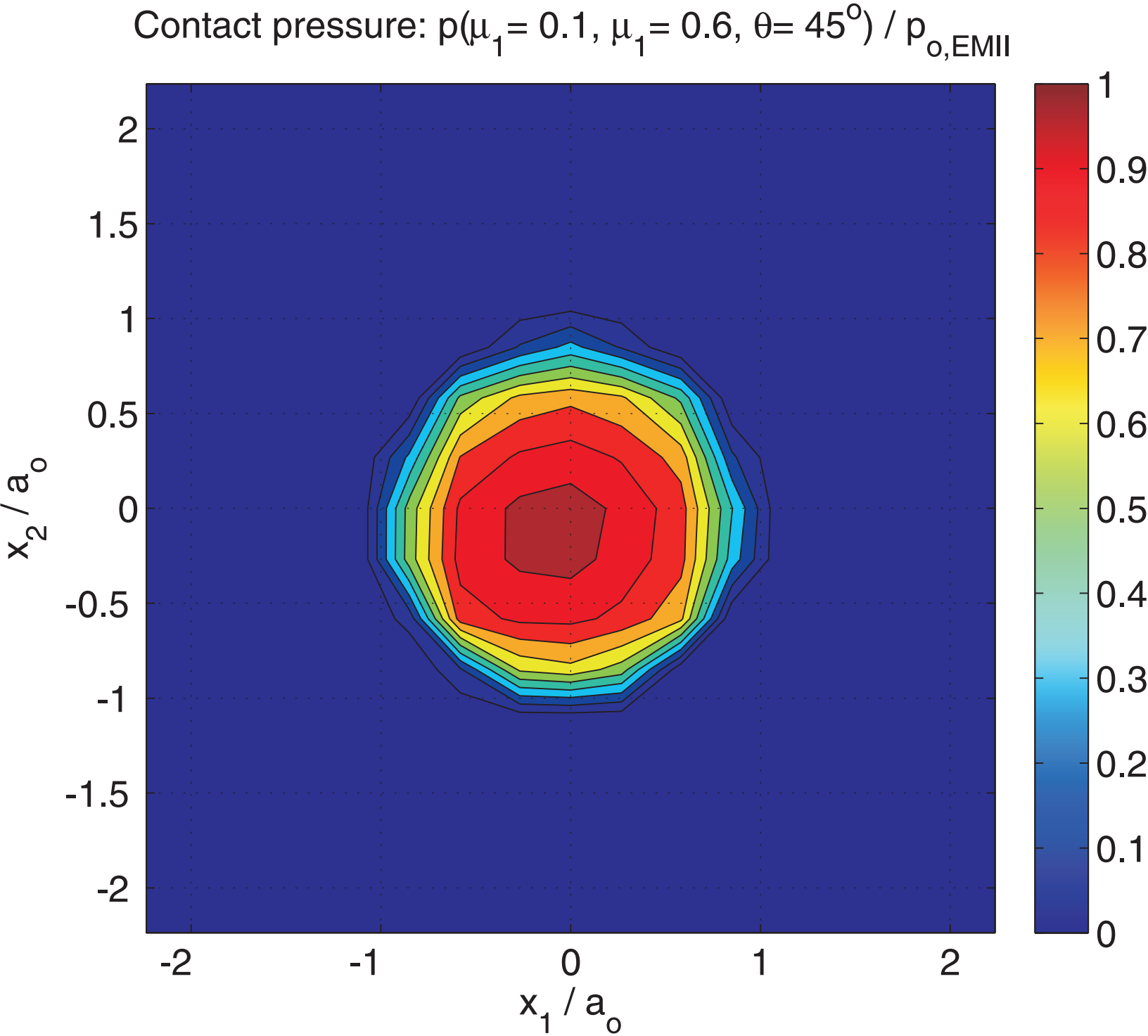
Contact pressure: p(μ1= 0.1, μ1= 0.6, θ= 45°) / po,EMII
2
1.5
1
0.5
0
-0.5
-1
-1.5
-2
x2 / ao
-2
-1
0
1
2
x1 / ao
1
0.9
0.8
0.7
0.6
0.5
0.4
0.3
0.2
0.1
0

Figure(s)

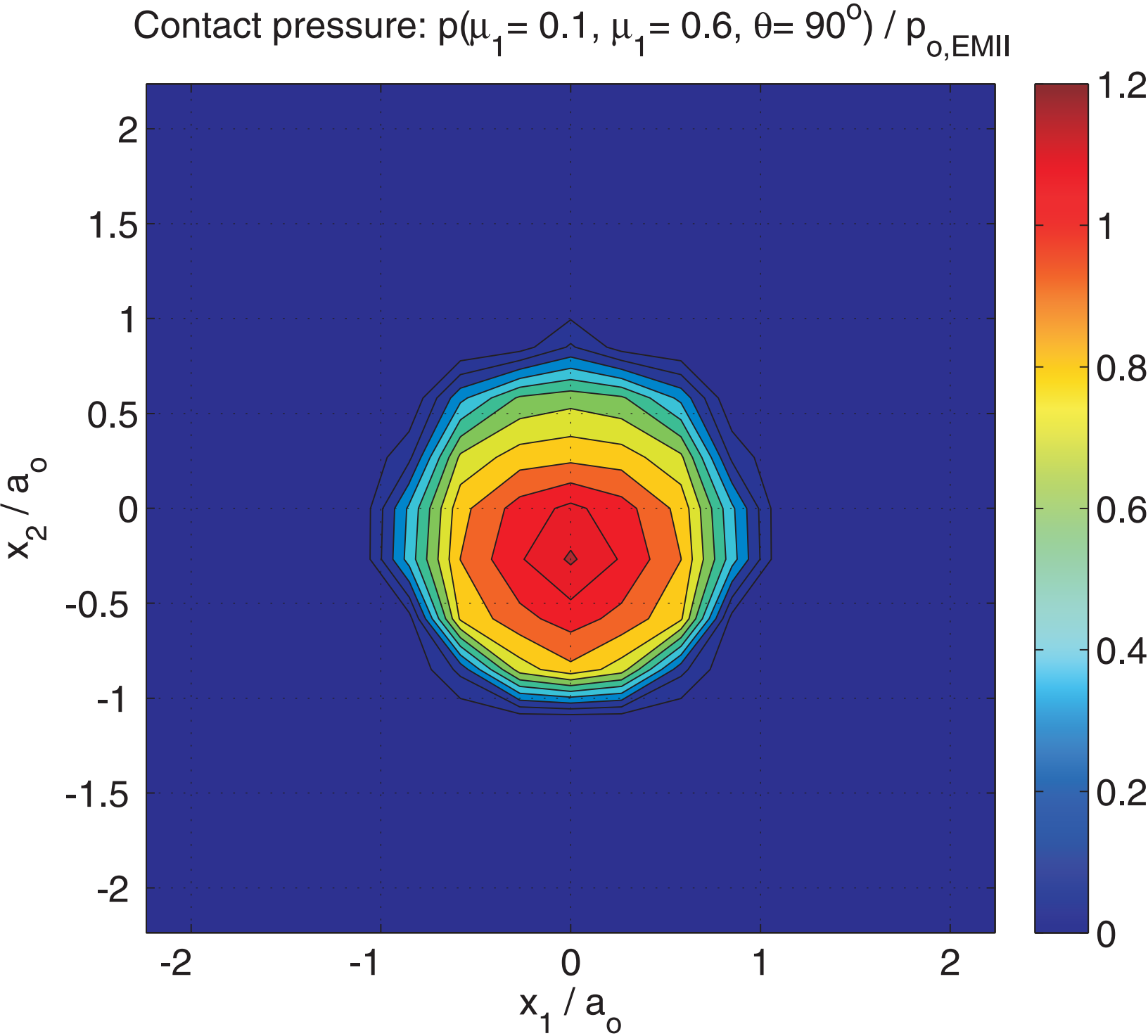
Contact pressure: p(μ1= 0.1, μ1= 0.6, θ= 90°) / po,EMII
2
1.5
1
0.5
0
-0.5
-1
-1.5
-2
x2 / ao
-2
-1
0
1
2
x1 / ao
1.2
1
0.8
0.6
0.4
0.2
0

Figure(s)

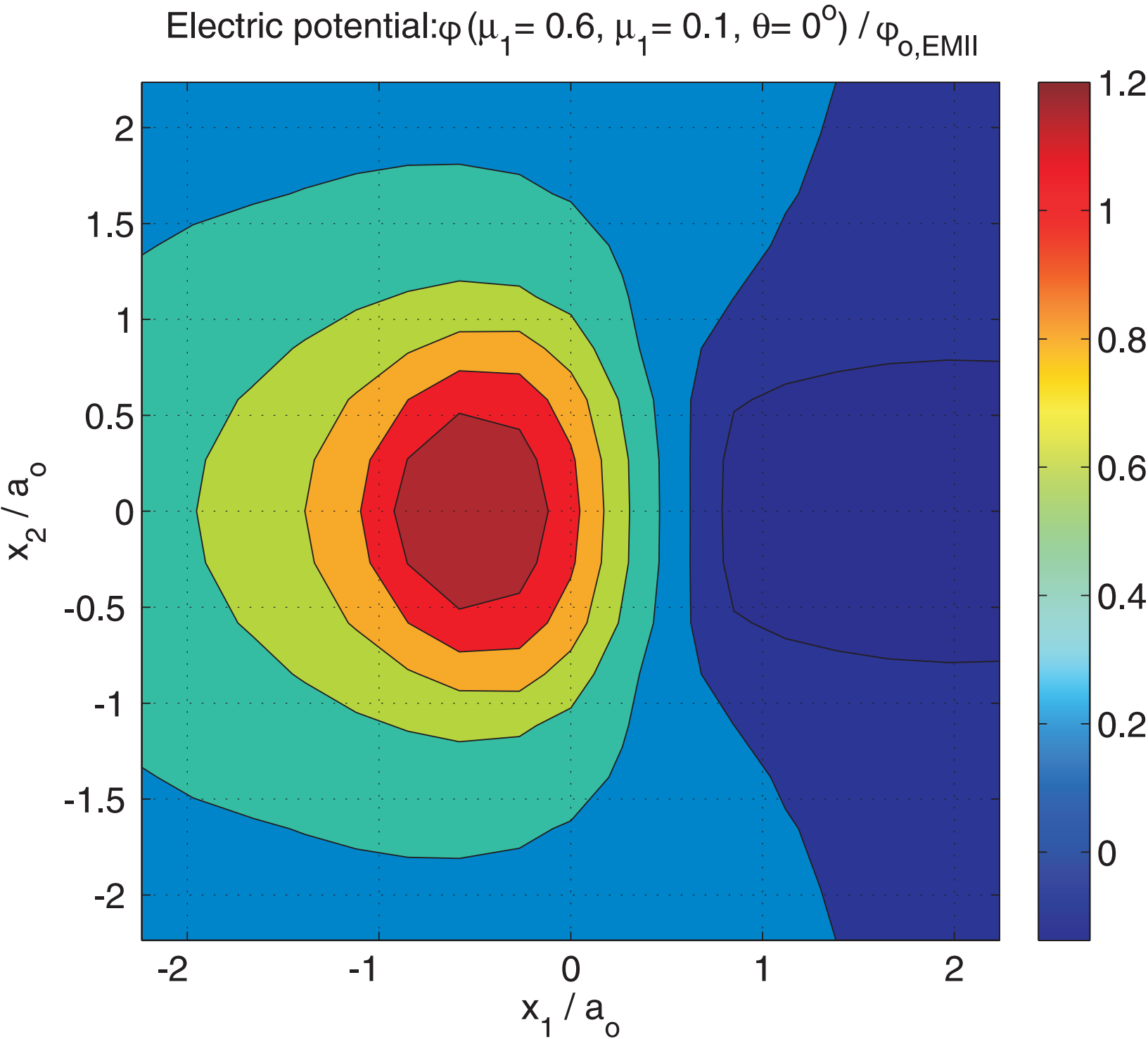
Electric potential:φ (μ1= 0.6, μ1= 0.1, θ= 0°) / φo,EMII
x2 / ao
x1 / ao
2
1.5
1
0.5
0
-0.5
-1
-1.5
-2
-2
-1
0
1
2
1.2
1
0.8
0.6
0.4
0.2
0

Figure(s)

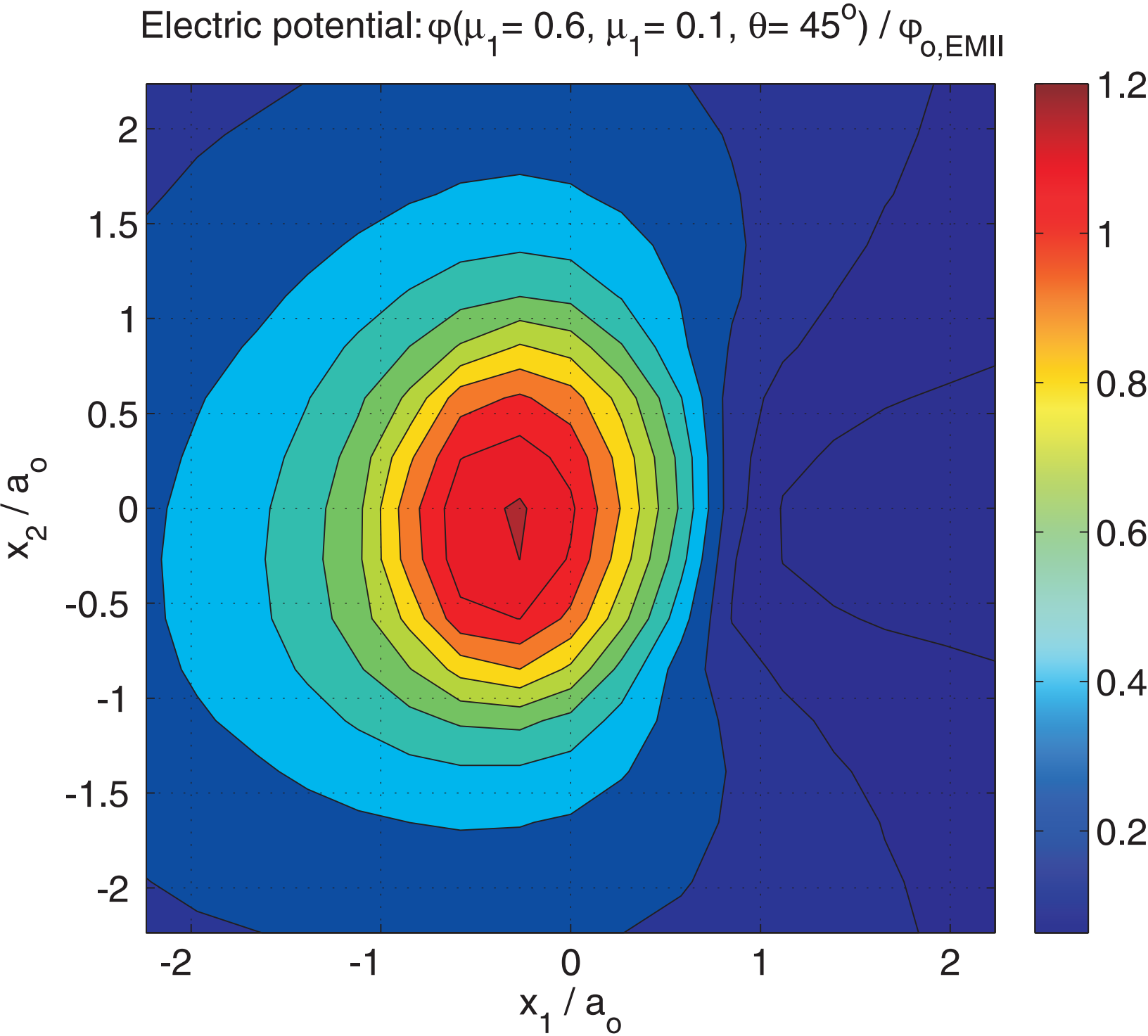
Electric potential: φ(μ1= 0.6, μ1= 0.1, θ= 45°) / φo,EMII
x2 / ao
x1 / ao
2
1.5
1
0.5
0
-0.5
-1
-1.5
-2
-2
-1
0
1
2
1.2
1
0.8
0.6
0.4
0.2

Figure(s)

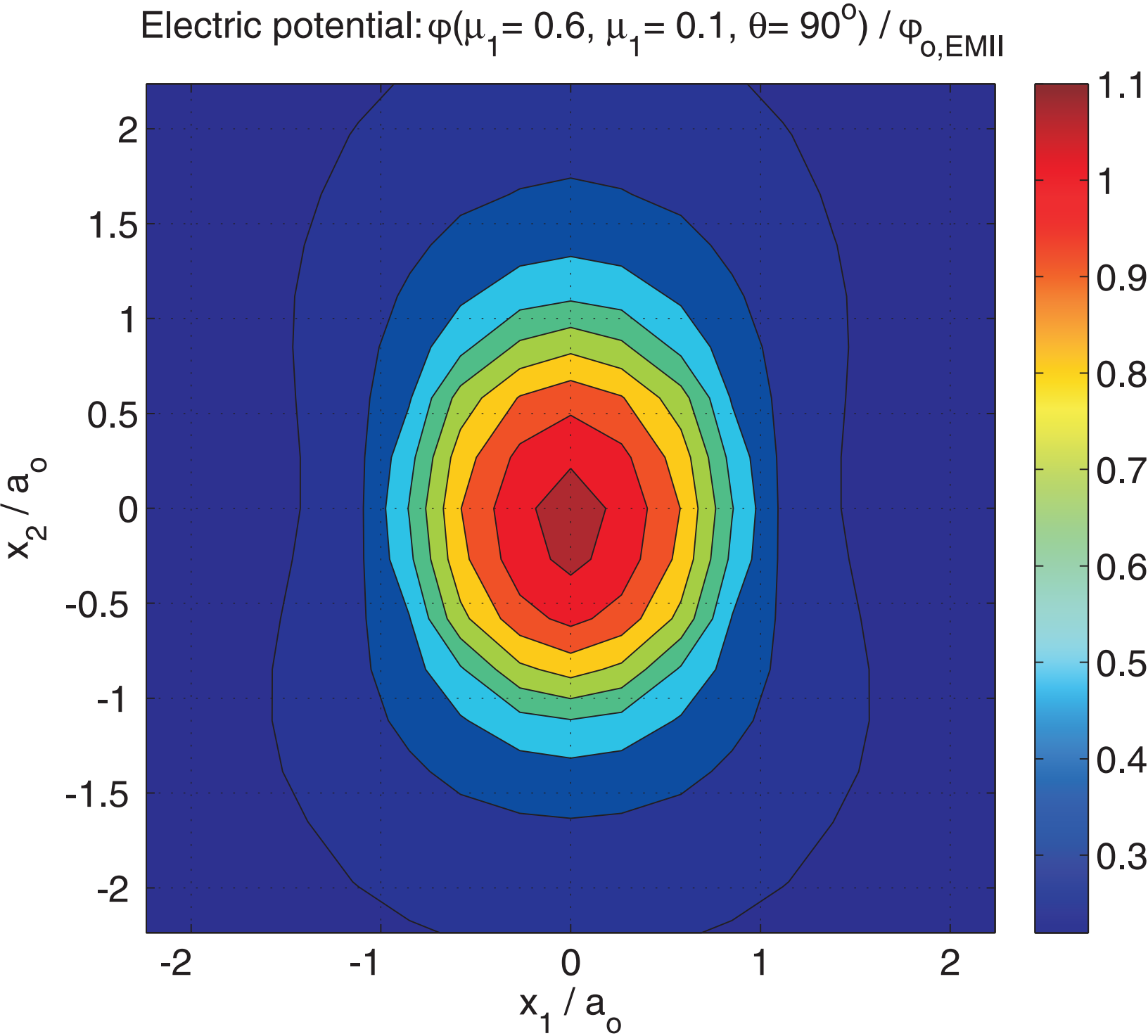
Electric potential: φ(μ1= 0.6, μ1= 0.1, θ= 90°) / φo,EMII
2
1.5
1
0.5
0
-0.5
-1
-1.5
-2
x2 / ao
-2
-1
0
1
2
x1 / ao
1.1
1
0.9
0.8
0.7
0.6
0.5
0.4
0.3

Figure(s)

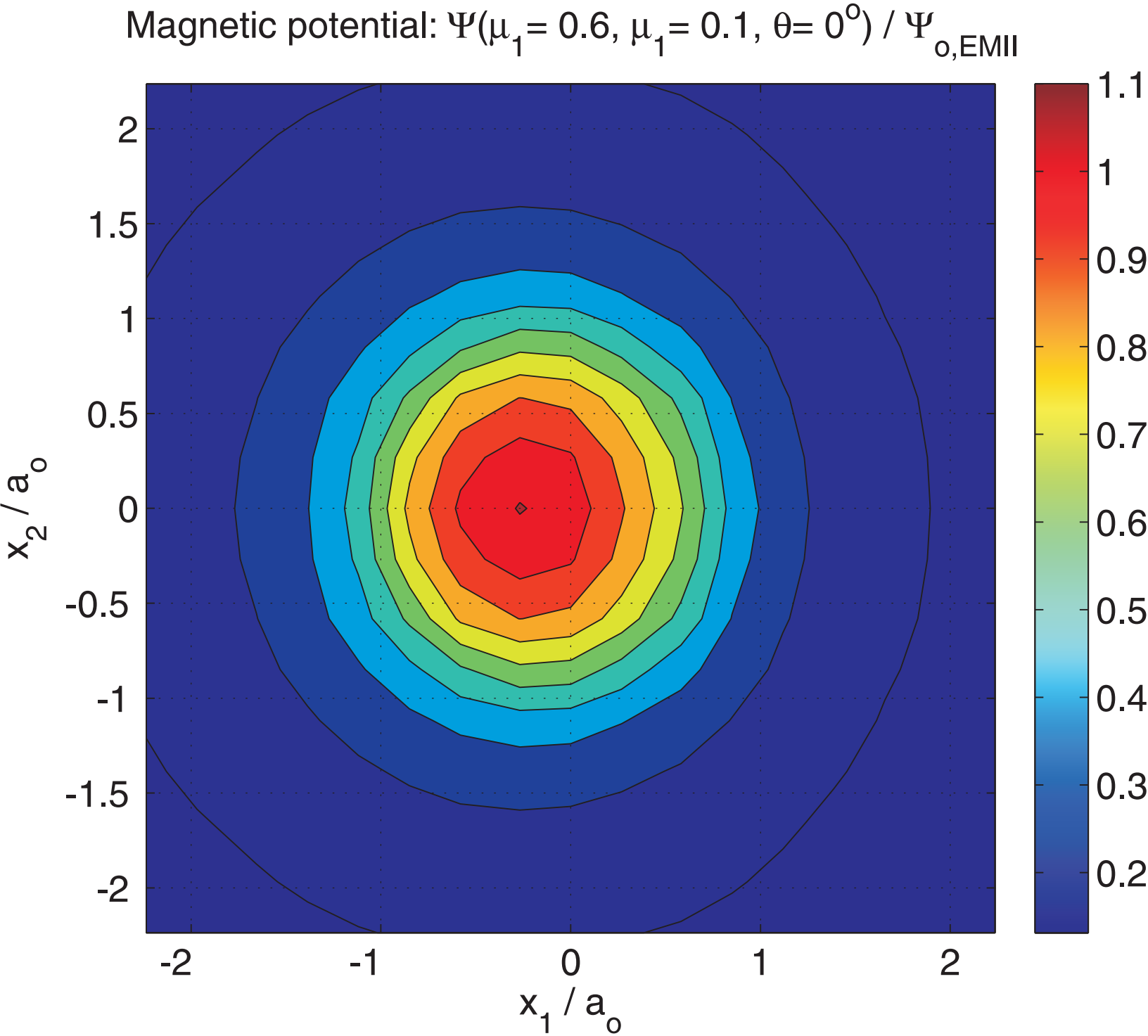
Magnetic potential: Ψ(μ1= 0.6, μ1= 0.1, θ= 0°) / Ψo,EMII
x2 / ao
x1 / ao
2
1.5
1
0.5
0
-0.5
-1
-1.5
-2
-2
-1
0
1
2
1.1
1
0.9
0.8
0.7
0.6
0.5
0.4
0.3
0.2

Figure(s)

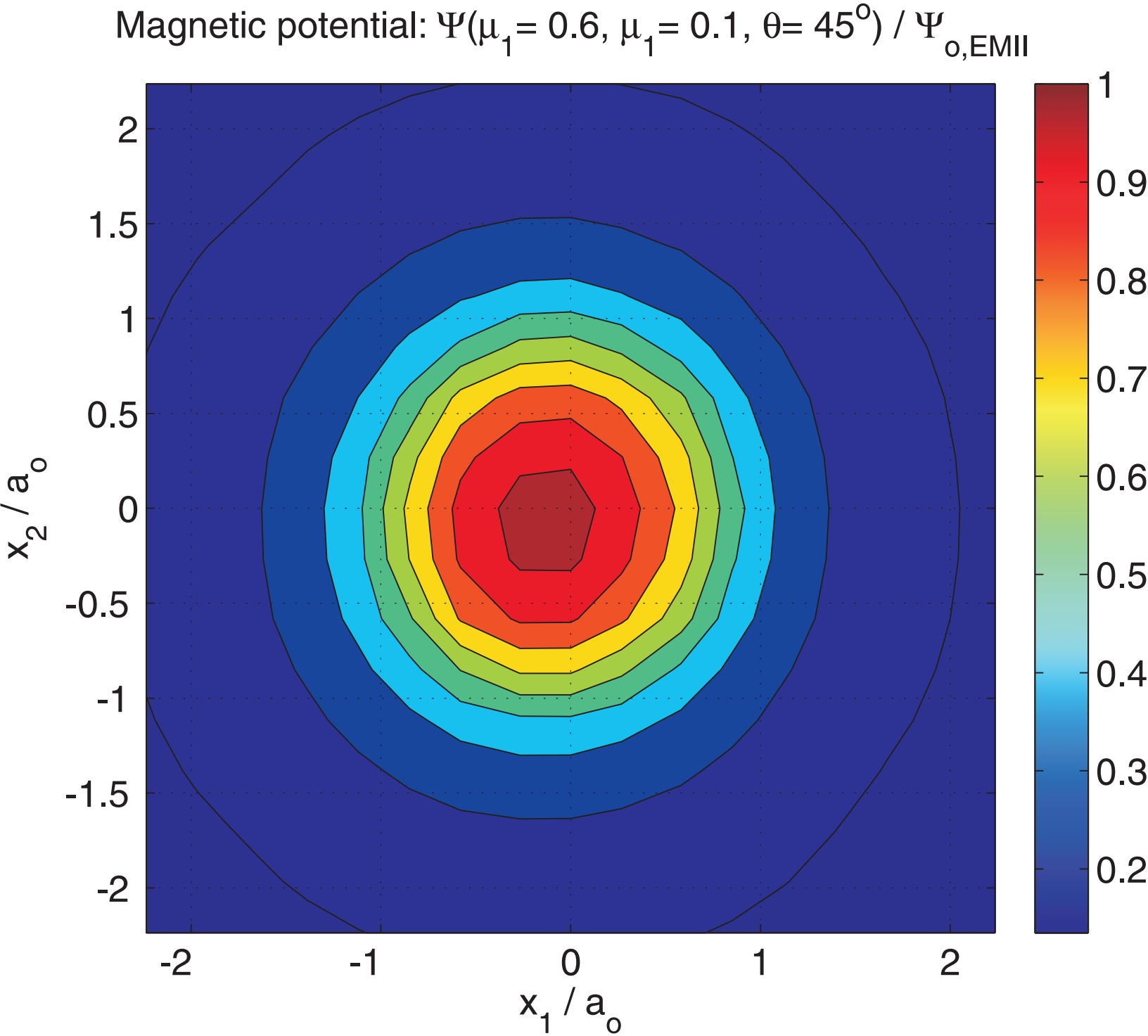
Magnetic potential: Ψ(μ1= 0.6, μ1= 0.1, θ= 45°) / Ψo,EMII
x2 / ao
x1 / ao
2
1.5
1
0.5
0
-0.5
-1
-1.5
-2
-2
-1
0
1
2
1
0.9
0.8
0.7
0.6
0.5
0.4
0.3
0.2

Figure(s)

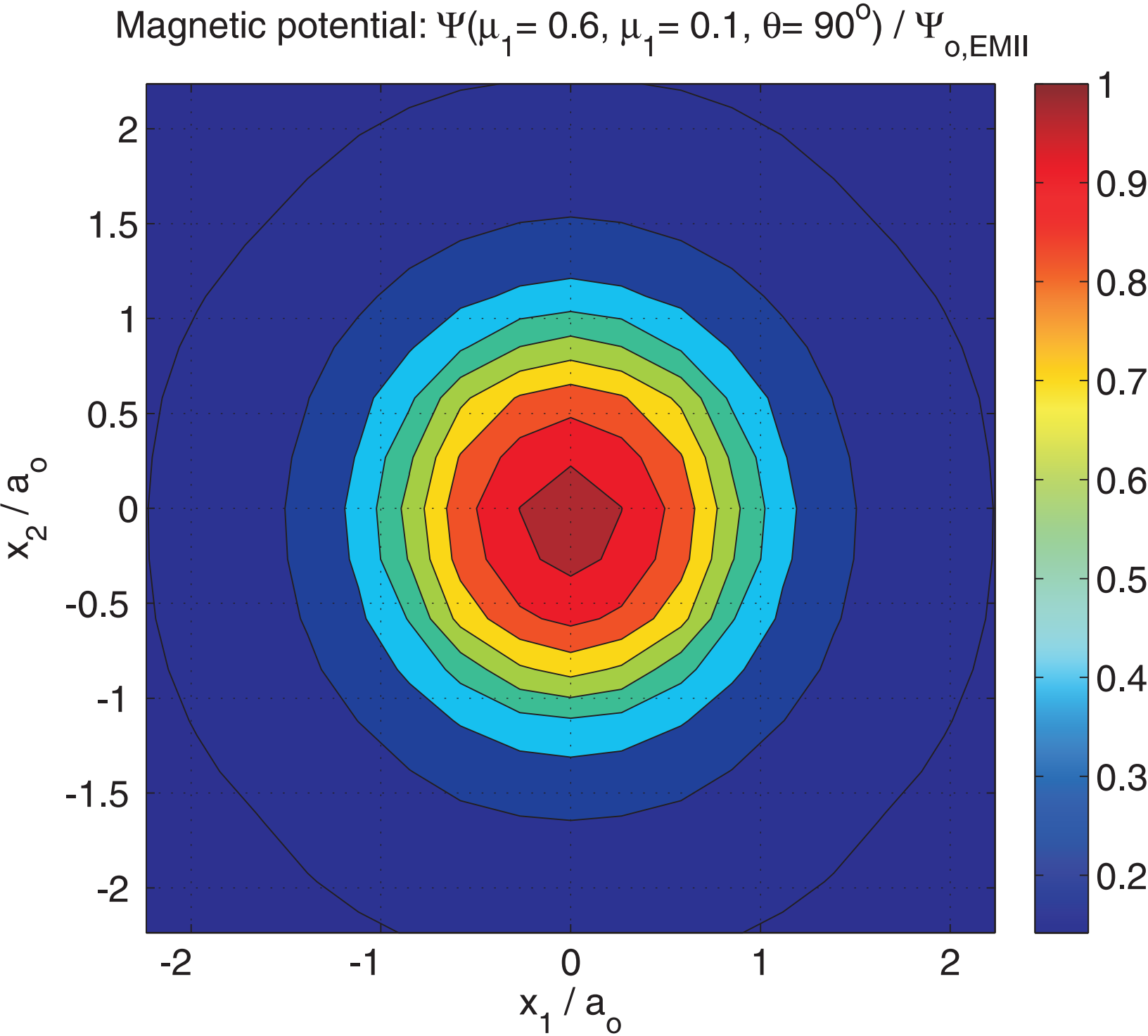
Magnetic potential: Ψ(μ1= 0.6, μ1= 0.1, θ= 90°) / Ψo,EMII
2
1.5
1
0.5
0
-0.5
-1
-1.5
-2
x2 / ao
-2
-1
0
1
2
x1 / ao
1
0.9
0.8
0.7
0.6
0.5
0.4
0.3
0.2

Figure(s)

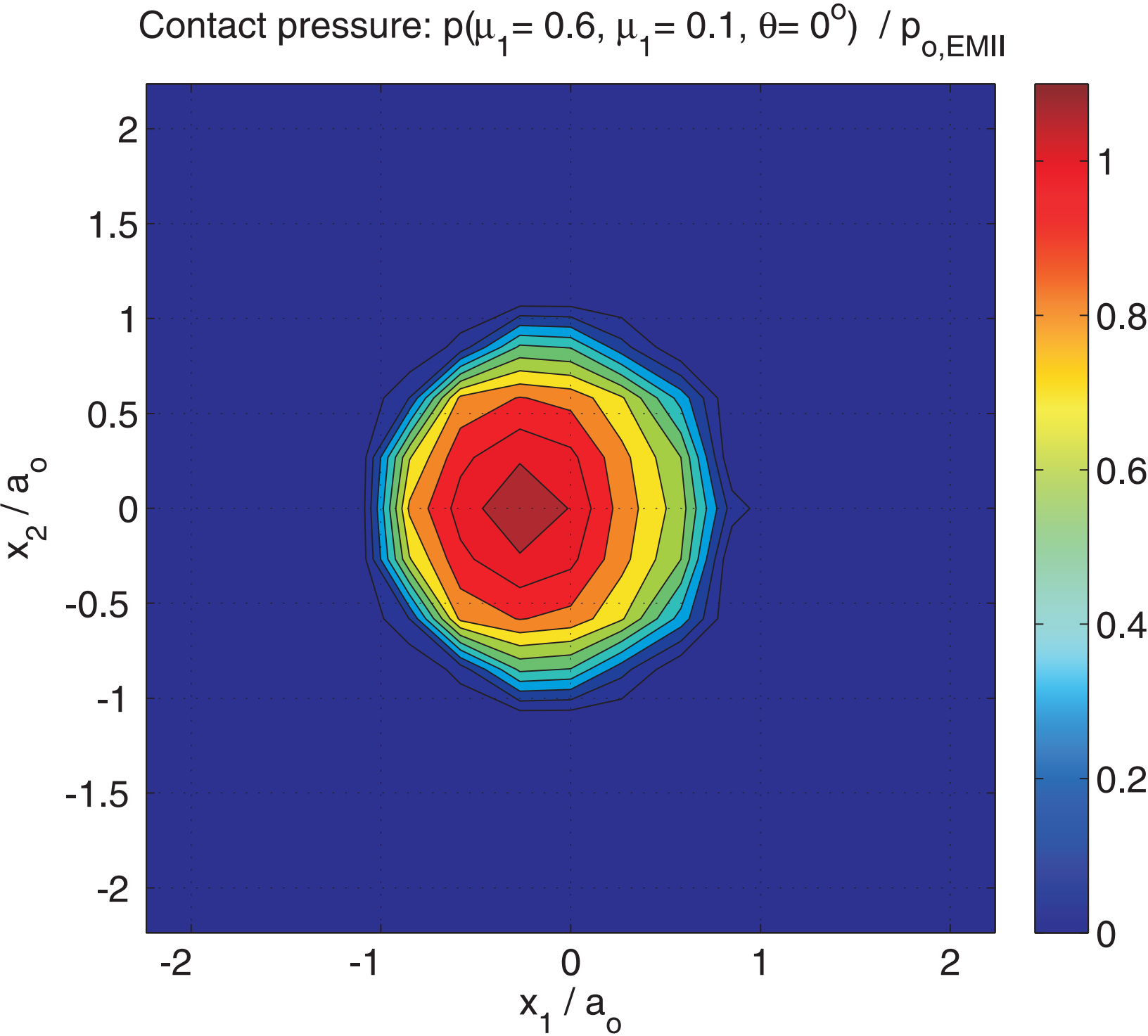
Contact pressure: p(μ1= 0.6, μ1= 0.1, θ= 0°) / po,EMII
x2 / ao
x1 / ao
2
1.5
1
0.5
0
-0.5
-1
-1.5
-2
-2
-1
0
1
2
1
0.8
0.6
0.4
0.2
0

Figure(s)

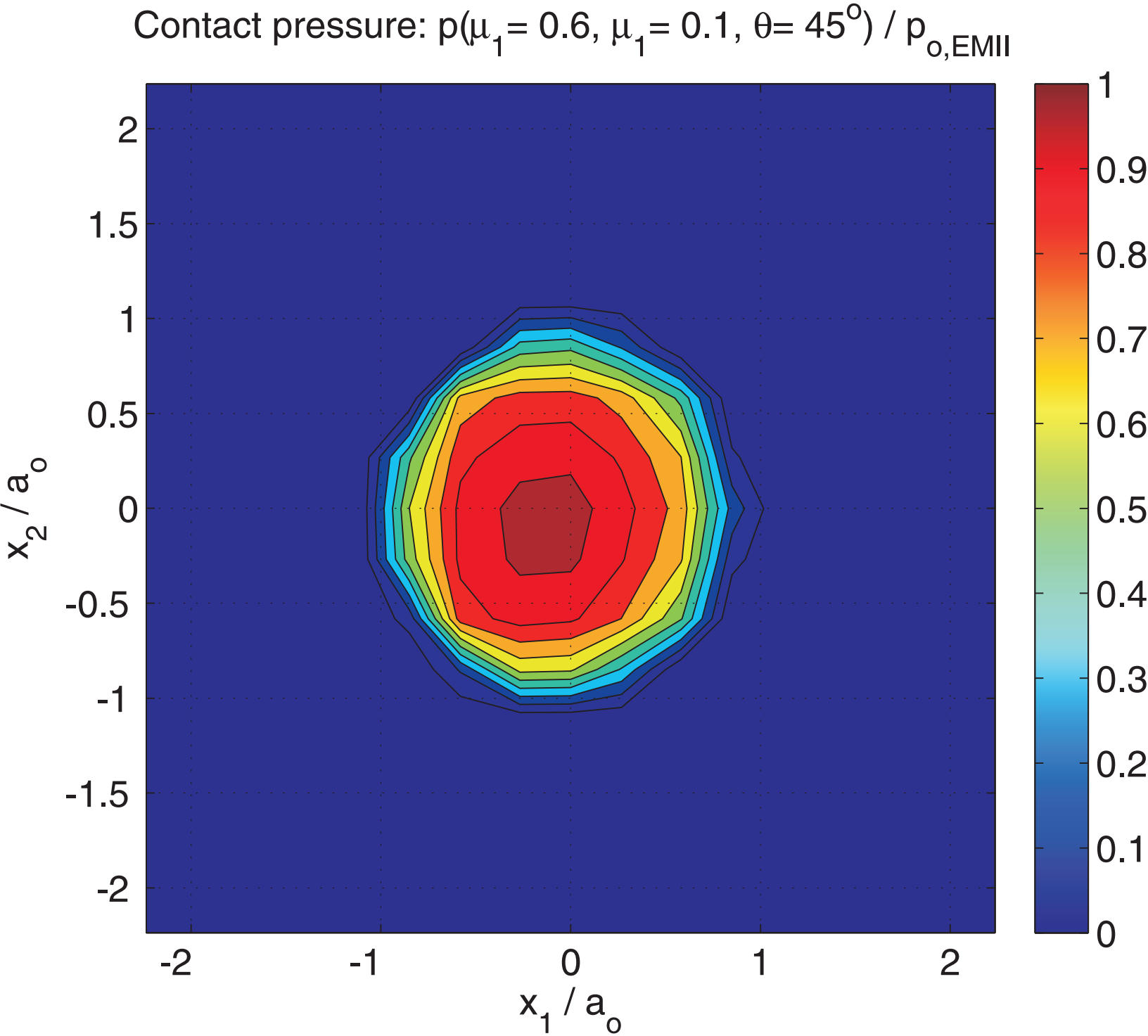
Contact pressure: p(μ1= 0.6, μ1= 0.1, θ= 45°) / po,EMII
x2 / ao
x1 / ao
2
1.5
1
0.5
0
-0.5
-1
-1.5
-2
-2
-1
0
1
2
1
0.9
0.8
0.7
0.6
0.5
0.4
0.3
0.2
0.1
0

Figure(s)

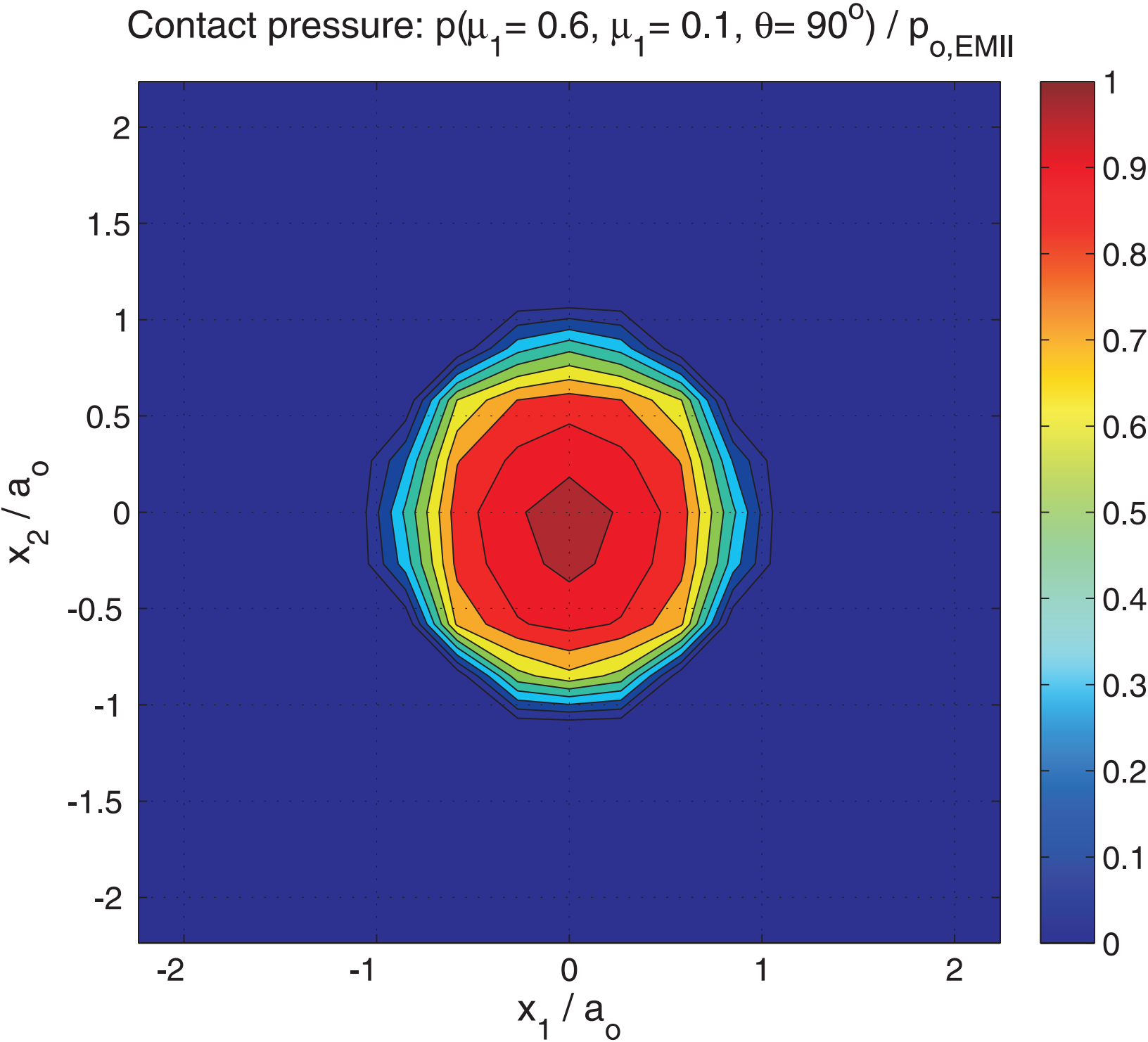
Contact pressure: p(μ1= 0.6, μ1= 0.1, θ= 90°) / po,EMII
x2 / ao
x1 / ao
2
1.5
1
0.5
0
-0.5
-1
-1.5
-2
-2
-1
0
1
2
1
0.9
0.8
0.7
0.6
0.5
0.4
0.3
0.2
0.1
0

LaTeX Source Files

Click here to download LaTeX Source Files: MainDocument.tex